Measurement of charm, bottom and Drell-Yan in p+Au collisions in Run15 via dimuons at $\sqrt{s} = 200$ GeV

September 18, 2018

Abstract

This analysis note documents the analysis of the Run15 p+Au unlike- and like-sign dimuons.

Contents

1 Introduction

This analysis note documents the analysis of the Run15 p+Au unlike and like sign dimuons. We focus on the extraction and separation of charm, bottom and Drell-Yan via a multi-dimensional analysis of the unlike- and like-sign dimuon spectra.

The p+p dimuon analysis is extensively documented in AN1306 [1]. We apply a similar strategy for signal extraction for p+Au. It is strongly recommended to first read [1] and view this document as chapters following the end of [1].

2 Data set, QA, analysis cuts

The good run list is provided by Sanghoon, and is identical to the J/ψ dimuon analysis in small systems, see AN1354 [2].

3 Analysis cuts

A summary of all cuts applied for single muons and dimuons are listed in Tables 1 and 2.

4 Simulation Framework

The construction of efficiency files to the MuTr and MuID are documented in AN1354. It is important to note that the the z-collision vertex is unusual, due to the fact that the MuIDLL1-2D is combined with different BBC triggers in different runs, either BBCLL1-novtx, BBCLL1-narrowvertex or BBCLL1. The z-collision vertex obtained from data is shown in Fig. 1. For each run, we choose the BBC sample triggered with the specific BBC trigger combined with the MuIDLL1-2D, scaled with the corresponding scaledown of the run.

5 Like-sign analysis

5.1 Modification of templates

For like-sign analysis, the aim is to obtain pair yield of dimuons from $b\bar{b}$. The backgrounds of $b\bar{b}$ is the combinatorial background and correlated hadronic pairs. The main contributions to correlated

Table 1: Summary of single cuts applied in this analysis.

	South	North
MuID last gap	$= 4$	$= 4$
$\|p\|$	> 3 GeV	> 3 GeV
p_z	< -2 GeV	> 2 GeV
y	$(-2.2, -1.2)$	$(1.2, 2.2)$
MuTr χ^2	< 15	< 20
no. hits in MuTr	> 10	> 10
MuID χ^2	< 5	< 5
no. hits in MuID	> 5	> 5
Fiducial cuts		
$DG0(\|p\|)$	3σ	3σ
$DDG0(\|p\|)$	3σ	3σ
$\|p\|$	< 20 GeV	< 20 GeV
1D software trigger cut		

Table 2: Summary of pair cuts applied in this analysis.

MuID gap 0 track Δx	> 20cm
MuID gap 0 track Δy	> 20cm
muon pair should not share same MuTr octant	
χ^2_{vtx}	< 5
$\|p_1 - p_2\|/\|p_1 + p_2\|$	< 0.55

hadronic pairs are hadron-hadron pairs and charm-hadron pairs. All contributions may be modified in p-Au collisions, and are described in the following:

5.1.1 Combinatorial background

Event mixing is carried out using p+Au single muons from MuIDLL1-1D. One additional modification to the p+p analysis is in addition to z-vertex bins, we also divide data into 5 centrality bins, $0-20\%$, $20-40\%$, $40-60\%$, $60-84\%$. The multiplicity as a function of bbc_z, $N_{trk}/N_{bbcz}(z)$ are shown in Fig. 2. From $N_{trk}/N_{bbcz}(z)$, and the z vertex shown in Fig. 1, we can calculate the relative expected no. of combinatorial pairs as a function of z, for each sign combination, according to Eq. 1, which is shown in Fig. 3.

$$N_{uncorr}(z) = (\frac{\Delta N_{trk}(z)}{\Delta N_{bbcz}(z)})^2 * N_{bbcz}(z) * \epsilon_{pair}, \quad (1)$$

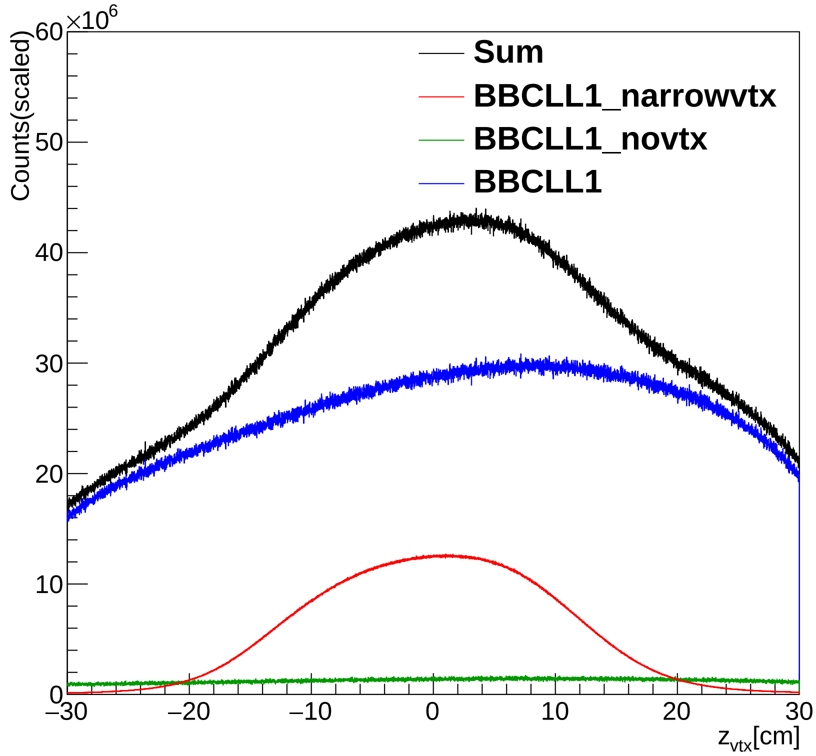

Figure 1: z vertex distribution for Run15 p+Au different BBC triggered samples. The vertex distribution is weighted with the no. of events when the MuIDLL1-2D is combined with a certain BBC trigger and the corresponding scaledown.

5.1.2 Correlated hadronic pairs

1. **Modification of input hadron p_T spectra**

   The input hadron(K and π) p_T spectra is modified according to the R_{pAu} of inclusive hadrons, from AN1341 [3], as in Fig. 4. Each hadron in simulations is weighted according to the R_{pAu} as a function of p_T in Fig. 4 for the p-going and Au-going side. The corresponding correlated hadronic background(ZYAM applied) for the p-going and Au-going side as a function of mass is shown in Fig. 5 as solid colored lines. The mass spectrum for the p-going side is harder, due to the harder input p_T spectrum; high p_T hadrons less suppressed than low p_T hadrons, while for the Au-going side, the mass spectrum is softer, due to the softer input p_T spectrum; high p_T hadrons more suppressed than low p_T hadrons (see Sec. 5.6 for an extended discusion). The modified mass-p_T spectrum is also shown as solid colored lines in Fig. 6 and 7. The figures show only one case of the applied R_{pA}, a full account of the systematic uncertainties will be discussed in Sec. 5.6.

2. **Modification of input charm p_T spectra**
   In addition to the modification of K,π p_T spectra, the charm p_T spectra may be modified. Since there are no existing heavy flavor muon measurement in p+Au collisions, we estimate

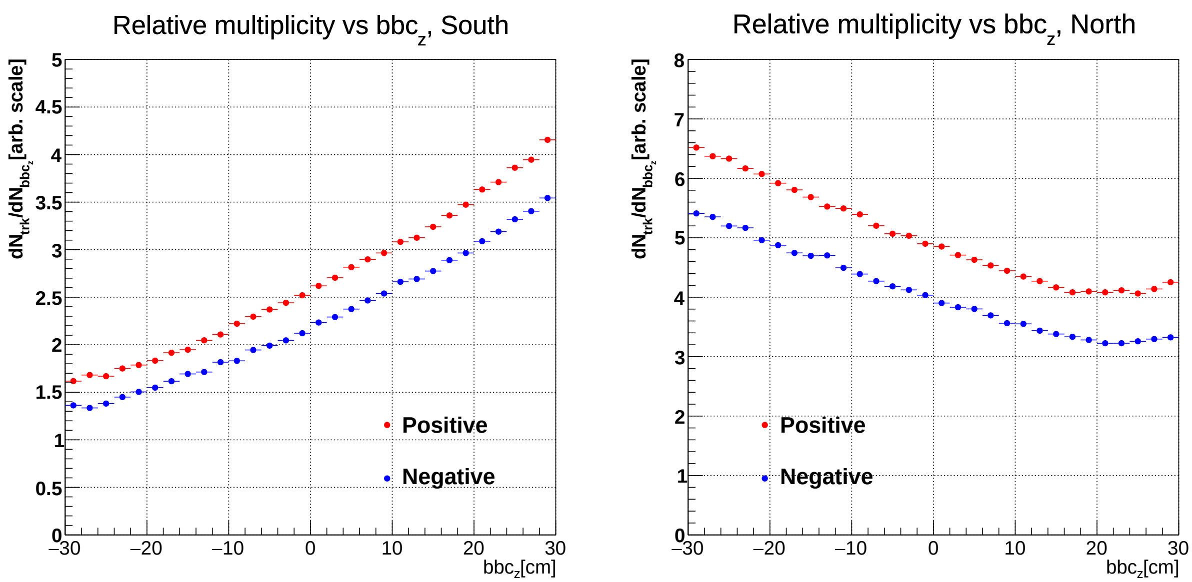

Figure 2: $N_{trk}/N_{bbcz}(z)$ in South and North arms.

this effect by applying R_{dAu} of heavy flavor muons, documented in PPG153 [4]. The R_{dAu} of heavy flavor muons at forward and backward rapidity is shown in Fig. 8. We apply the central value of the R_{dAu} to charm-hadron pairs. The modified correlated hadronic pairs as a function of mass, and mass and p_T are shown as dotted colored lines in Figs. 5, 6 and 7. The figures show only one case of the applied R_{pA}, a full account of the systematic uncertainties will be discussed in Sec. 5.6.

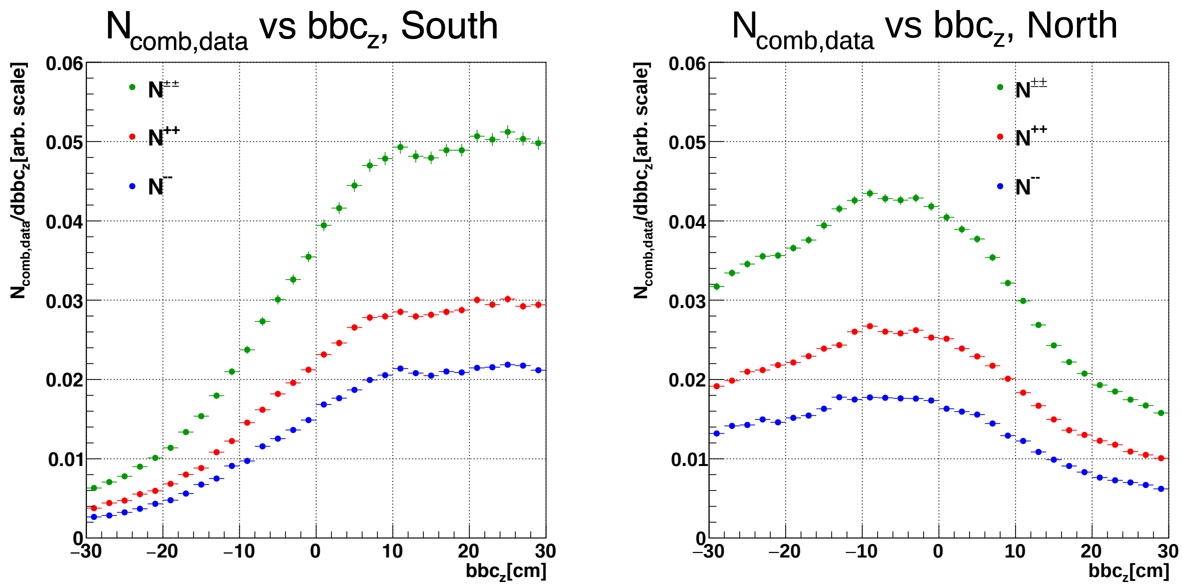

Figure 3: N_{uncorr} in South and North arms.

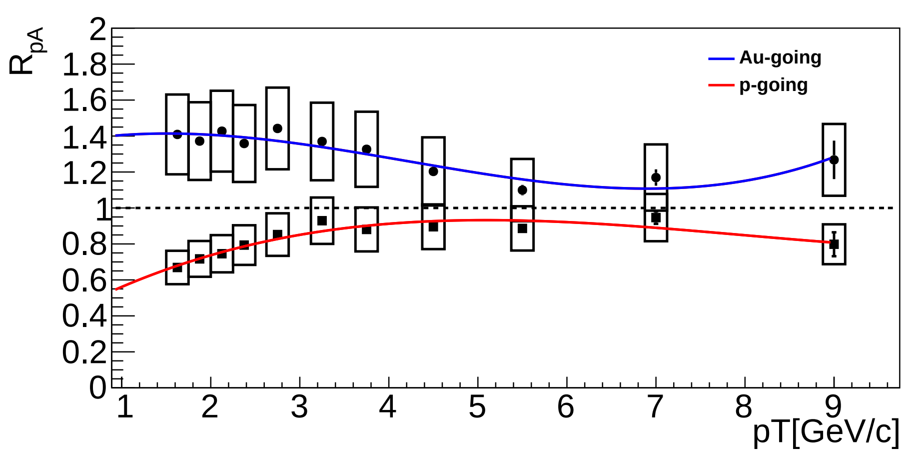

Figure 4: R_{pAu} of inclusive hadrons and fit.

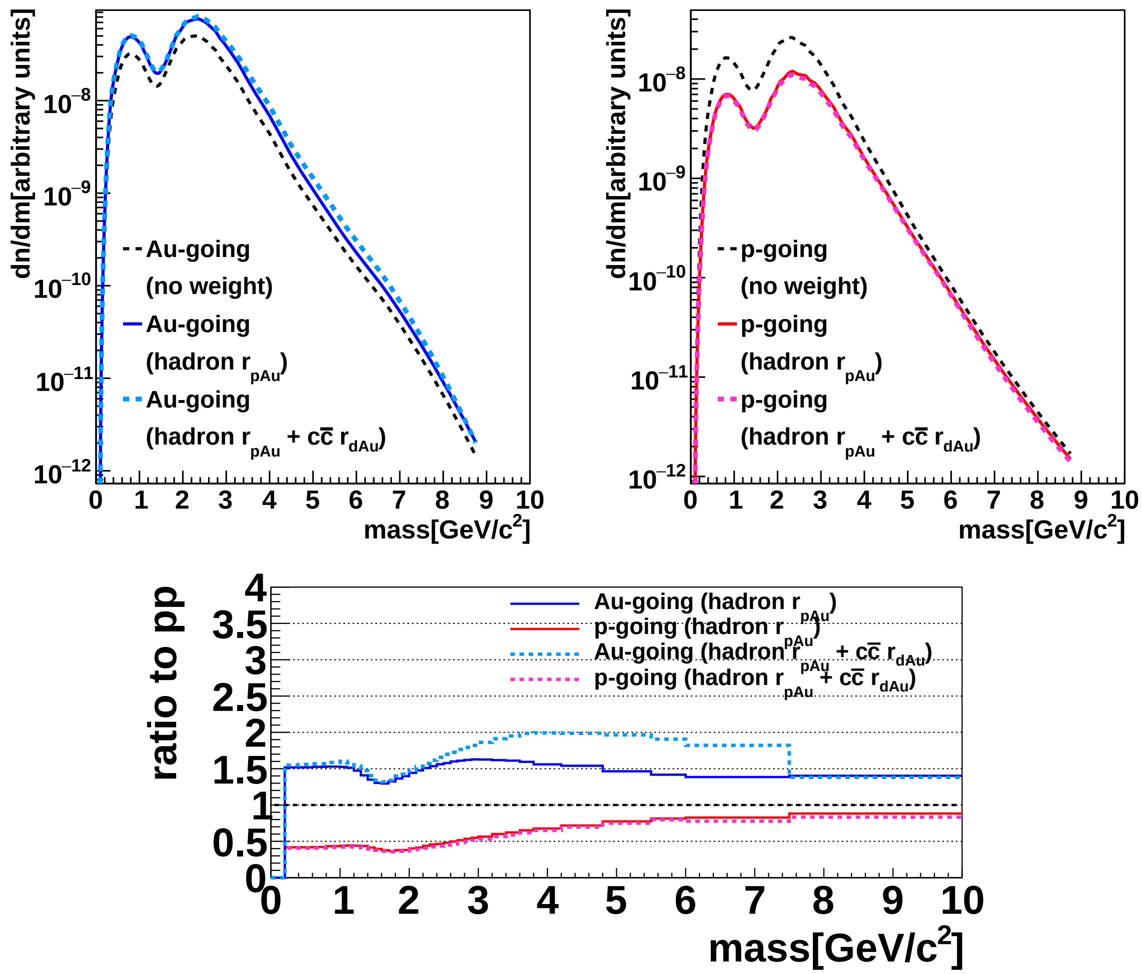

Figure 5: Correlated hadronic pairs as a function of mass, modified with nuclear modifications of hadrons (kaons and pions)(solid colored) and also charm (dotted colored).

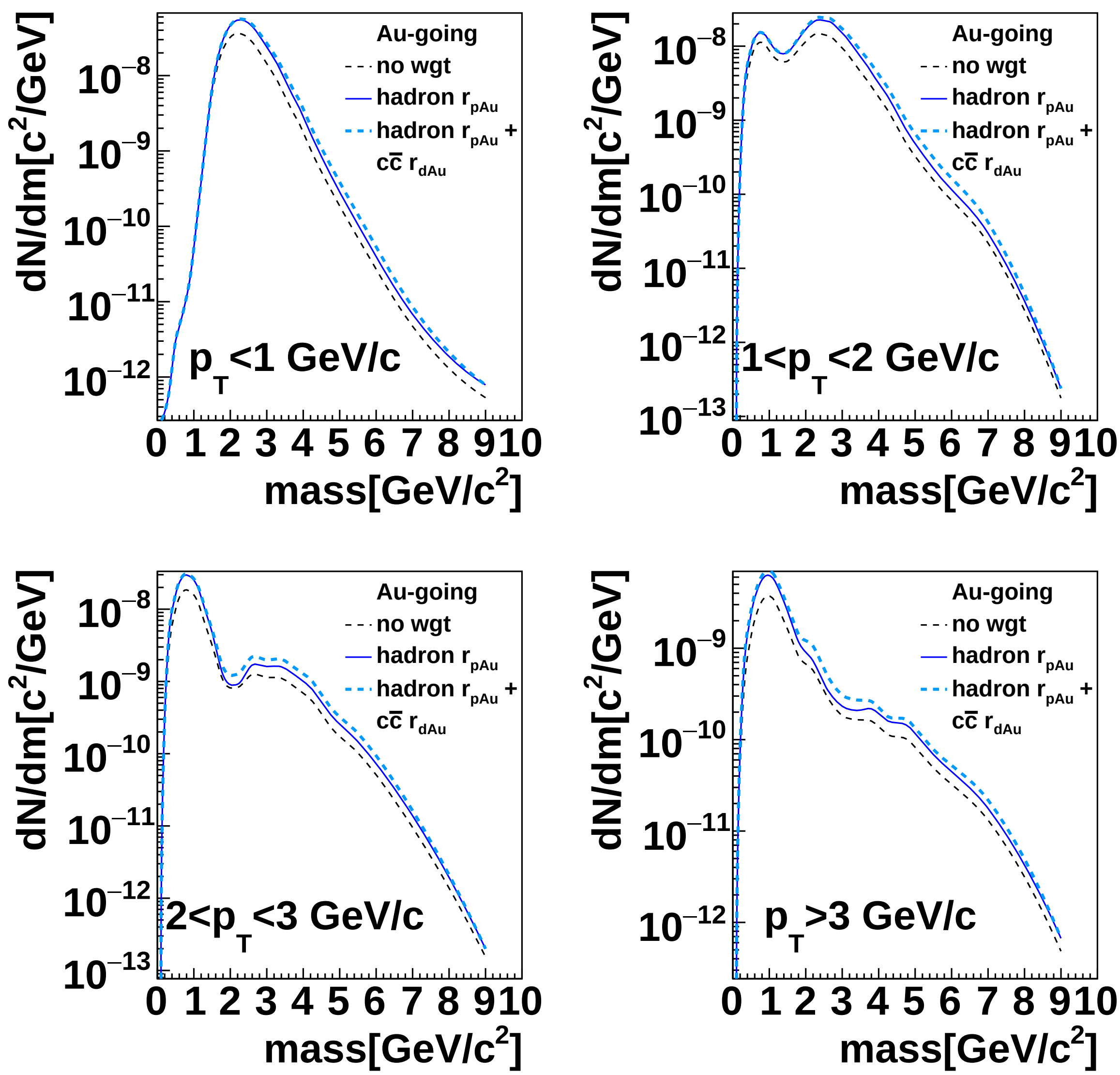

Figure 6: Correlated hadronic pairs as a function of mass and p_T, modified with nuclear modifications of hadrons (kaons and pions) (solid colored) and also charm (dotted colored) for the Au-going side.

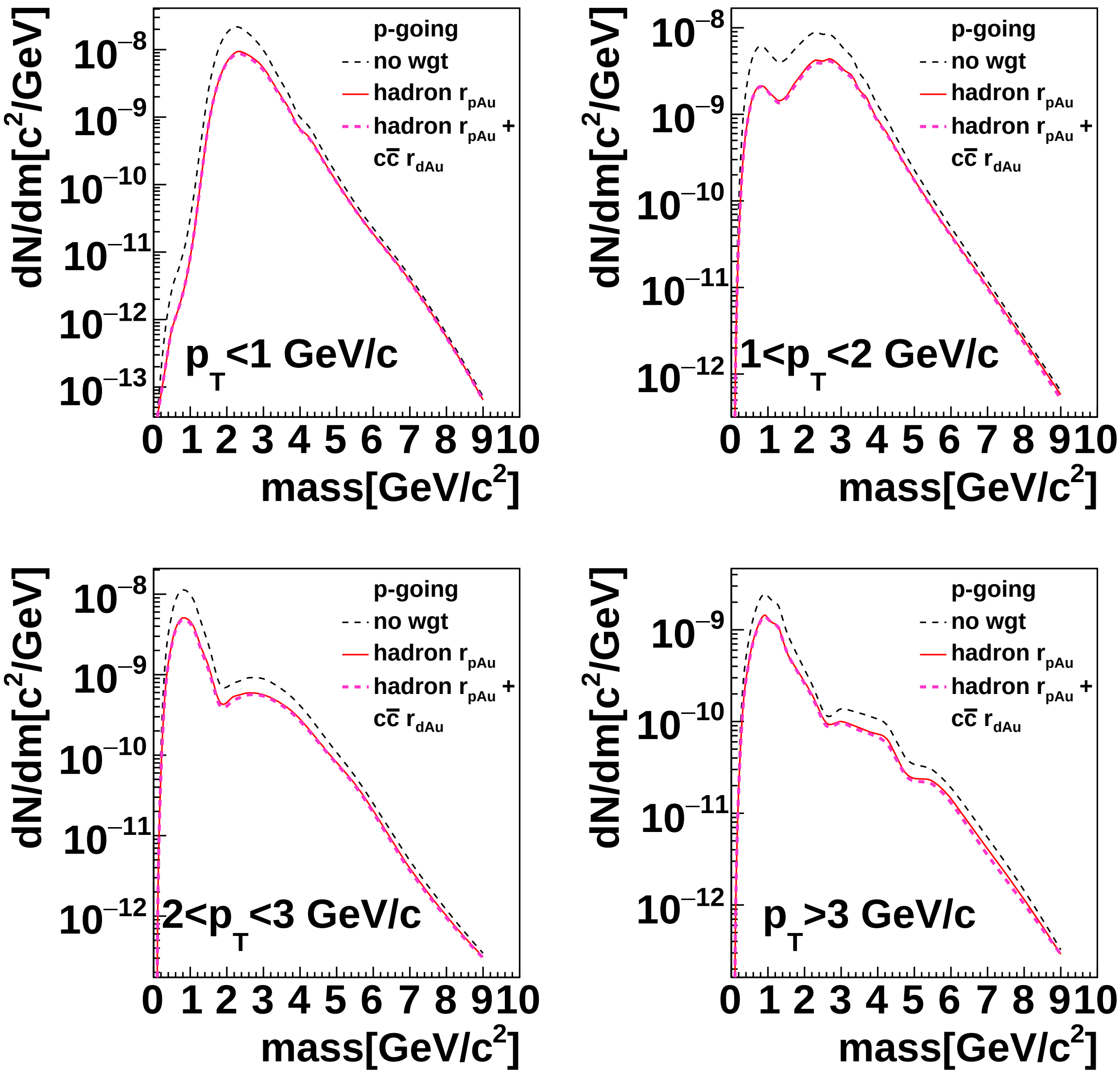

Figure 7: Correlated hadronic pairs as a function of mass and p_T, modified with nuclear modifications of hadrons (kaons and pions) (solid colored) and also charm (dotted colored) for the p-going side.

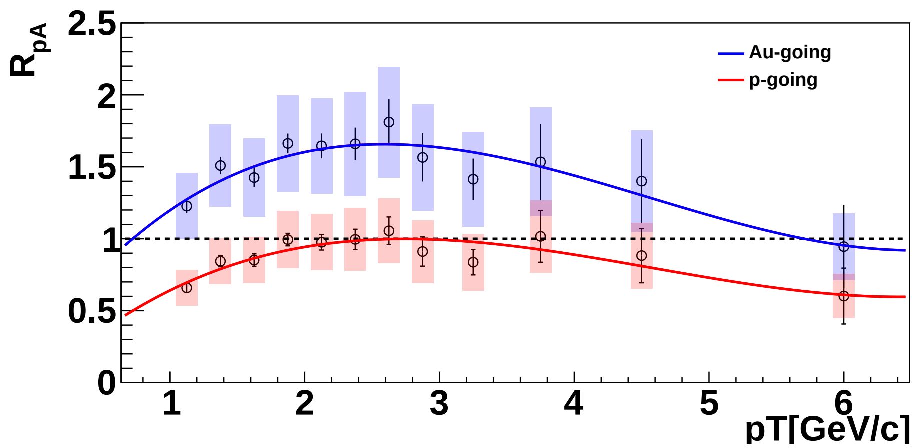

Figure 8: r_{dAu} of inclusive heavy single muons and fit.

5.2 Normalization of templates

The normalization of the correlated hadronic background is obtained the p+p analysis, i.e. θ_h as documented in [1]. Note here θ_h is a normalization constant for the hadronic background, which contains a mixture decay muons/punchthrough hadrons/secondary particles from showers. These components are uncorrected and hence θ_h is not a cross-section in the usual sense. The mixture of such components depends on the input p_T spectra, input vertex distribution, as well as detector configuration. The input p_T spectrum is modified through scaling with N_{coll} and folding with the nuclear modifications of hadrons and charm. The input vertex distribution is modified through weighting in z in fastMC simulations, and the detector configuration is unmodified between p+p and p+Au.

An additional effect to be considered is the drop in MuTr/MuID efficiency, especially in the South muon arm. This effect is not in the fastMC and needs to be estimated using simulations. In principle, if the decrease in MuTr/MuID efficiency, is a random effect and not localized in certain geometrical regions, this would result in a global scale factor, rather than changes in shapes of templates. This is verified by comparing $b\bar{b}$ simulations through GEANT4 and reconstruction, using p+Au detector efficiency and p+p detector efficiency, as shown in Fig 9. One can see that the detector efficiency is similar on the North arm, but a significant drop is observed in the South arm.

One thing to note is that these are muon simulations, not hadron simulations. To check for efficiency difference of hadrons between p+Au and p+p, one simply needs to run hadron simulations and plot reconstructed muons, e.g. as a function of p_T. The resulting ratio should be, to first order, flat, since the hadronic background are dominated by decay muons and punchthrough hadrons, both of which has similar/same characteristics as a prompt muon as far as the MuTr and MuID are concerned. This, however has not been done due to time constraints and we therefore assign a 15% uncertainty on the normalization of the hadronic background due to possible efficiency effects for both muon arms as a conservative measure.

In addition, the high multiplicity in the South arm may give rise background hits, leading to additional efficiency loss. This can be estimated by embedded simulations. Again, we carried out full GEANT4 and reconstruction on $b\bar{b}$ simulations, and compared the case of embedded simulations and non-embedded simulations. The embedding set-up is identical with AN1354, which filters minimum bias data samples for embedding based on MuID activity. The results are shown in Fig. 10. Again, we see no mass dependence on efficiency loss due to background hits. The efficiency loss (11.5% for South, 2.5% for North) is larger than South and North as expected. We assign a $\pm5\%$ uncertainty for both arms in the normalization of the hadronic background due to uncertainties in embedding simulations.

The normalizations of the bottom contribution and the combinatorial background is obtained by a two parameter fit in mass, p_T and z, corresponding to θ_h an $\theta_{b\bar{b}}$ in [1].

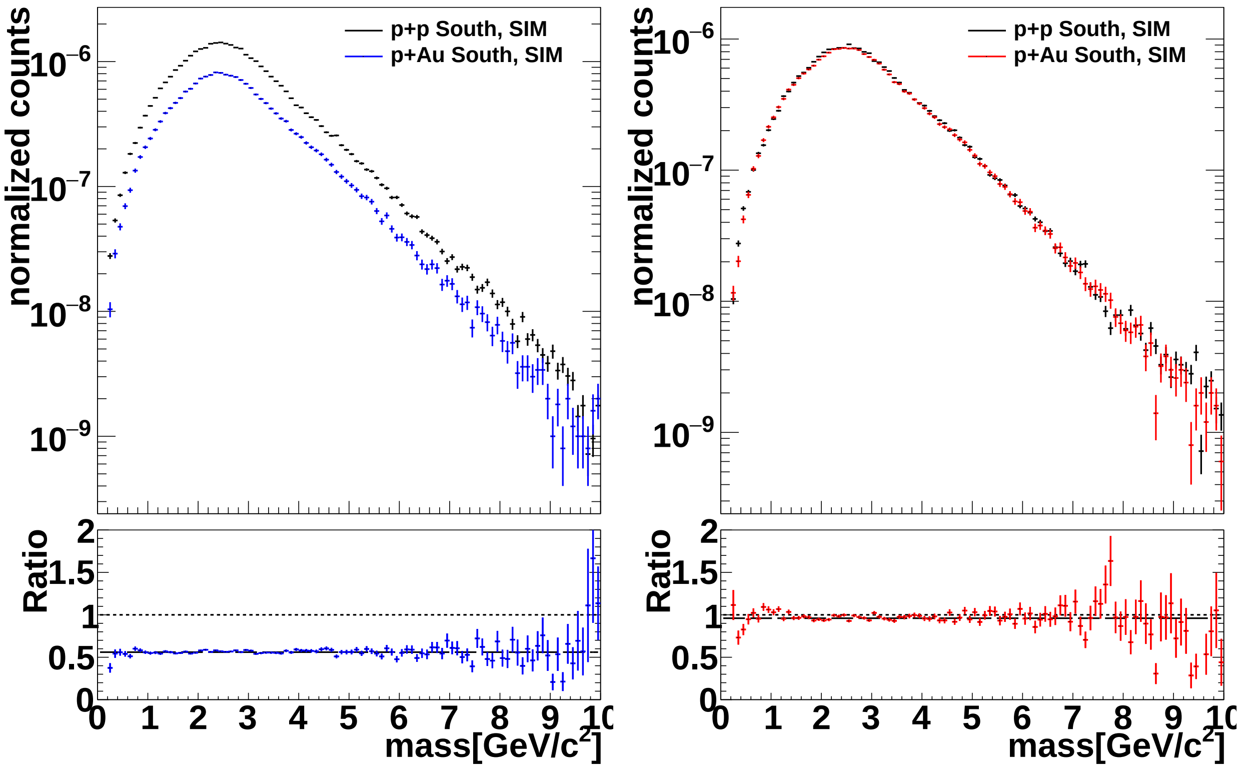

Figure 9: Pairs from $b\bar{b}$ simulations through GEANT4 and reconstruction, using p+p detector configuration (black) and p+Au configuration (colored).

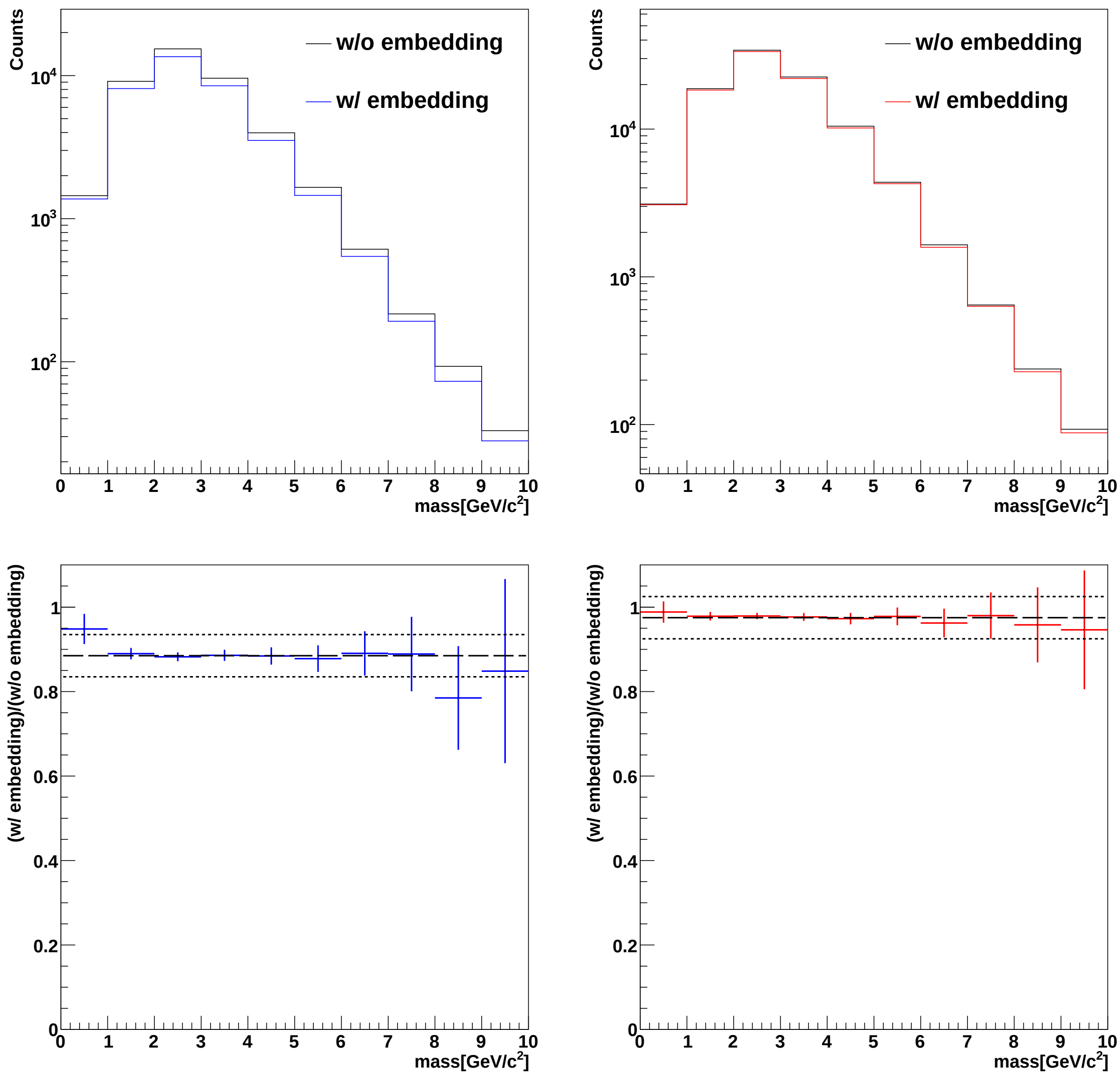

Figure 10: Pairs from $b\bar{b}$ simulations through GEANT4 and reconstruction, without embedding (black) and with embedding (colored).

5.3 Reproducing the combinatorial background using FastMC

Here we discuss efforts to reproduce the combinatorial background in p+Au using FastMC. A similar check has been done in p+p collisions, as in Fig. 11.

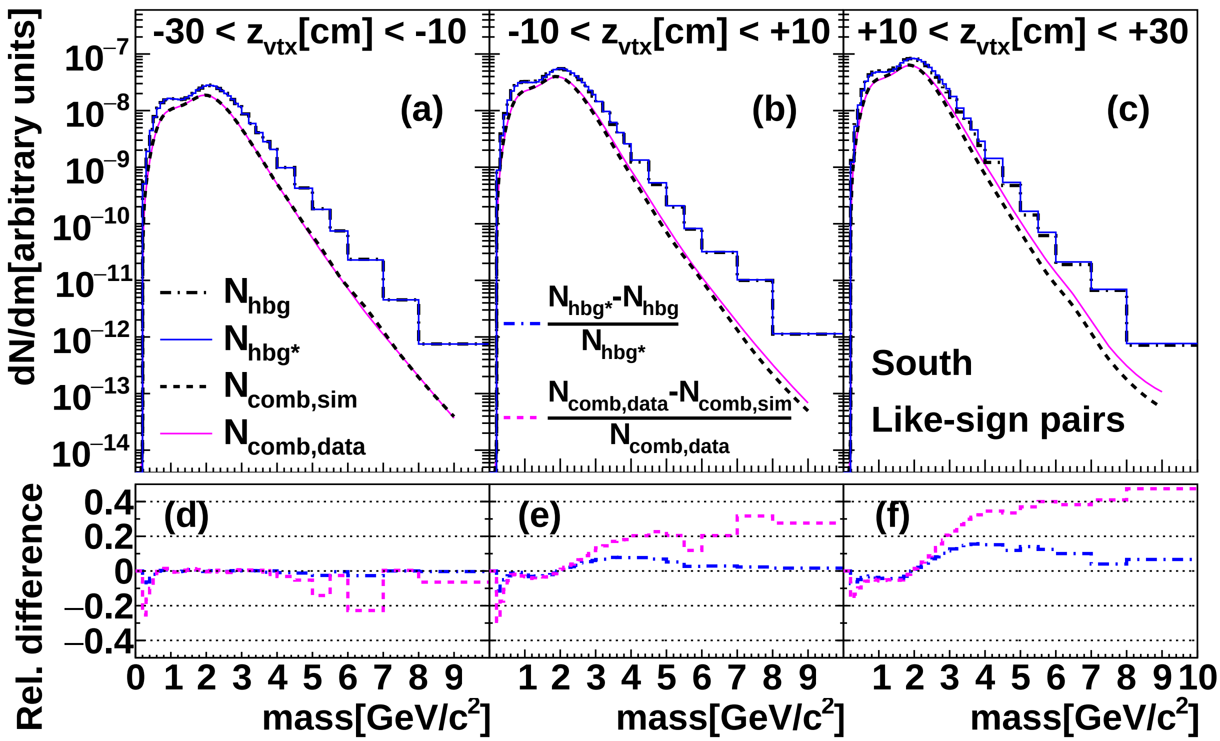

Figure 11: Comparison of combinatorial background in data and FastMC in p+p collisions.

Fig. 11 shows the combinatorial background generated using default p+p input hadron spectra. The description is not perfect, which worsens as the collision vertex moves away from the absorber. However, this level of discrepancy is covered by uncertainties in the p+p input hadron spectra (using BRAHMS and PHENIX mid-rapidity to bracket systematic uncertainties). We hope to reproduce similar level of agreement in p+Au collisions.

The construction of the combinatorial background is naturally sensitive to the input hadron spectra. In the case of p+Au, these are modified. One thing to note is that the shape of the combinatorial background is also sensitive to hadrons with low p_T ($\sim$ 1 GeV), which gives rise to pairs with mass $<$ 2 GeV. Thus, there is a complication due to the fact that the R_{pA} measurement shown in Fig. 4 only extends to 1.6 GeV, i.e. one would need to extrapolate down to around $\sim$ 0.8 GeV (the acceptance threshold) in order to reproduce an accurate combinatorial background using fastMC.

Note that the naive fit as shown in Fig. 4 gives a flat R_{pA} for p_T $1.0-1.6$ GeV. This contrasts to the mid-rapidity π^0 result 12 as well as HIJING simulations (see slide 13: https://indico.cern.ch/event /433345/contributions/2358479/attachments/1408900/2154126/ NovitzkyQM2017-final.pdf), where a steep decline is observed/predicted. As a qualitative check, we look at a sample of gap4 single muons between p+p and p+Au. Note here the samples are arbitrarily normalized, we only compare the shape of the raw p_T spectra in Fig. 13.

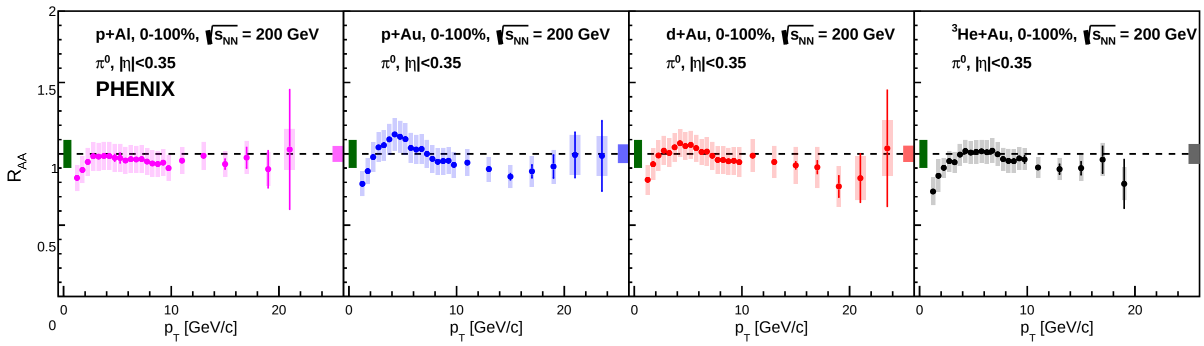

Figure 12: Mid-rapidity π^0 R_{AA} in small systems.

The interpretation of raw p_T spectra is complicated due to various reasons, we make qualitative arguments in the following. For the comparison in the North arm, we see that the ratio of p+Au,N to p+p decreases with p_T. As low p_T muons are dominated by decay muons from hadrons, this is completely consistent with the naive fit to hadron R_{pA} for the North arm shown in Fig. 4. However, the case for the South is inconsistent with the naive fit for South in Fig. 4, which gives a flat R_{pA} from $1.0 - 1.6$ GeV. If the R_{pA} from $1.0 - 1.6$ GeV is constant, then we should see an enhancement for single muons in $1.0 - 1.6$ similar to p_T between $1.6 - 3.0$ GeV, where the R_{pA} is almost constant at around 1.3. However, we clearly see a decreasing trend in the raw muon yield from 1.6 GeV. This clearly implies that the R_{pA} should decrease below 1.6 GeV. In addition, the raw yield hints that the decline may be steep.

With the qualitative information from the raw gap4 tracks, we consider the following three cases of R_{pA} (see Fig. 14), which we call soft, default, and hard input p_T spectra as a systematic study:

The corresponding combinatorial background generated using soft, default, and hard input p_T spectra are shown in Fig. 15 for the North arm and Fig. 16 for the South arm.

This study clearly illustrates the sensitivity of the lower mass region of the combinatorial background to the low p_T input spectra. We observe that the soft spectra for North and hard spectra for South can reasonably reproduce the data, at least to the level of the p+p analysis. This implies that the input spectra for the fastMC reasonably reproduce the data.

The hard spectra from the naive fit clearly underestimates the combinatorial background, which is an obvious result based on the raw p_T spectra as shown in Fig. 13.

We also generate the correlated hadronic background using the three spectra. The results for the South arm are shown in Fig. 17.

Note that there are three components of uncertainties in the input hadron spectra: 1. uncertainties in the baseline p+p spectra; 2. uncertainties in the R_{pA} in the measured region; 3. uncertainties in the extrapolation of R_{pA} beyond the measured region. All three should be accounted for in the systematic uncertainties of the correlated hadronic background, as discussed in Sec. 5.6.

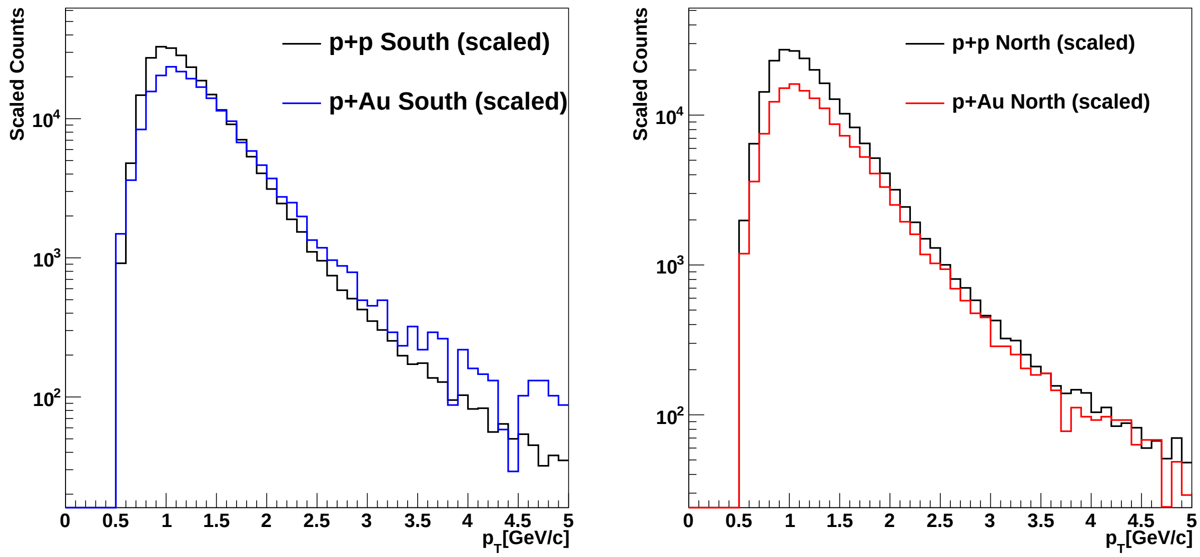

Figure 13: Comparison of single raw p_T spectra in p+p and p+Au collisions.

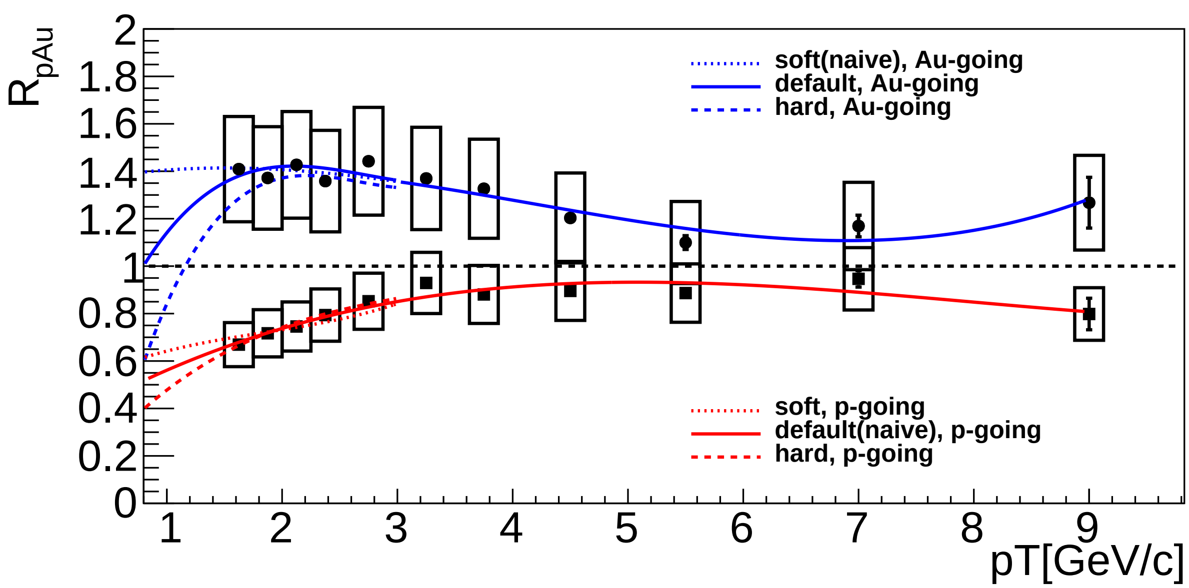

Figure 14: Extrapolation of R_{pA} to low p_T. Different extrapolations are for systematic studies.

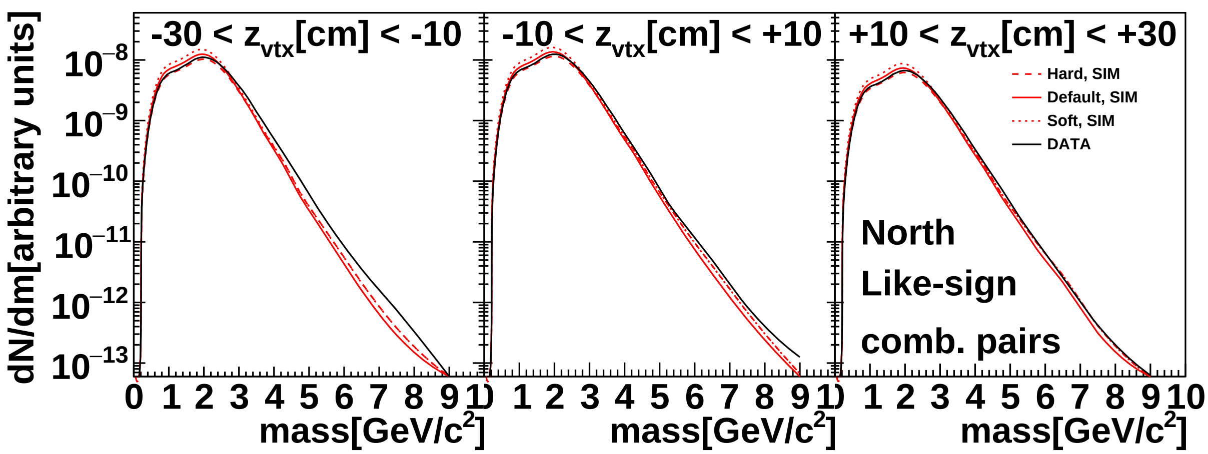

Figure 15: Generation of combinatorial background using FastMC in p+Au using hard(dashed), default(solid) and soft(dotted) input spectra for the North arm.

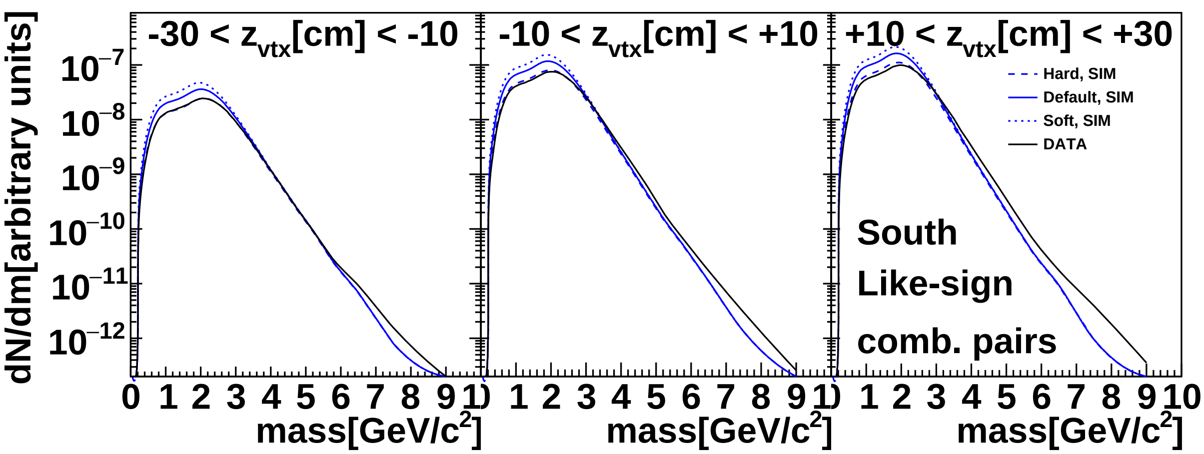

Figure 16: Generation of combinatorial background using FastMC in p+Au using hard(dashed), default(solid) and soft(dotted) input spectra for the South arm.

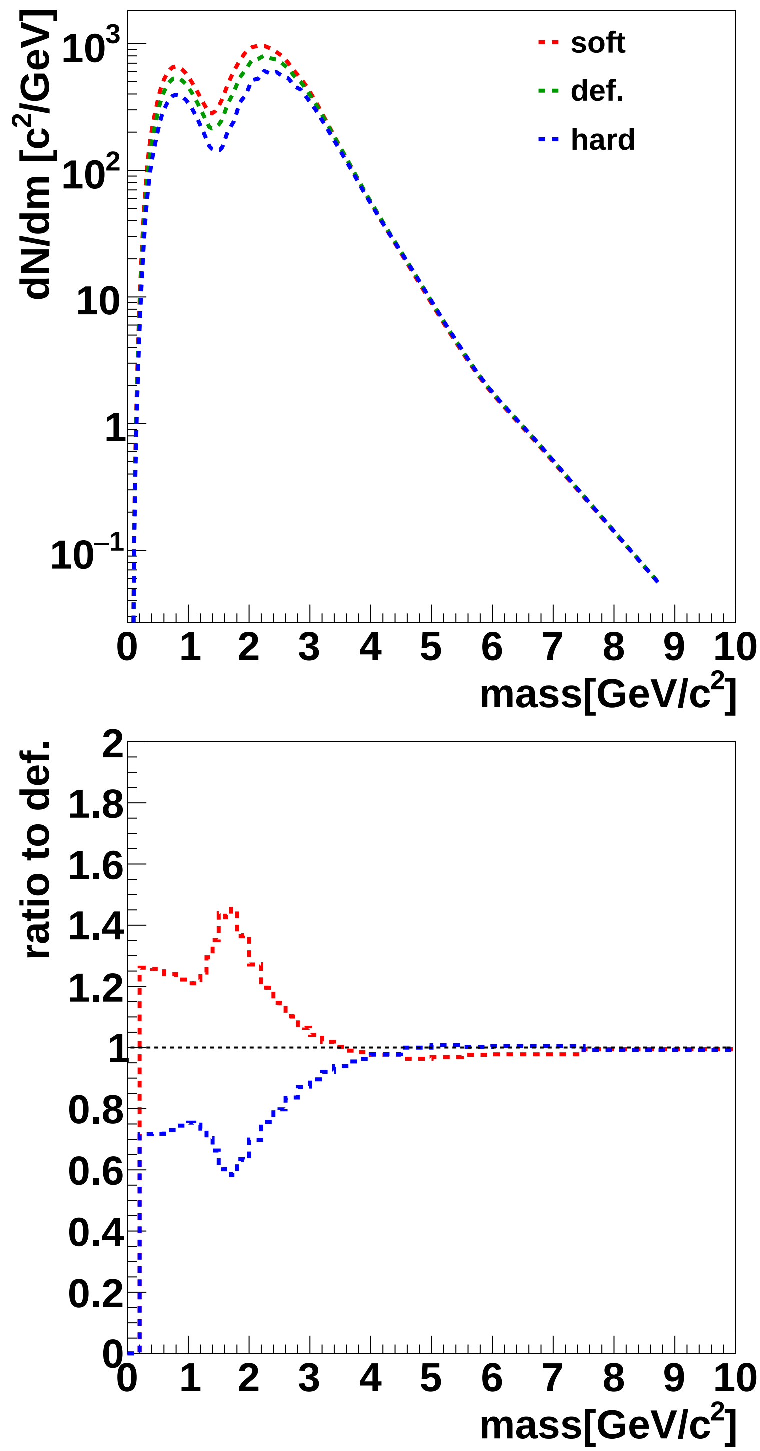

Figure 17: Generation of correlated hadronic background using FastMC in p+Au using soft(red), default(green) and hard(blue) input spectra for the South arm. The ratio to the default spectra is shown in the bottom panel.

5.4 Fitting results

Like-sign pairs compared to fitted cocktail are shown in Fig. 18 as a function of mass, Figs. 19 as a function of mass-z and Figs. 20 as a function of mass-p_T. We use the default spectra for the above figures, the fit quality is on par with the p+p analysis.

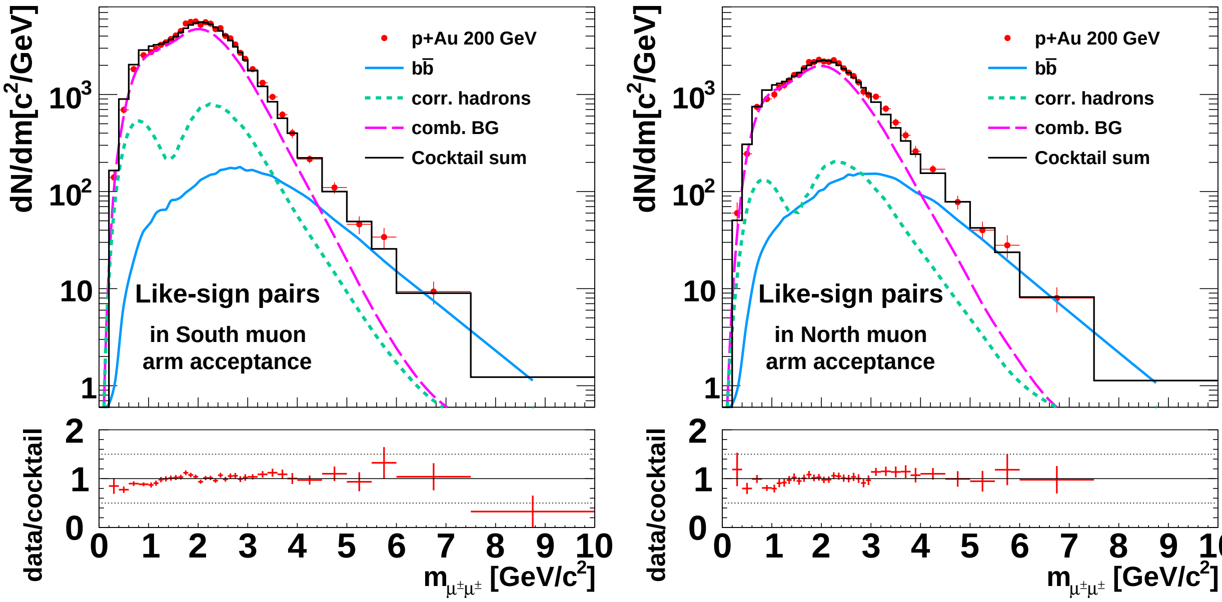

Figure 18: Like-sign pairs for the Au-going(left) and p-going(right) side as a function of mass compared to cocktail.

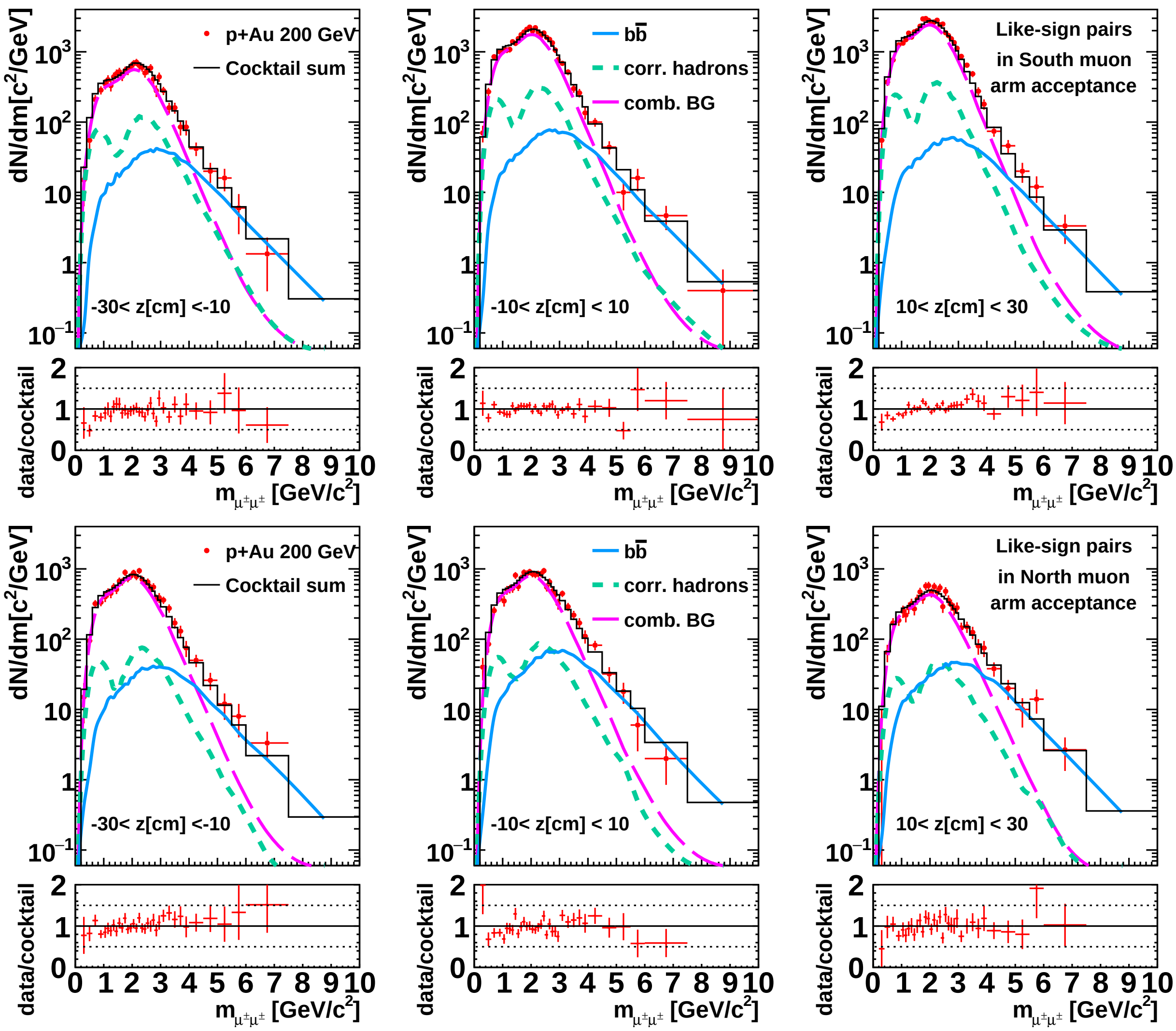

Figure 19: Like-sign pairs for the Au-going(left) and p-going(right) side as a function of mass and z compared to cocktail.

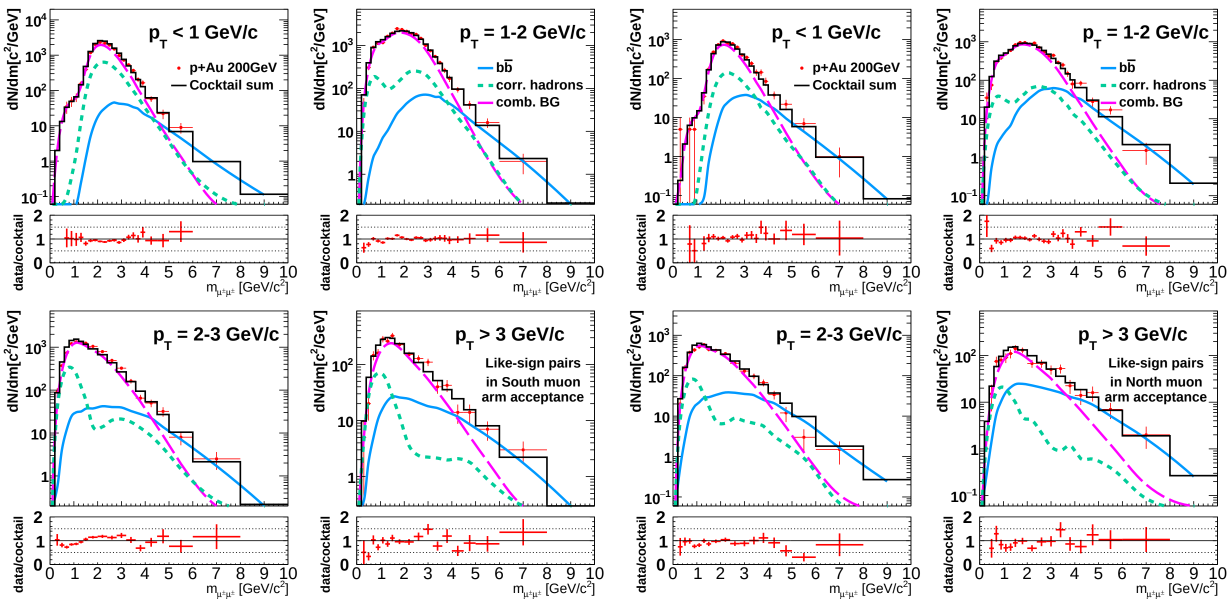

Figure 20: Like-sign pairs for the Au-going(left) and p-going(right) side as a function of mass and p_T compared to cocktail.

5.5 Background subtraction

After the normalization of the combinatorial background in the previous section, the correlated hadronic background and the combinatorial background are subtracted from the data as a function of $\Delta\phi$ or p_T and subsequently corrected for efficiency. Fig. 21 shows the background components as a function of $\Delta\phi$, and fig. 21 shows the background components as a function of p_T. Background levels are significantly higher in the South arm, which will lead to larger systematic uncertainties.

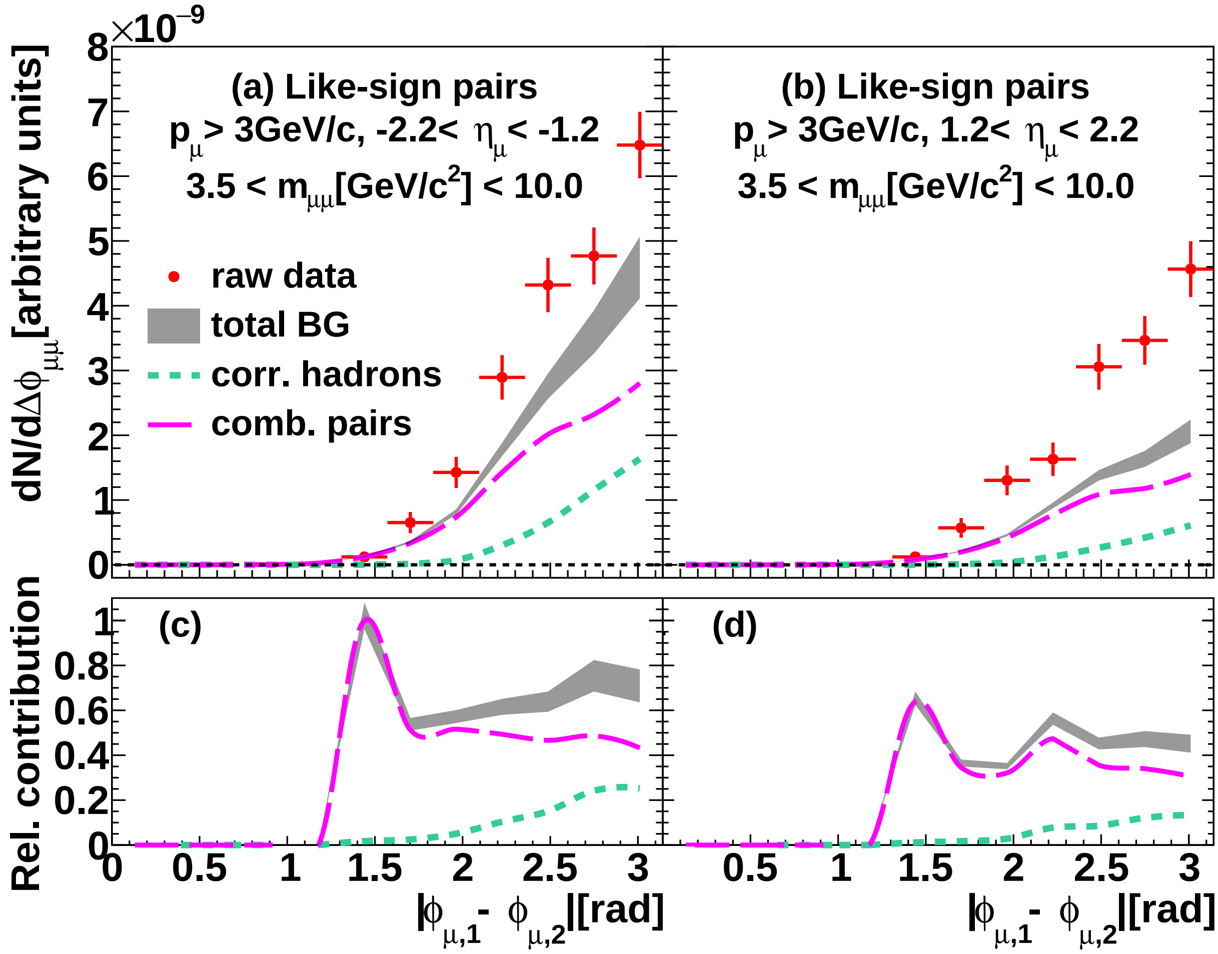

Figure 21: Background components as a function of $\Delta\phi$.

The subtracted yield is corrected for efficiency, estimated using POWHEG and PYTHIA $b\bar{b}$ simulations. We also estimate effects from embedding as a function of $\Delta\phi$ (Fig. 23) and $\Delta\phi$ (Fig. 24). For $\Delta\phi$, embedded studies show no $\Delta\phi$ dependent efficiency loss. For p_T we see some $\sim 5\%$ p_T dependent effects, which may arise due to momentum smearing from background hits. We assign 5% systematic uncertainties for background hits.

The effect from background hits are small in both Au-going and p-going sides. To show this, we plot the percentage of single tracks after embedding background hits against the fraction of mis-associated hits in the MuTr or the MuID in Fig. 25. We see a very large fraction (80% tracks for

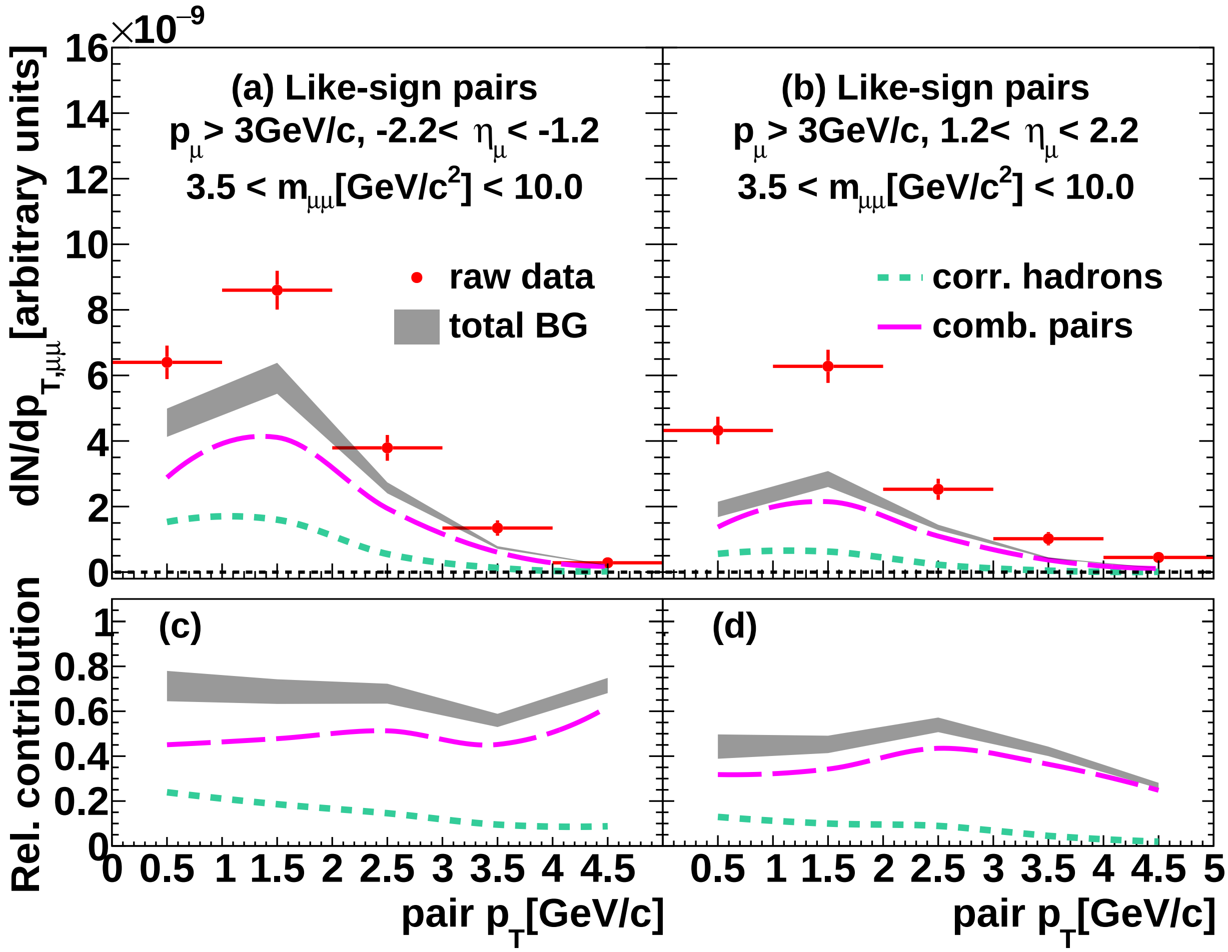

Figure 22: Background components as a function of p_T.

the Au-going side and 92% tracks for the p-going side), corresponding to the peak at 0, where there are no mis-associated background MuTr hit. A secondary peak at 0.06 corresponds to cases where there is 1 mis-associated background hit, (out of 15+ total MuTr hits), and is extremely unlikely to significantly affect the momentum determination. Cases where there are more than 2 mis-associated hits are rare (< 5% for Au-going side and < 2% for the p-going side). The background contamination is even smaller for the MuID trackets. This indicates that the templates generated by the simulations, fast or default, not significantly affected by background hits and should well be covered by the assigned systematic uncertainties.

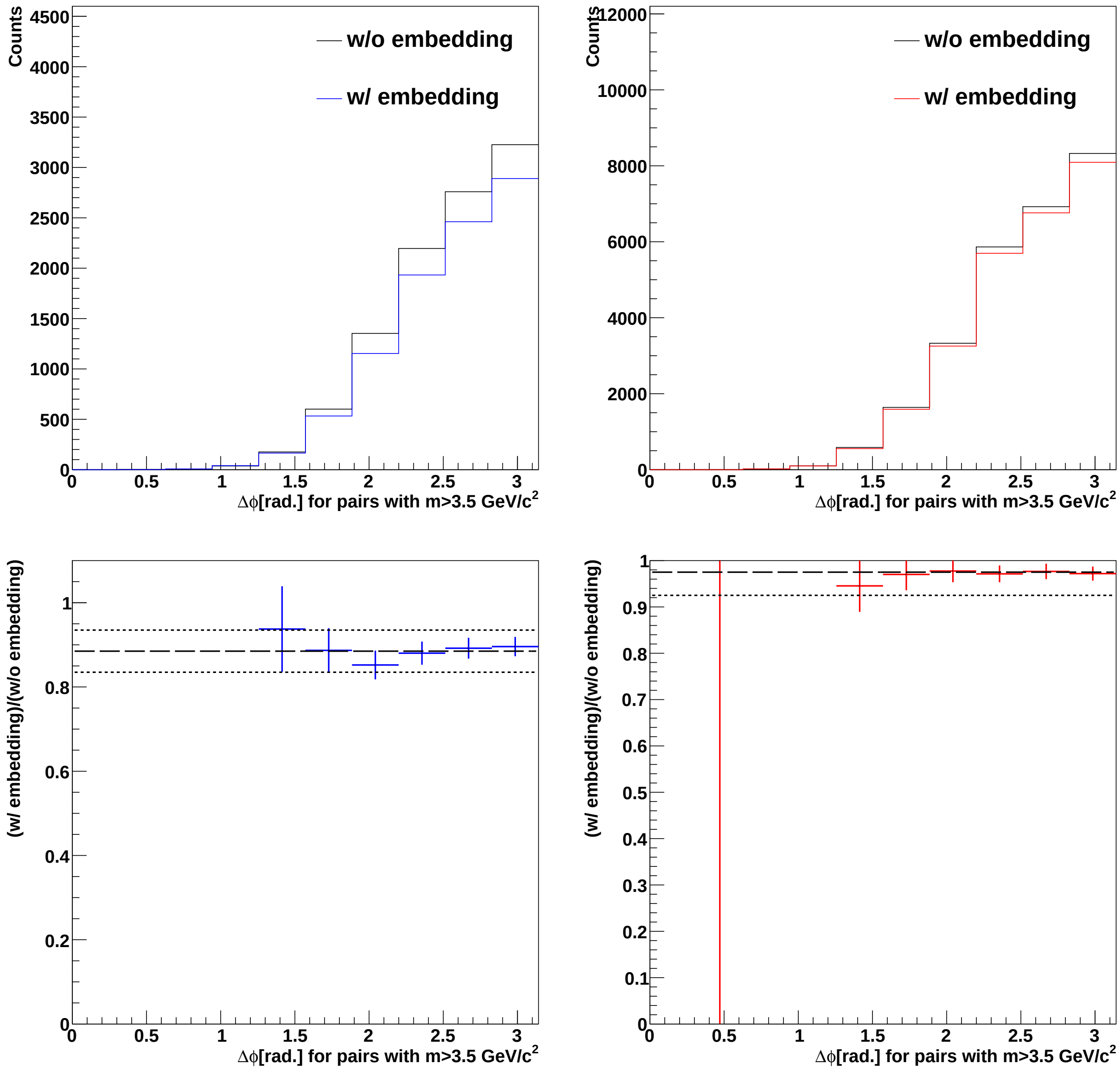

Figure 23: Comparison between embedded and non-embedded simulation as a function of $\Delta\phi$.

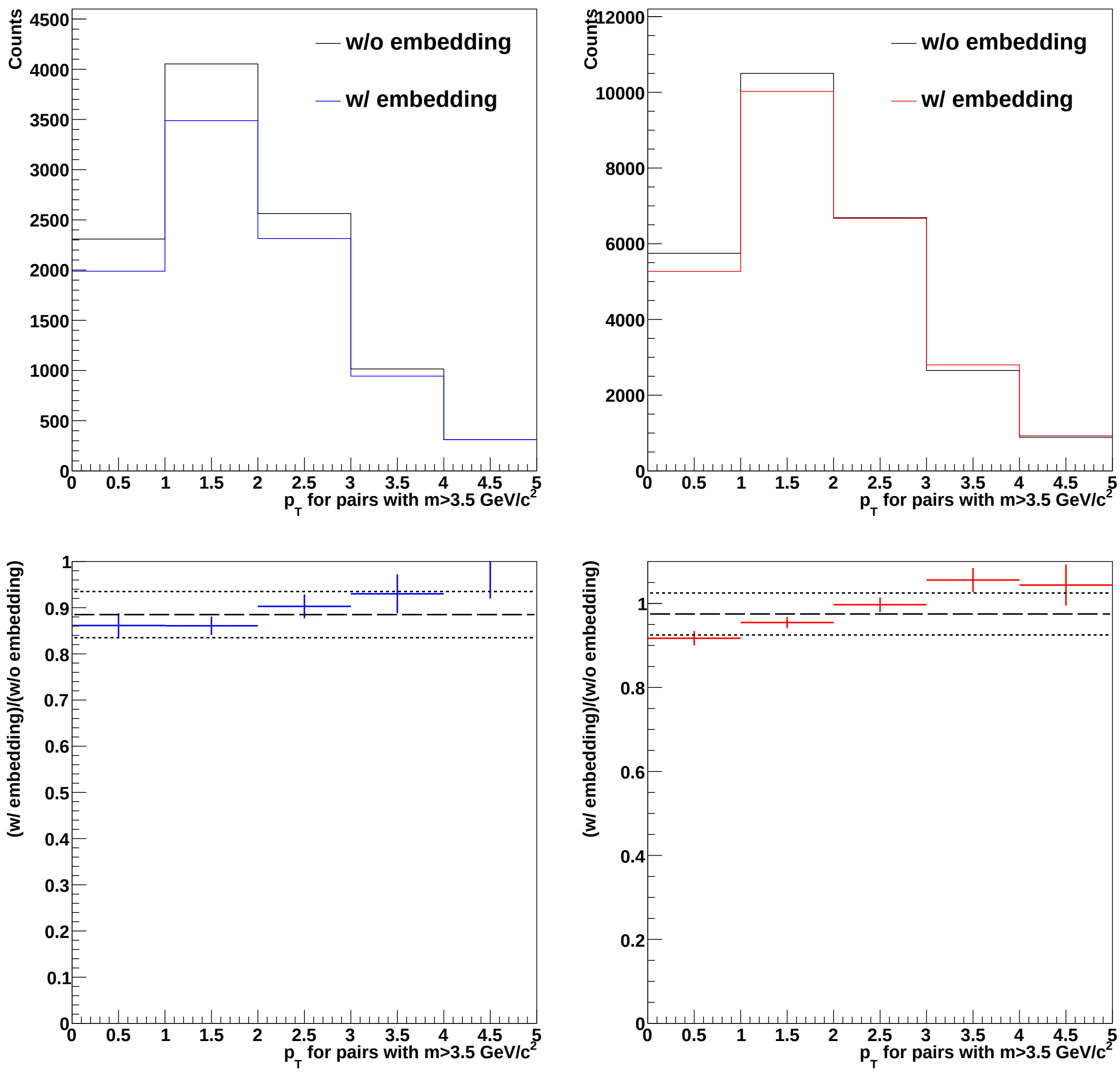

Figure 24: Comparison between embedded and non-embedded simulation as a function of p_T.

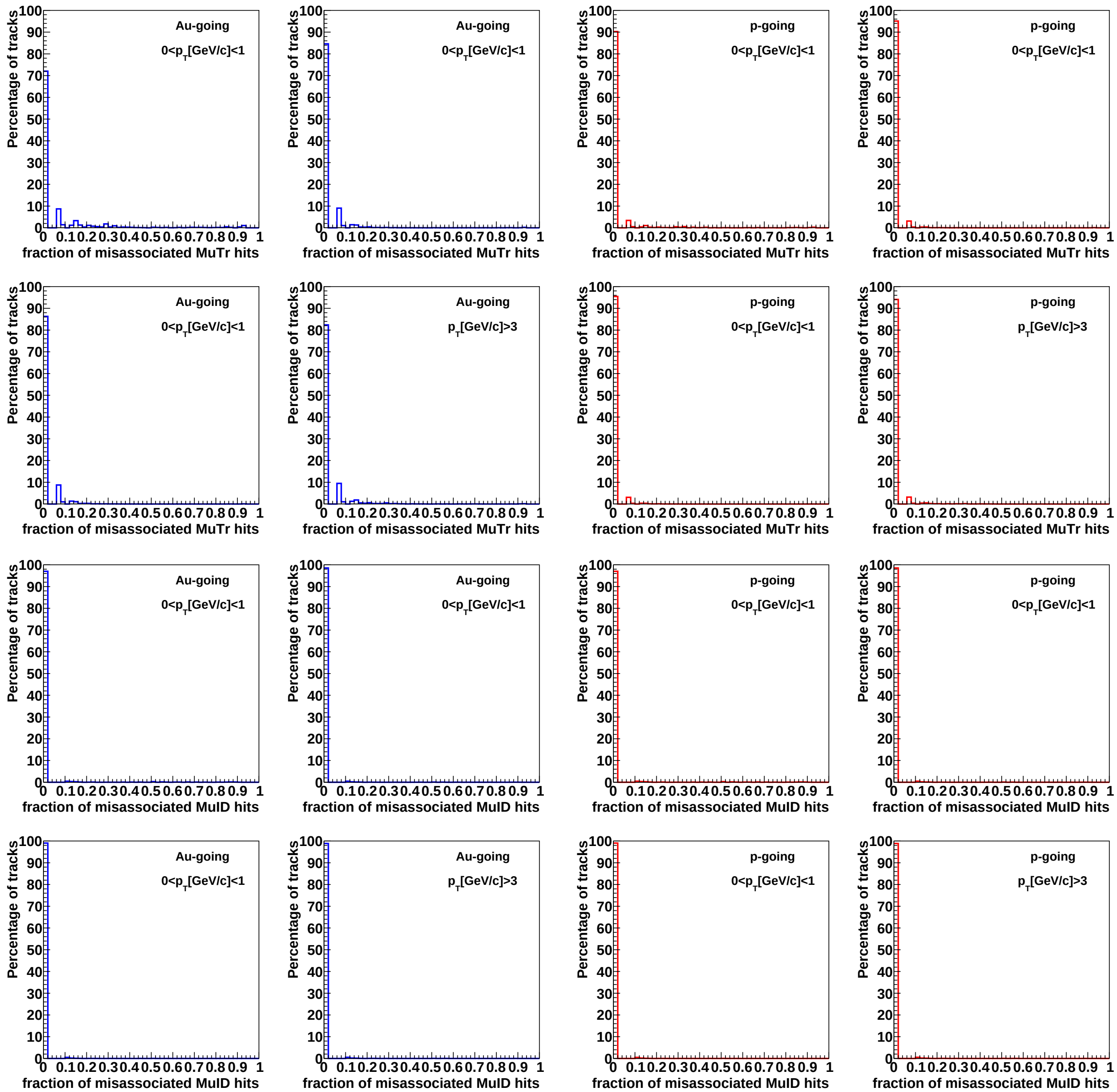

Figure 25: Percentage of tracks against mis-associated MuTr (upper panels) MuID (lower panels) hits for the Au-going (left panels) and the p-going (right panels) sides.

5.6 Systematic uncertainties

All the systematic uncertainties in p+p analysis apply to p+Au analysis. A summary of all systematic uncertainties for the $b\bar{b}$ yields as a function of $\Delta\phi$ and p_T can be found in Fig. 32 and 33.

We describe the uncertainties in the p+p analysis briefly here:

5.6.1 Input hadron spectra (p+p)

This is a dominant source of uncertainty, estimated by taking the BRAHMS hadron spectra at very forward rapidity ($y = 2.95$) and PHENIX mid-rapidity results.

5.6.2 Fitting range

The fitting range is varied from $1.0 - 10.0$ GeV/c^2 to $2.0 - 10.0$ GeV/c^2.

5.6.3 Charm p+p

Uncertainties in the charm cross-section as well as p_T spectra, estimated from difference between PYTHIA and POWHEG.

5.6.4 Fit uncertainties

Normalization of combinatorial and hadronic background has uncertainties due to statistical uncertainties in fit and should be propagated to the $b\bar{b}$ yields.

5.6.5 FastMC

FastMC description of ϕ has an associated uncertainty due to approximations taken in the FastMC formalism.

5.6.6 Model dependent acceptance and efficiency

Estimated using PYTHIA and POWHEG.

5.6.7 MuTr, MuID, trig efficiency

Same uncertainties assigned to p+Au analysis.

In addition, we have five additional sources of uncertainty for p+Au.

5.6.8 Background hits

As shown in the previous section, background hits causes additional efficiency losses. We assign 5% uncertainty.

5.6.9 Input hadron spectra (R_{pA})

The uncertainty in the input hadron spectra can factorized divided into three components, 1. the uncertainty in the p+p input hadron spectra; 2. the uncertainty in measured R_{pA}; 3. the uncertainty in extrapolation of R_{pA} to unmeasured region.

The uncertainty in measured R_{pA} is estimated by constructing fits to extrema: Fig 26. The uncertainty in the hadron spectra is estimated by fitting with variations of hadron spectra within the band, and then to the obtained pair yield from bottom. We assume half of the uncertainty gives a variation such that all points are shifted up and down (upper panel of Fig 26), while the other half gives a variation in the slope (lower panel of Fig 26). These two variations are added in quadrature and assigned as the uncertainty.

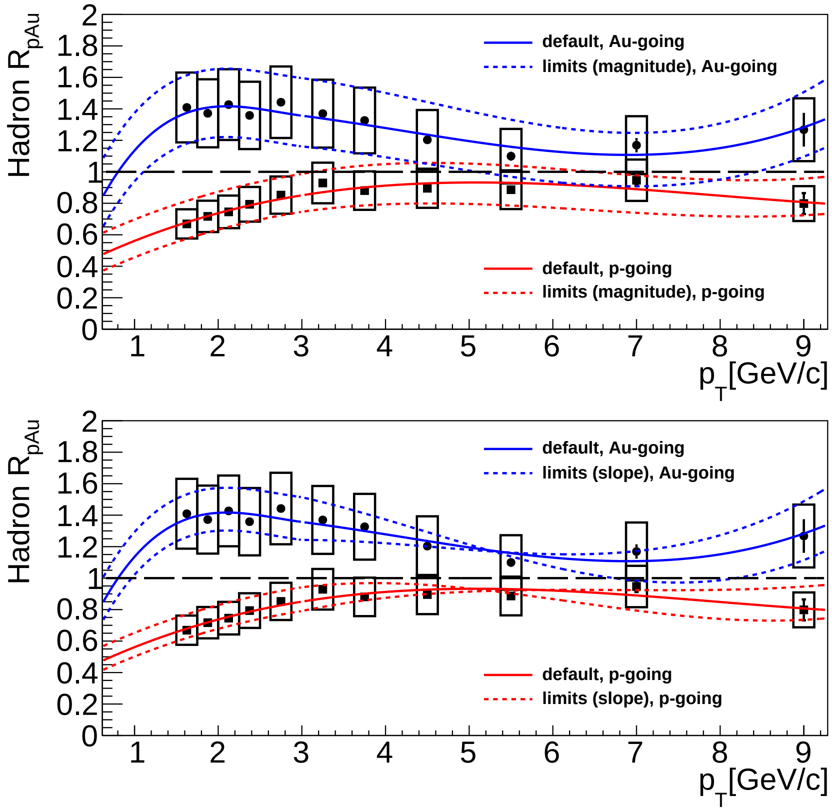

Figure 26: Uncertainty band for hadron R_{pA}.

5.6.10 Input hadron spectra (extrapolation)

The low p_T extrapolation cannot affect the $b\bar{b}$ yield directly; since in the high mass region $m > 3.5$ GeV, the minimum p_T is around 1.8 GeV. However, the extrapolation can affect the $b\bar{b}$ yield indirectly; a smaller yield in the low mass region increase the normalization of the combinatorial background in the fitting procedure, thus producing more combinatorial background in the high mass region. The soft and hard spectra as defined in Fig. 14 and shown in Fig. 27. The motivation is the fact that the R_{pA} corresponding to the uncertainty limits gives a reasonable description of the combinatorial background, thus indirectly implying that the input hadron spectra in simulations match the data. This uncertainty gives rise to 4.0(1.5)% uncertainty in the normalization of combinatorial pairs. The corresponding fitting results are shown in Figs. 29 and 30. The total uncertainty band combining the low p_T spectra and the high p_T uncertainties are shown in Fig. 28. This is slightly expanded as a conservative approach for preliminary request.

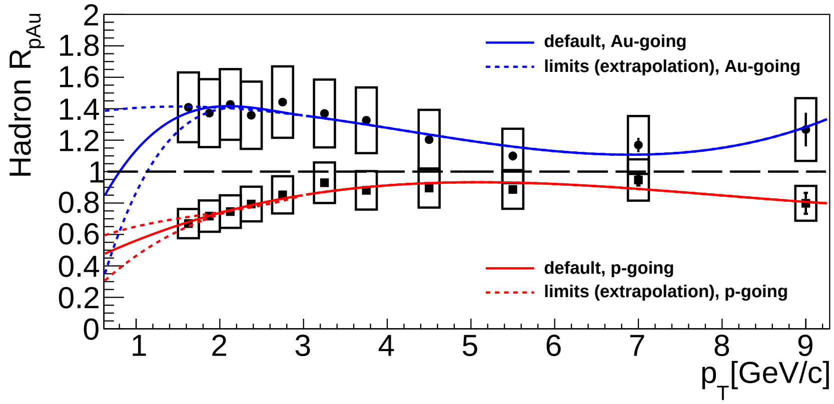

Figure 27: Uncertainty band for hadron R_{pA} related to low p_T extrapolation.

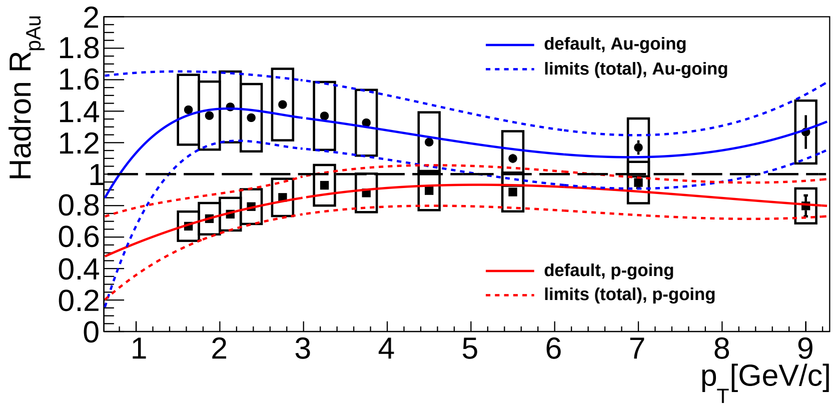

Figure 28: Total uncertainty band for hadron R_{pA}.

5.6.11 Input charm spectra

The uncertainty in the input charm spectra can factorized divided into two components, one is the uncertainty in the p+p charm hadron spectra, the other is the uncertainty in R_{pA}. The former is already documented in AN1306, the latter is estimated by constructing a by fitting with variations within the uncertainty band, as shown in Fig 31. The uncertainty in the charm spectra is is estimated by the maximum variation of charm spectra from the four fits shown.

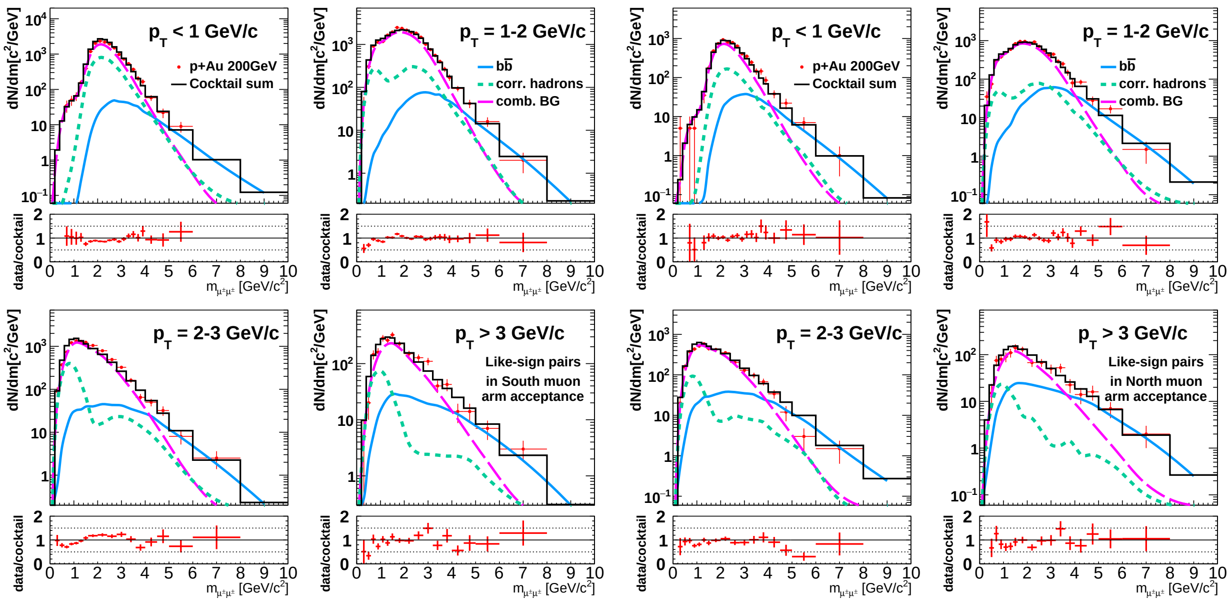

Figure 29: Fitting results using soft spectra.

5.6.12 Normalization of correlated hadronic background

We assign 16% uncertainty to the normalization of correlated hadronic background (see Sec. 5.2). The normalization is varied and the fitted to obtain the normalization of the combinatorial background. The resulting uncertainties are propagated to the $b\bar{b}$ yields.

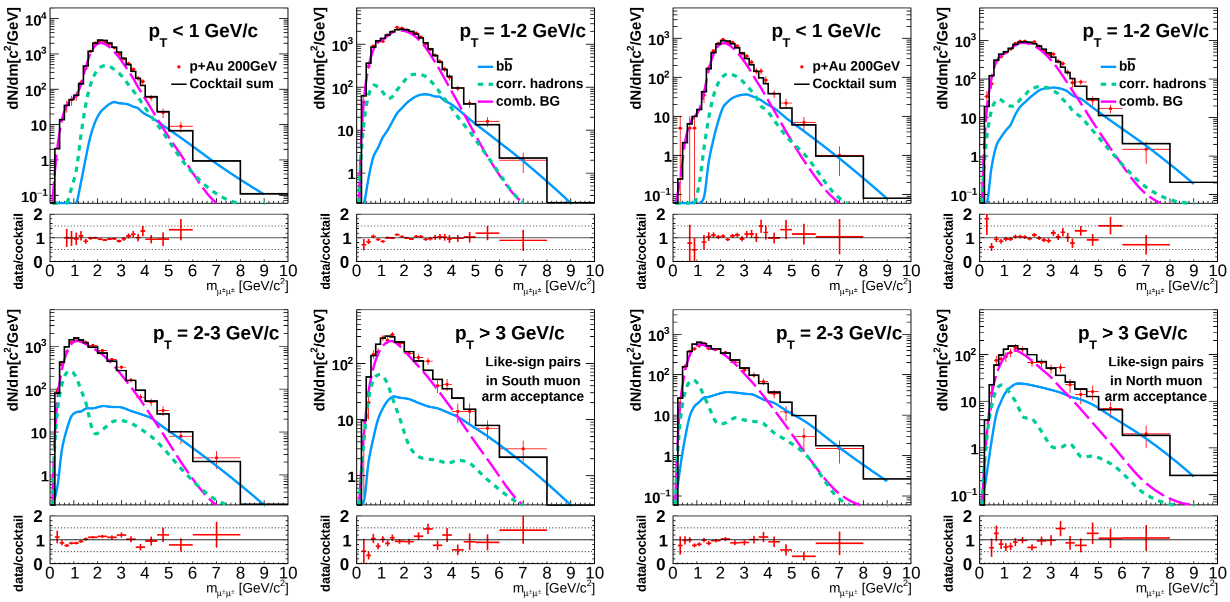

Figure 30: Fitting results using hard spectra.

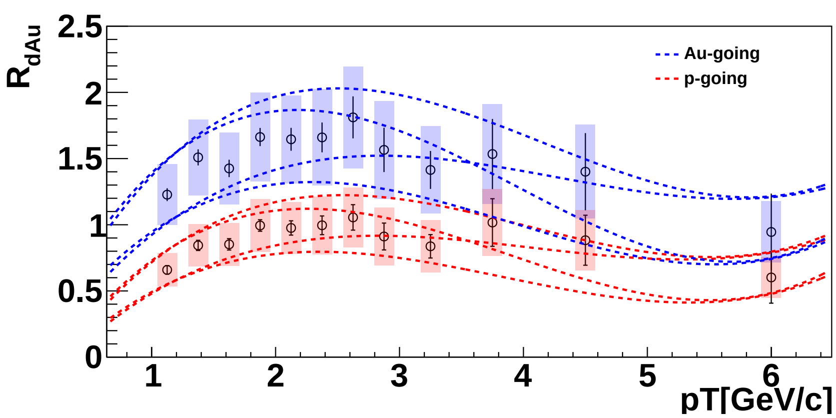

Figure 31: Uncertainty band for charm R_{pA}.

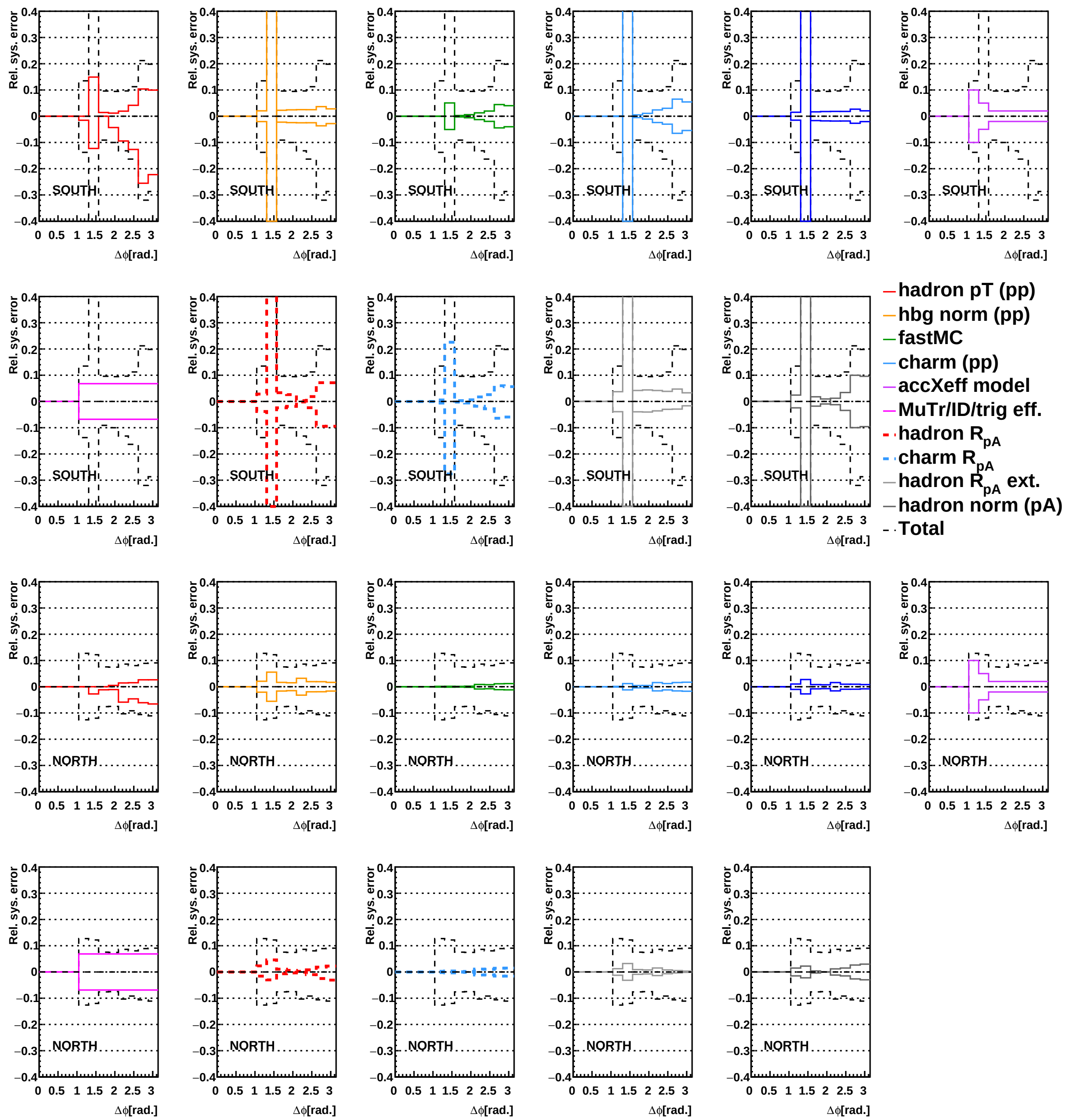

Figure 32: Summary of all systematic uncertainties as a function of $\Delta\phi$.

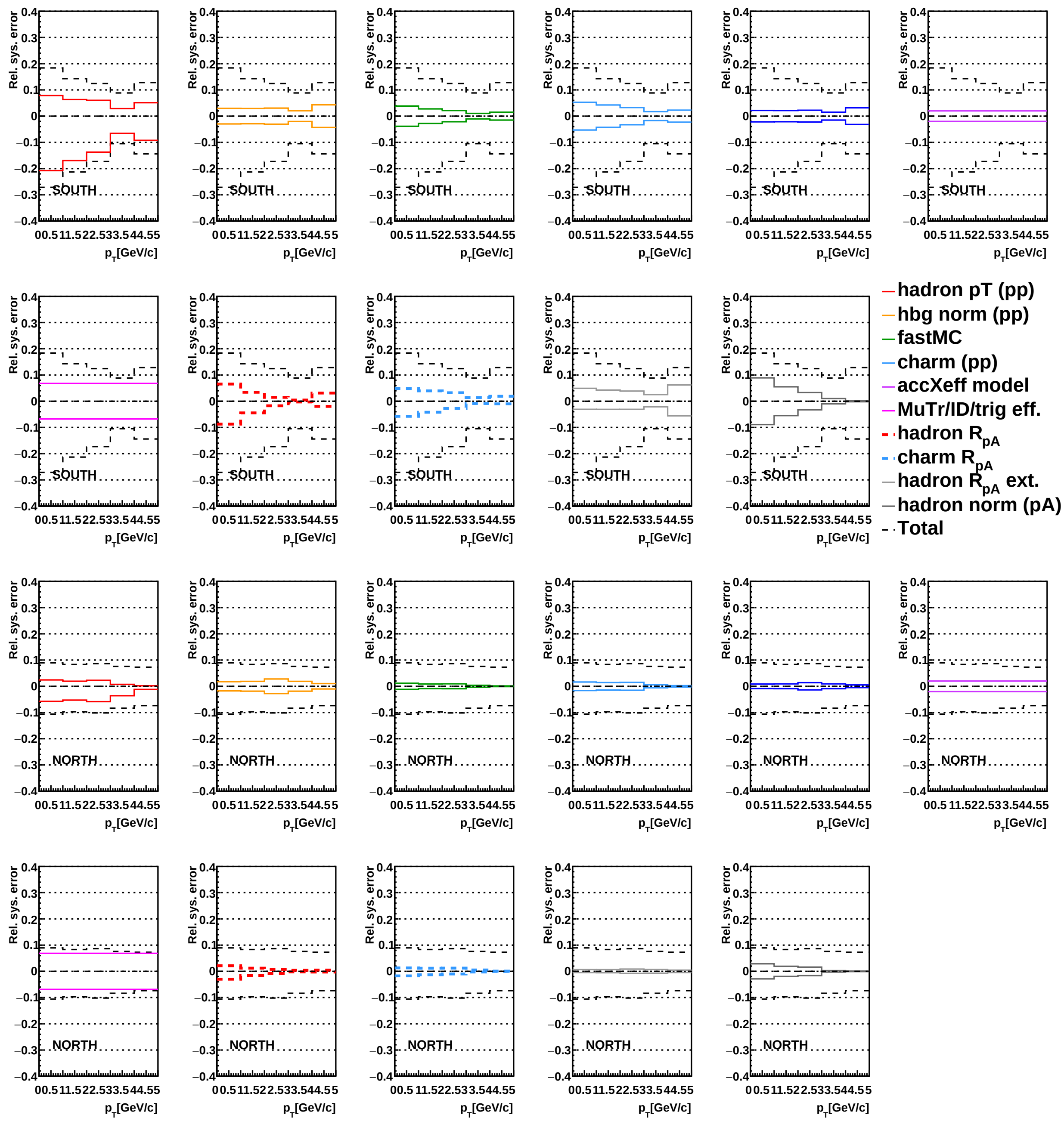

Figure 33: Summary of all systematic uncertainties as a function of p_T.

5.7 Results

Fig. 34 shows the corrected yields as a function of $\Delta\phi$ and p_T, compared to N_{coll}-scaled p+p. Fig. 37 shows the ratio to N_{coll}-scaled p+p. Note that in the calculation of the uncertainties for the ratio, common uncertainties like input hadron spectra (p+p) and charm spectra(p+p) may cancel (partially). Therefore, for the i^{th} source of systematic uncertainties that are common to p+p and p+Au, $\Delta N_{p+p,i}$ and $\Delta N_{p+Au,i}$ we estimate the corresponding systematic uncertainty for R_{p+Au} using the following relation:

$$(\Delta R_{p+Au})_i = \frac{(N_{p+Au} + \Delta N_{p+Au,i})}{N_{coll} \times (N_{p+p} + \Delta N_{p+p,i})} - \frac{(N_{p+Au})}{N_{coll} \times (N_{p+p})} \tag{2}$$

The p+p p+Au correlated and uncorrelated systematic uncertainties are then summed in quadrature.

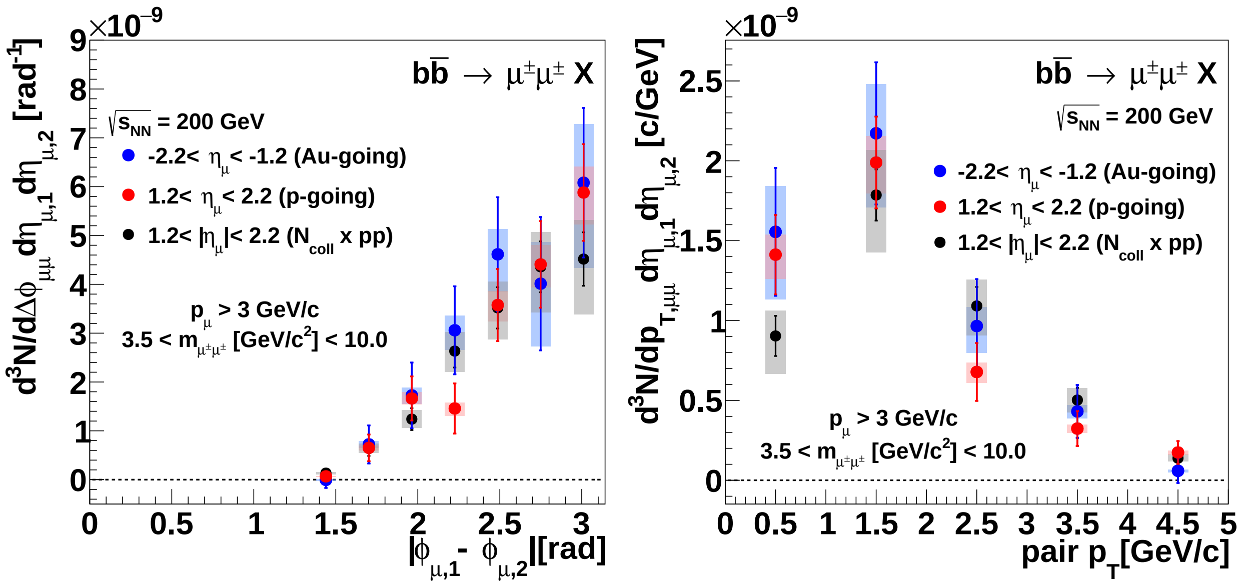

Figure 34: Corrected $b\bar{b}$ yields as a function of $\Delta\phi$ and p_T.

5.7.1 Results

We also compare to the result from EPPS16. See Fig. 36.

As a cross-check, we determine the R_{pA} for the soft, default and hard spectra, see Fig. 37. This does not lead to significant uncertainties and does not give a slope change.

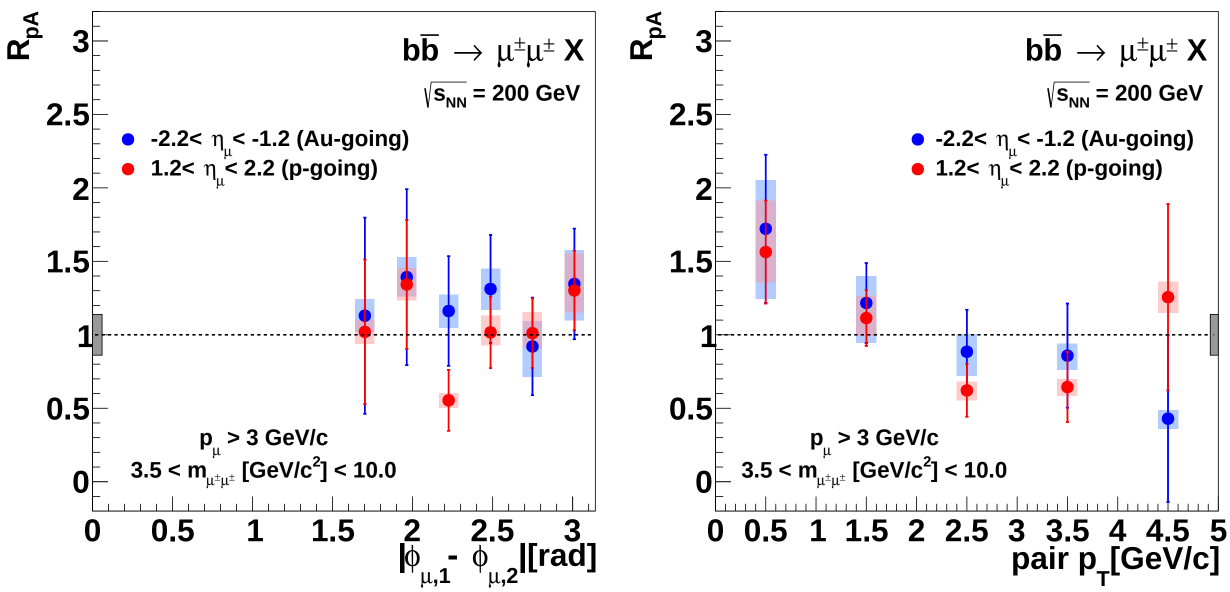

Figure 35: Ratio to N_{coll}-scaled $p+p$ as a function of $\Delta\phi$ and p_T.

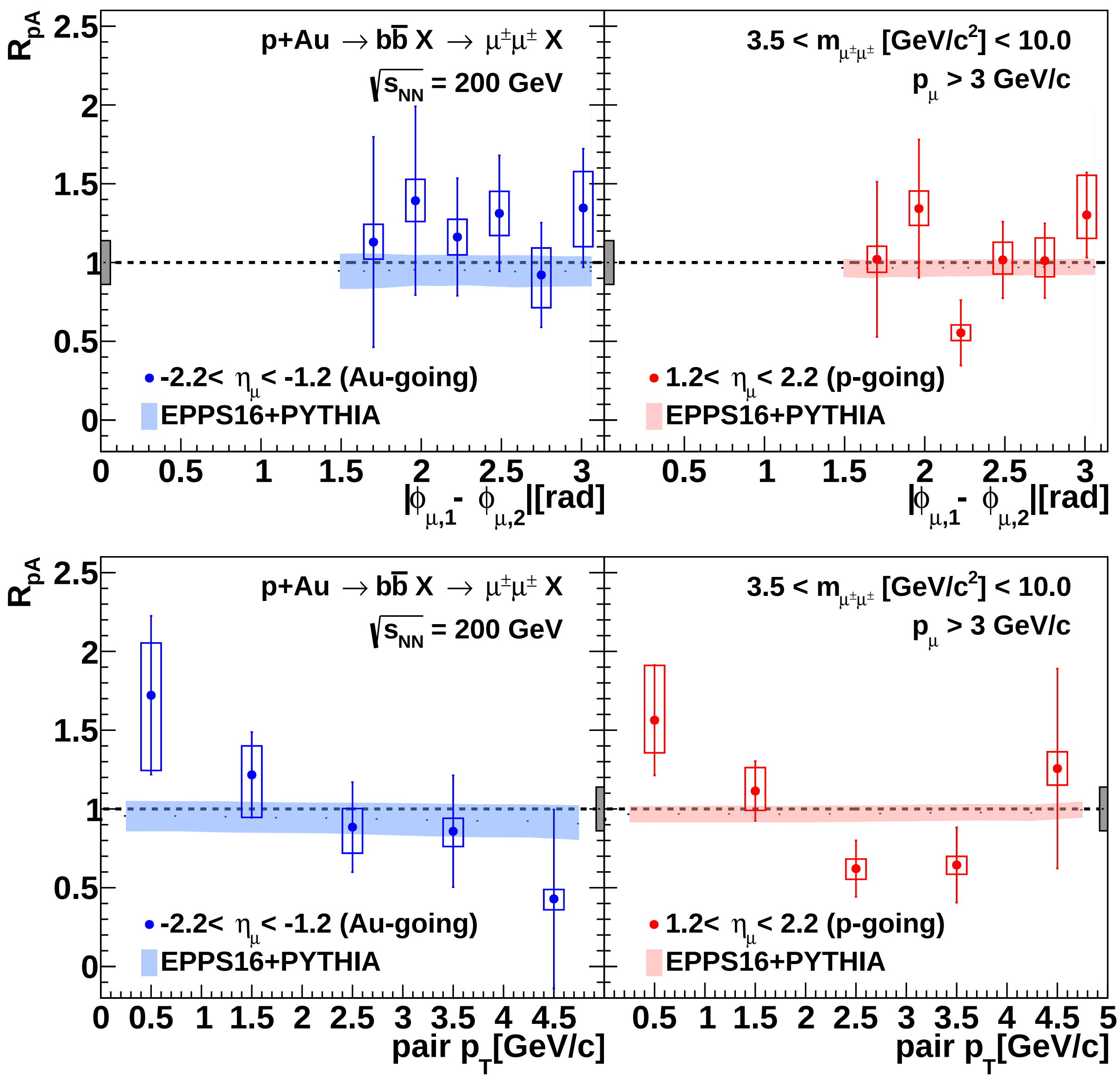

Figure 36: Ratio to N_{coll}-scaled $p+p$ as a function of $\Delta\phi$ and p_T.

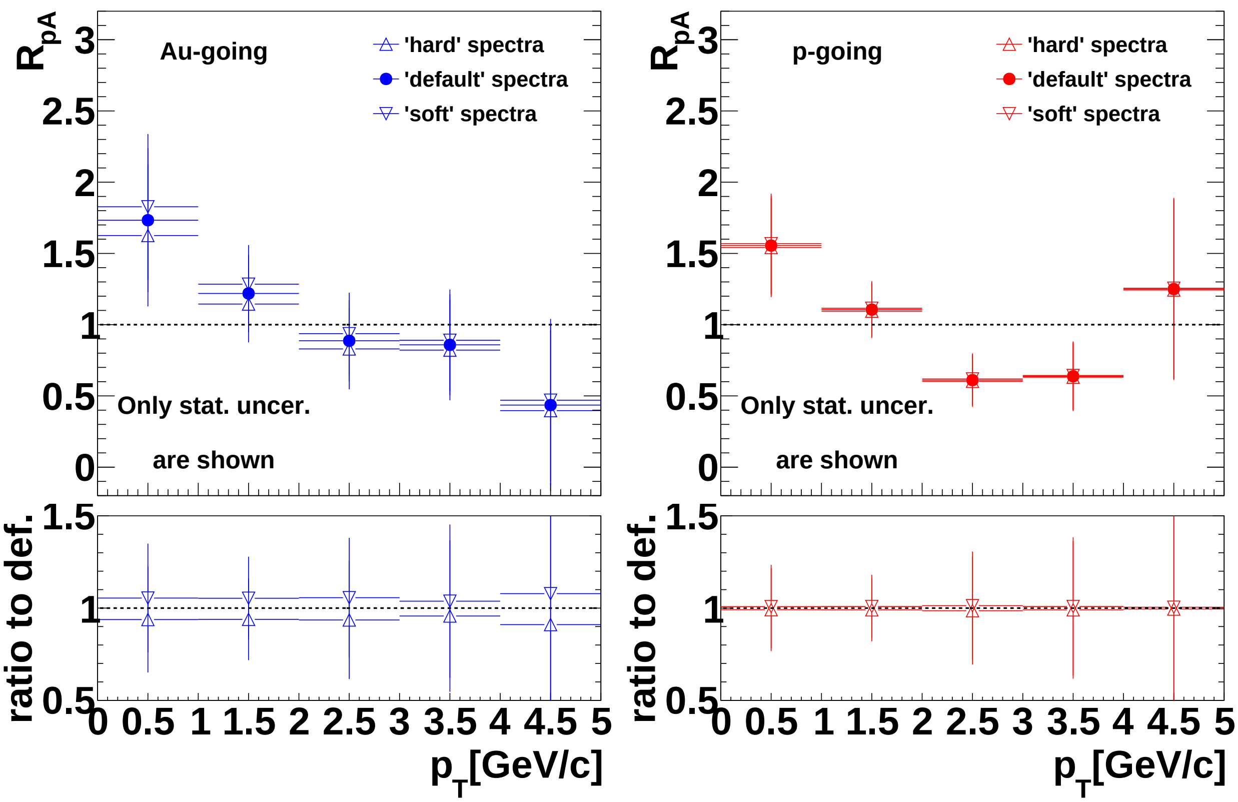

Figure 37: Ratio to N_{coll}-scaled p+p as a function of p_T to the South and North arms.

6 Unlike-sign analysis

We focus on the extraction of Drell-Yan cross-sections using high mass $(4.8-8.2)$ GeV/c^2 unlike-sign pairs.

6.1 Modification and normalization backgrounds

6.1.1 Mixed event background

The absolute normalization for the mixed event background has been obtained via fitting in mass-p_T-z slices using the like-sign pairs. The unlike-sign mixed event background is related to the like-sign mixed event background as according to Eq. 1 and Fig. 3. Thus, the mixed event background normalization is constrained by the like-sign pairs and can be readily subtracted.

6.1.2 Correlated hadronic background

As is identical to the like-sign analysis, the hadronic background is normalized using the normalization in p+p collisions scaled with the measured hadron R_{p+Au} according to Fig. 4 and muons from $c\bar{c}$ R_{d+Au} according to Fig. 8. The systematic uncertainties for the unlike-sign component is determined, again identical to the like-sign analysis, as documented in Sec. 5.6.9 and 5.6.10. For the mass region of interest $(4.8-8.2$ GeV/$c^2)$, the expected background is non-dominant and only contributes to 5(1)% of the inclusive pairs for the Au-(p-)going side. Thus, the actual modification of the hadronic backgrounds do not give rise to significant variations in the extracted Drell-Yan yields, but can give rise to variations indirectly through contributions from $b\bar{b}$, which are anti-correlated to the hadronic contributions via fitting to the like-sign spectra.

6.1.3 $c\bar{c}$

As in the like-sign analysis, the charm contribution is first normalized using the normalization obtained in p+p collisions, and then scaled with the measured R_{d+Au} as a function of the muon p_T, as shown in Fig. 8. Thus, for the unlike-sign $c\bar{c}$ pairs, the weighting factor for a pair of muons with transverse momentum $p_{T,1}$, $p_{T,2}$ respectively is $R_{d+Au}(p_{T,1}) \times R_{d+Au}(p_{T,2})$. The estimation of systematic uncertainties follow the like-sign analysis, as detailed in Sec. 5.6.11; i.e., we first shift all data points by one sigma up/down; and then we also vary the slope by shifting data points at the boundaries up/down by 1 sigma of systematic uncertainty, as shown in Fig. 38. The corresponding modifications (compared to the p+p case) of the $\mu^+\mu^-$ pairs from $c\bar{c}$ after applying the weighting factors are shown in Fig. 39.

In the mass region of interest, this leads to an enhancement for the Au-going side and a slight suppression for the p-going side. This would naturally lead to larger systematic uncertainties for the Au-going side compared to the p-going side.

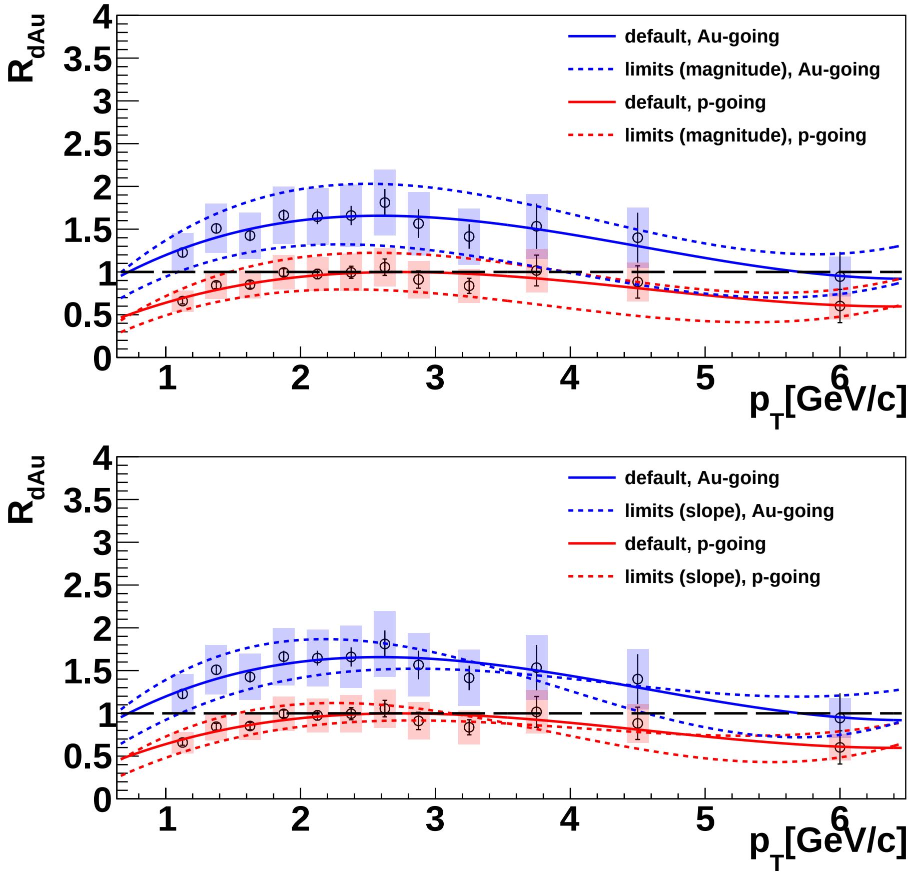

Figure 38: Measured R_{d+Au}, fits and systematic bands.

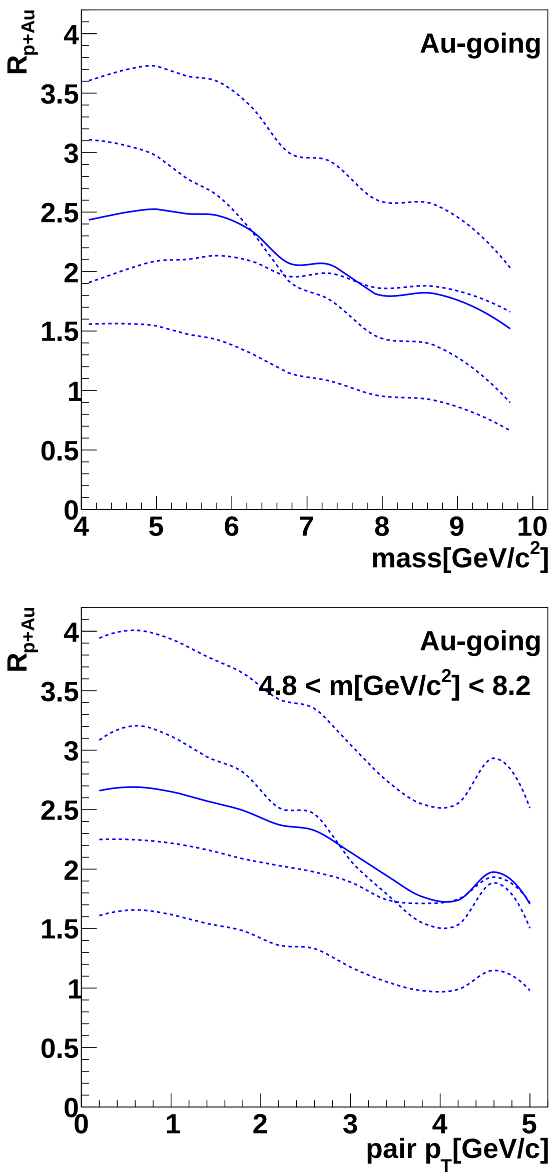

Figure 39: Modifications of the $c\bar{c}$ component, compared to the p+p case, for mass and p_T, for the central value (solid), and the systematic variations (dotted).

6.1.4 $b\bar{b}$

The R_{d+Au} for single muons from inclusive heavy flavor is dominated by contributions from $c\bar{c}$ in the p_T region of interest (approximately $2-4$ GeV/c single (not pair) p_T), hence the data is a good estimate of the modifications for $c\bar{c}$, but not necessarily $b\bar{b}$. **In particular, due to the much higher mass of the b-quark, the pair distributions of $\mu\mu$ are dominated by decay kinematics. i.e. The initial angular and momentum distributions of the b and $\bar{b}$-quarks (or the B and $\bar{B}$ mesons) does not have a significant impact on the resultant $\mu\mu$ pair mass and p_T distributions. This has been documented in detail in AN1156.** Hence we do not expect the $\mu\mu$ pair distributions to be largely modified in the p+Au case as compared to the p+p case.

There is no existing data to directly constrain the input distributions for $b\bar{b}$. For p/d+Au collisions at 200 GeV, PHENIX has measured pions and kaons at mid-rapidity, inclusive hadrons at forward and backward rapidities, inclusive heavy flavor leptons at mid-, forward and backward rapidities. In all cases, a broadening of p_T has been observed. The $R_{p/d+Au}$ can be characterized as a suppression at low p_T, followed by an increase to a peak at mid p_T, followed by a decrease to a constant at high p_T. Since the source of such a p_T broadening is unknown and also the mass of B-hadrons are different than D-hadrons, kaons, pions, the exact $R_{p/d+Au}$ cannot be estimated to good accuracy.

However we can assume that *if there is a modification*, then it should have the same features of p_T broadening as mentioned above, i.e. a peak structure at mid-p_T and constant at high p_T. The assigned systematic uncertainties should also constant with the flat R_{p+Au} case, i.e. *the case where there is no modification*; which may be possible since the mass of the B-hadrons is large.

We therefore explore different scenarios of B-hadron modification, more specifically, we vary the peak position, the peak strength and the peak width of the R_{p+Au} of the B-hadrons. After varying the p_T spectra of the B-hadrons, the dimuon mass and p_T distributions are generated using POWHEG. The resultant distributions are then fitted to the like-sign data to obtain a normalization in order to normalize the unlike-sign distributions for background subtraction for Drell-Yan extraction. Note here since the templates are normalized by fitting to the data, p-going and Au-going sides separately, the absolute normalization of the input R_{p+Au} of the B-hadrons is irrelevant, only the shape of the input R_{p+Au} of the B-hadrons is important.

We start with a generic input R_{p+Au} with the p_T broadening features and vary the peak position from 0.6 GeV/c to 3.6 GeV/c, as shown in Fig. 40.

To increase the confidence that these modifications are to first order reasonable guesses, one can compare the resultant dimuon distributions, or more specifically the simulated R_{p+Au} of these distributions, as a function of pair p_T or $\Delta\phi$ to real like-sign data, obtained in the like-sign analysis, as shown in Fig. 41.

One can see that the resultant simulated R_{p+Au} as a function of $\Delta\phi$ is flat and is consistent with data. For pair p_T, a decreasing trend is observed and again agrees with the data. One can quantify the agreement by determing the χ^2 values, as shown in Tab. 3. The agreement is best when the peak position sits at around 2 GeV/c.

Since we want to extract Drell-Yan cross-sections using unlike-sign pairs as a function of mass (mass $= 4.2-15.0\text{GeV}/c^2$) and as a function of p_T (mass $= 4.2-8.2\text{GeV}/c^2$), we need to estimate the $b\bar{b}$ background in the unlike-sign phase space. The simulated modifications are shown in Fig. 42.

In addition to varying the peak position, we also vary the peak strength and the peak width. The

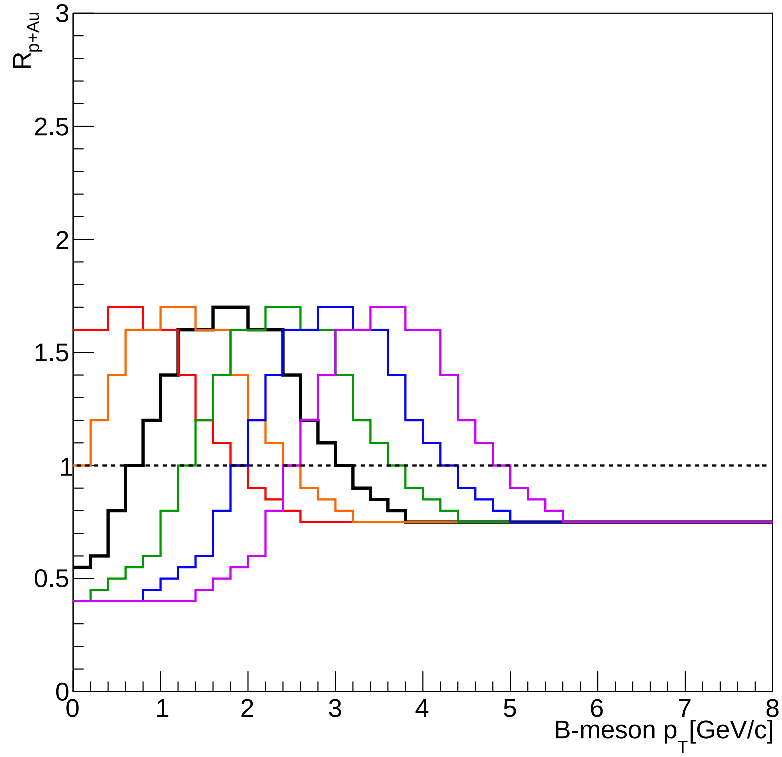

Figure 40: Input R_{p+Au} of the B-hadrons with varying peak positions. Different colored lines correspond to different peak positions: 0.6 (red), 1.2 (orange), 1.8 (black), 2.4 (green), 3.0 (blue), 4.6 magenta (magenta) GeV/c.

variations are shown in Fig. 43.

The extreme cases are chosen such that the maximum variation of the peak strength goes from $R_{p+Au} = 2.3$ at maximum and $R_{p+Au} = 0.75$ at high p_T, more than a factor of 3, which is very unlikely and arguably unphysical as this variation is much larger than the measured R_{d+Au} for single muons from heavy flavor for minimum bias, which is $R_{p+Au} = 1.6$ at maximum and $R_{p+Au} = 1.0$ for high p_T. The other limiting case is a very wide peak width which gives results which is basically flat and is consistent with the p+p case.

The corresponding simulated R_{p+Au} for like-sign muon pairs with mass $= 3.5 - 10.0$ GeV/c^2 are shown in Fig. 44 and 45. We see that the like-sign data may be reasonably reproduced.

In order to assign choose a reasonable central value and assign systematic uncertainties for the possible modifications of the B-hadron modifications, we take into account all aforementioned variations of the B-hadron p_T spectra. All variations for the unlike-sign pairs are shown in Fig. 46, as a function of mass or p_T. We take the average value to be the central value, and the maximum variation to be the systematic uncertainty. This is shown in Fig. 47.

Table 3: Summary of χ^2 values for different peak positions.

Peak position [GeV/c]	0.6	1.2	1.8	2.4	3.0	3.6
Au-going χ^2 (NDF=4)	4.2	3.5	2.8	2.6	2.8	3.5
p-going χ^2 (NDF=4)	7.4	6.4	6.0	6.3	7.2	8.3

6.1.5 Quarkonia

Since we deliberately excluded the mass regions from quarkonia, the modifications of quarkonia will not affect the results of this analysis. Nevertheless, we inserted modifications for quarkonia according to measured values, J/ψ R_{p+Au} from preliminary result, ψ' to J/ψ ratio from PPG188 and Υ R_{d+Au} from PPG142.

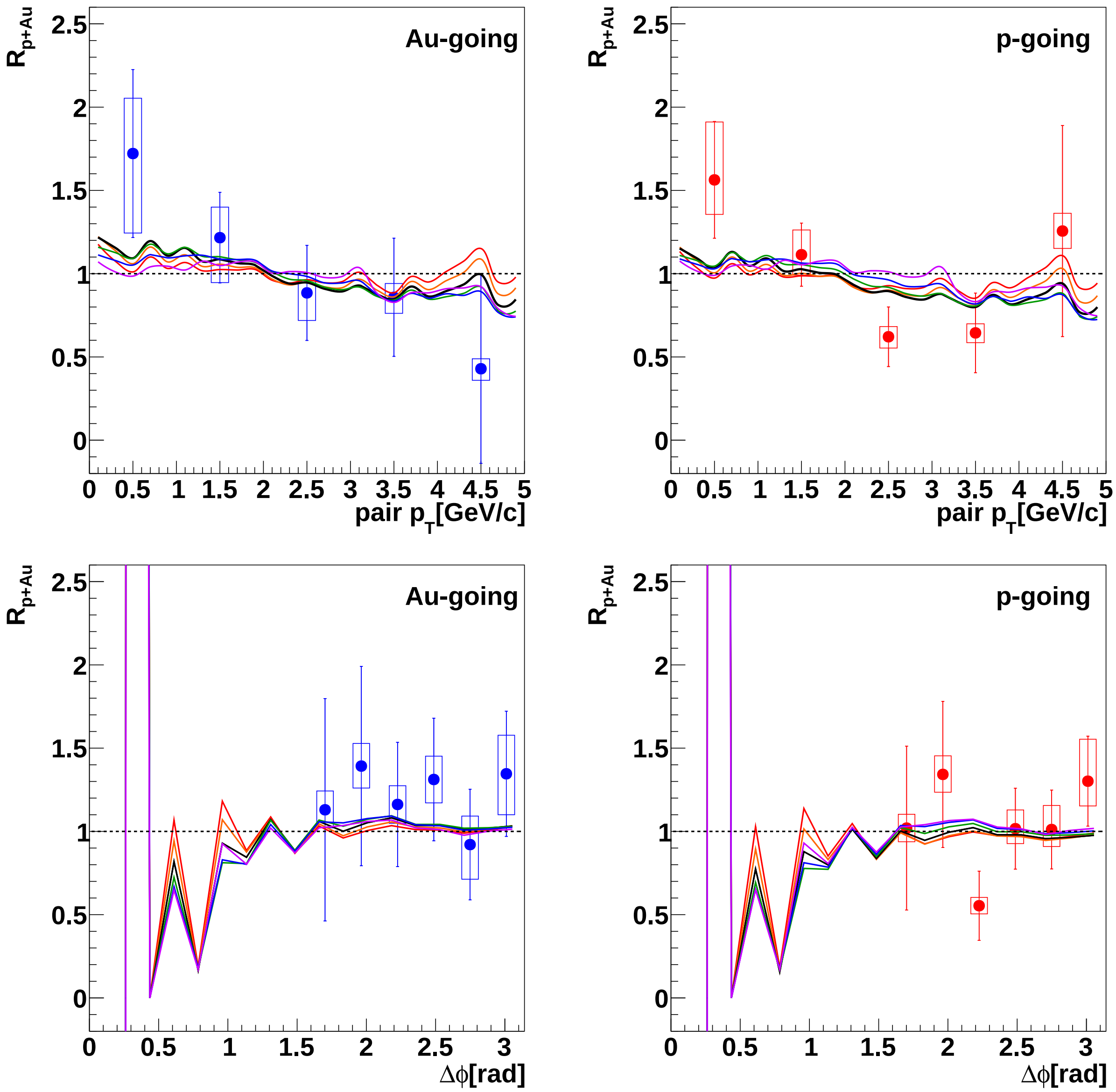

Figure 41: Resultant simulated R_{p+Au} of like-sign muon pairs with mass (3.5-10.0) GeV/c^2 compared to real data. The input R_{p+Au} the B-hadrons have varying peak positions. Different colored lines correspond to different peak positions: 0.6 (red), 1.2 (orange), 1.8 (black), 2.4 (green), 3.0 (blue), 4.6 magenta (magenta) GeV/c.

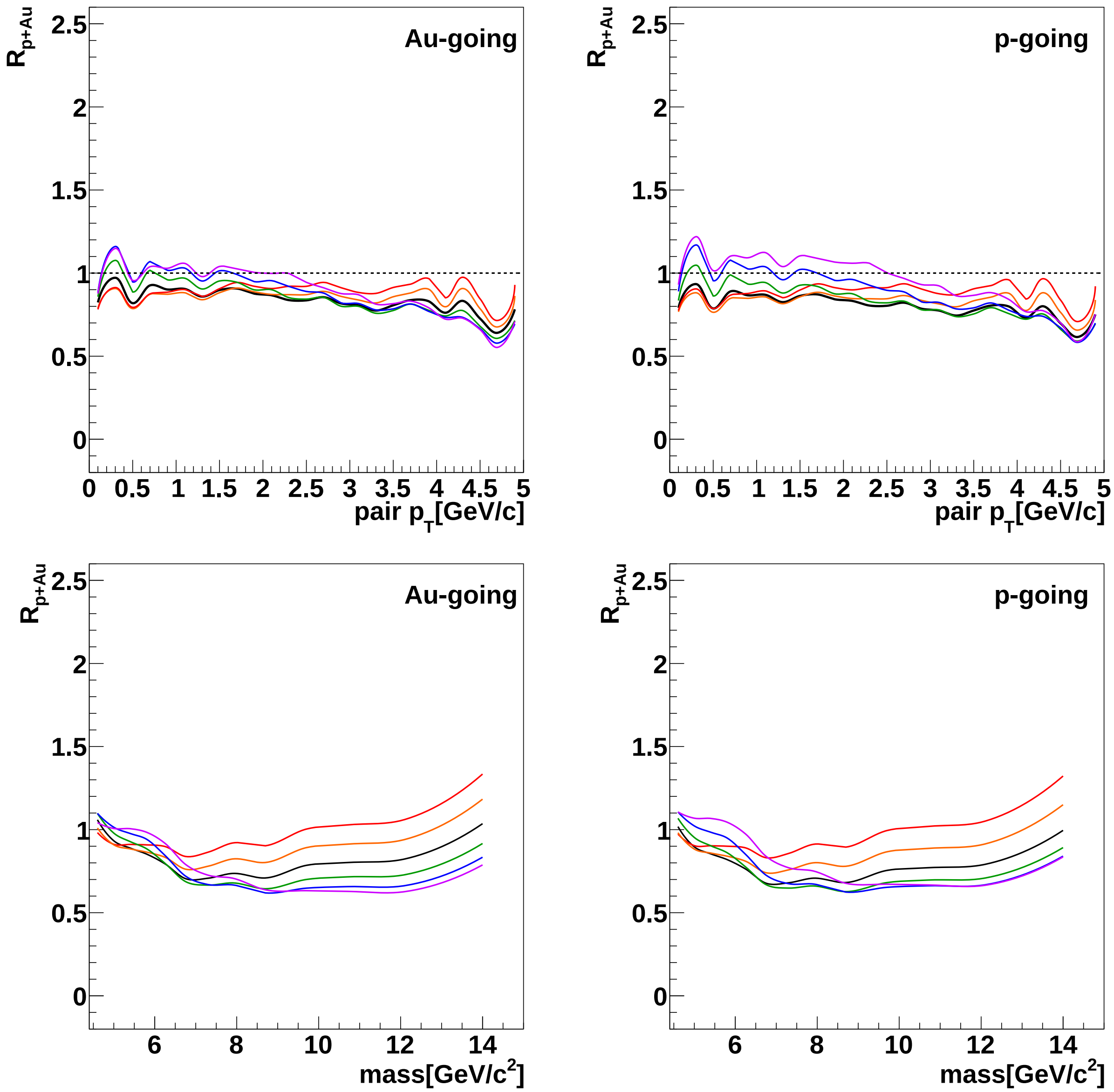

Figure 42: Resultant simulated R_{p+Au} of unlike-sign muon pairs (upper panel: with mass (4.8-8.2) GeV/c^2). The input R_{p+Au} the B-hadrons have varying peak positions. Different colored lines correspond to different peak positions: 0.6 (red), 1.2 (orange), 1.8 (black), 2.4 (green), 3.0 (blue), 4.6 magenta (magenta) GeV/c.

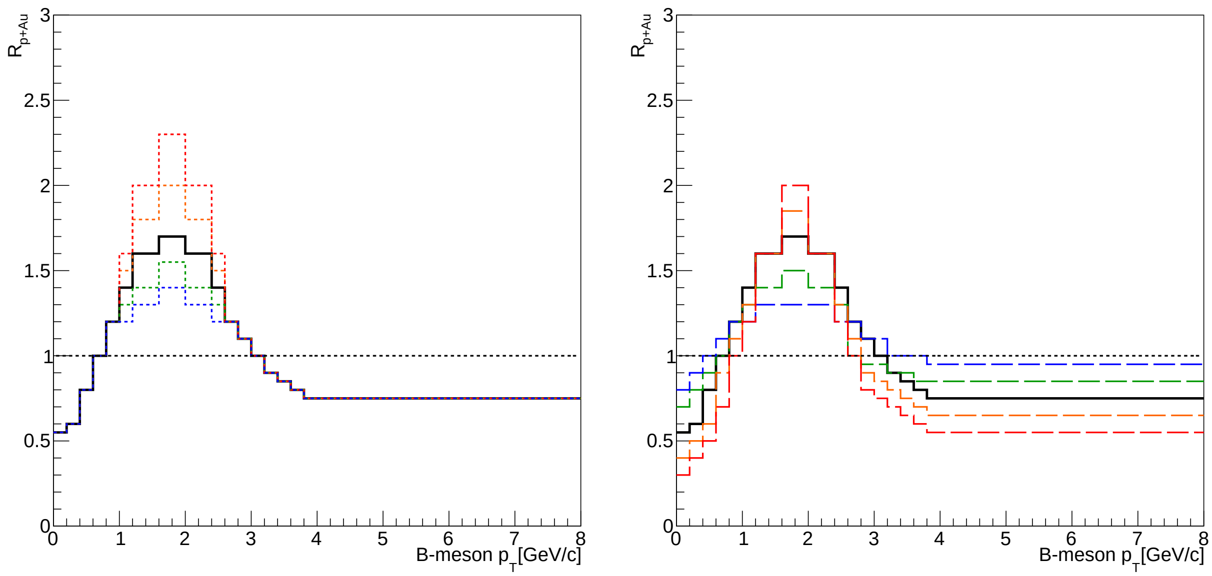

Figure 43: Input R_{p+Au} of the B-hadrons with varying peak strength (left) and peak width (right).

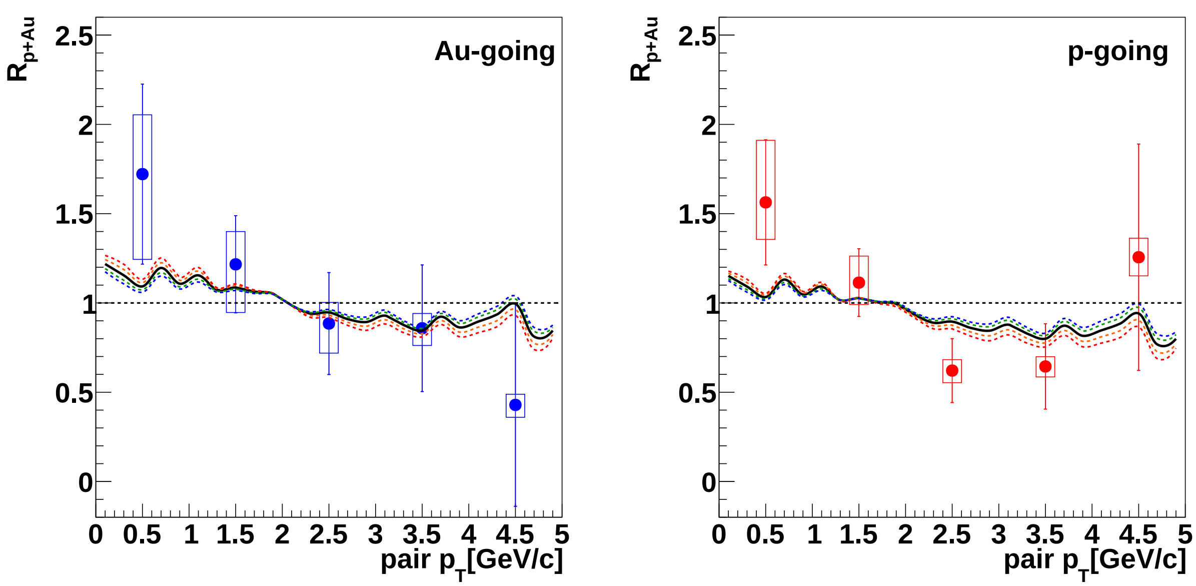

Figure 44: Resultant simulated R_{p+Au} of like-sign muon pairs with mass= $(3.5 - 10.0)$ GeV/c^2 compared to real data. The input R_{p+Au} the B-hadrons have varying peak strengths, with the same color code as Fig. 43.

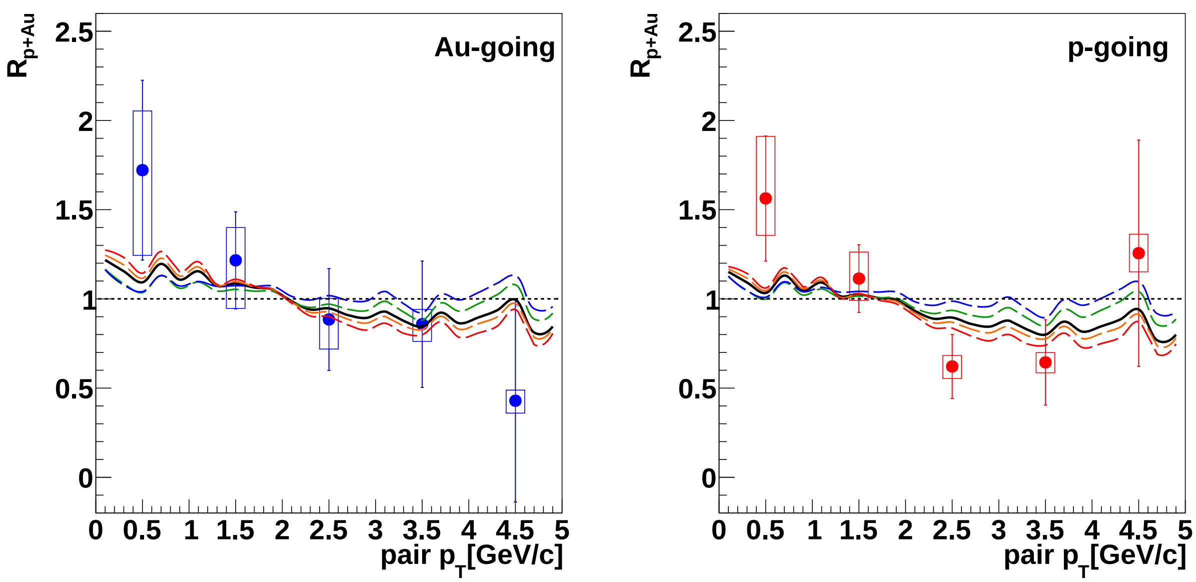

Figure 45: Resultant simulated R_{p+Au} of like-sign muon pairs with mass= $(3.5-10.0)$ GeV/c^2 compared to real data. The input R_{p+Au} the B-hadrons have varying peak widths, with the same color code as Fig. 43.

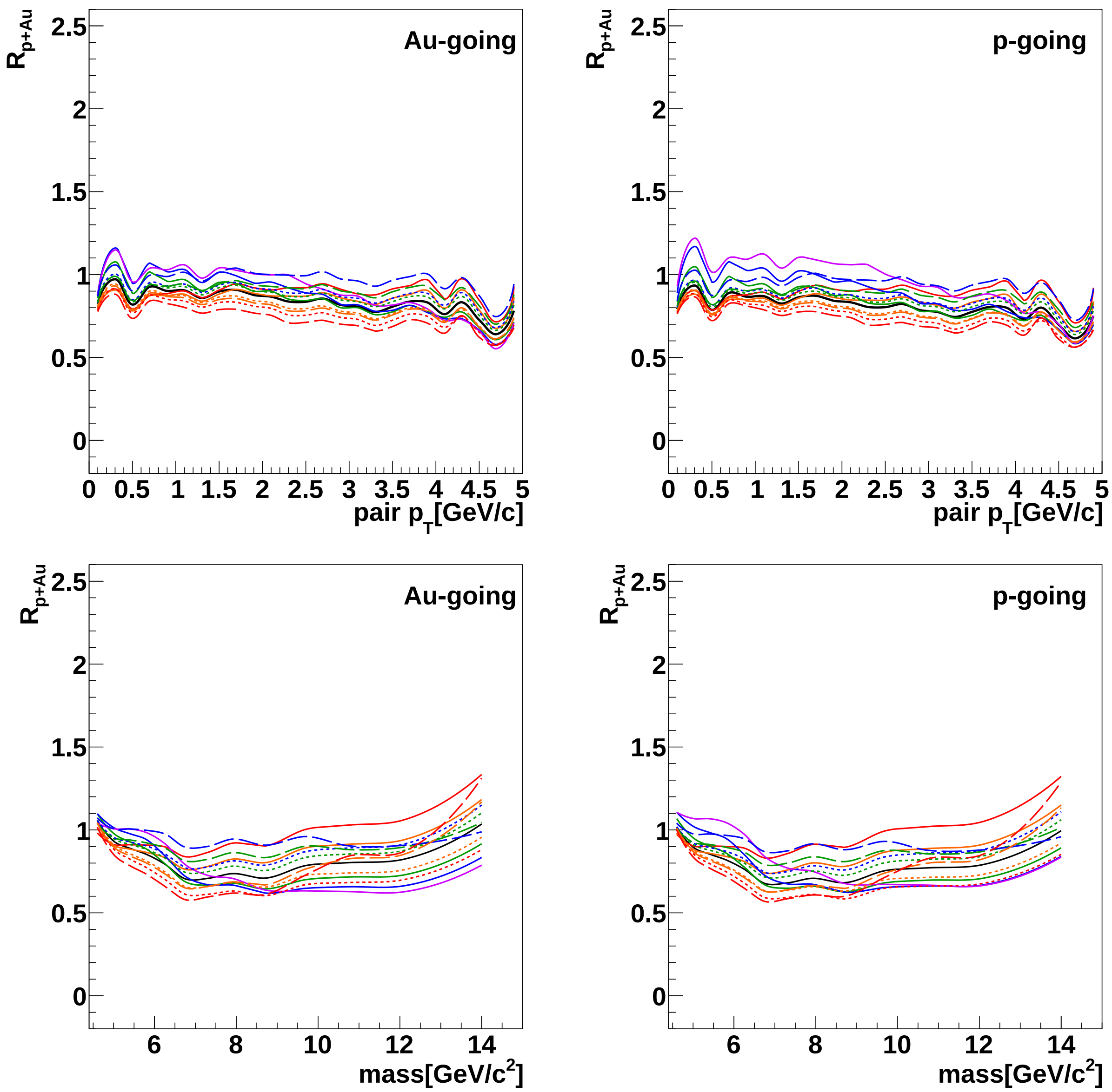

Figure 46: Resultant simulated R_{p+Au} of unlike-sign muon pairs (upper panels: with mass= $(3.5-10.0)$ GeV/c^2). The input R_{p+Au} the B-hadrons have varying peak positions, strengths and widths with consistent color code.

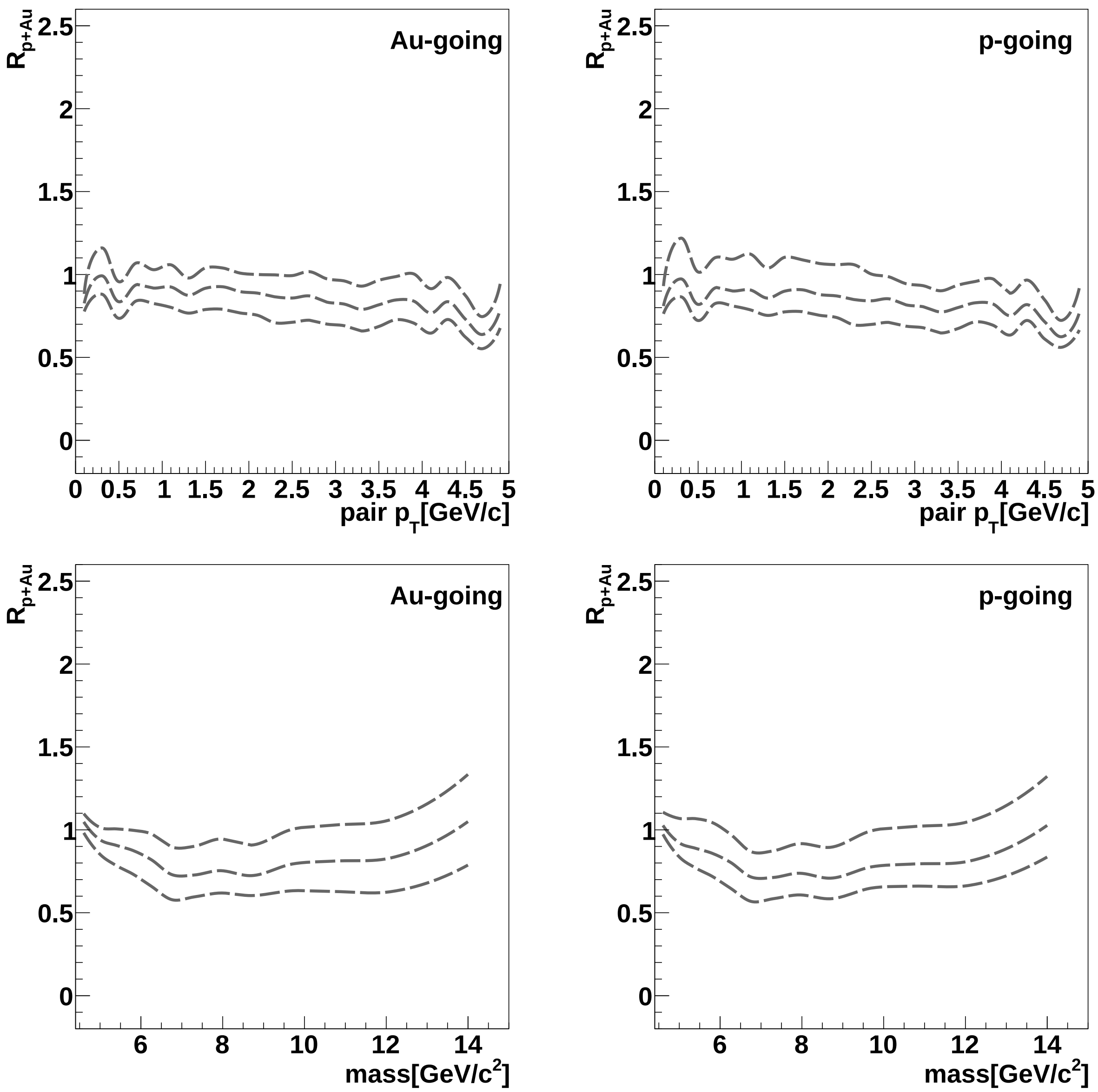

Figure 47: Resultant simulated R_{p+Au} of unlike-sign muon pairs (upper panels: with mass= $(3.5-10.0)$ GeV/c^2). Only the central values and systematic bands are plotted.

6.2 Background subtraction

The modified backgrounds are normalized as detailed in the previous section and subtracted from the inclusive yield as a function of mass or pair p_T, as shown in Fig. 48 and 49 respectively.

$$N_{DY} = N_{inclusive} - N_{b\bar{b}} - N_{c\bar{c}} - N_{corr.hadrons} - N_{comb.bg} - N_{J/\psi} - N_{\psi'} - N_{\Upsilon} \quad (3)$$

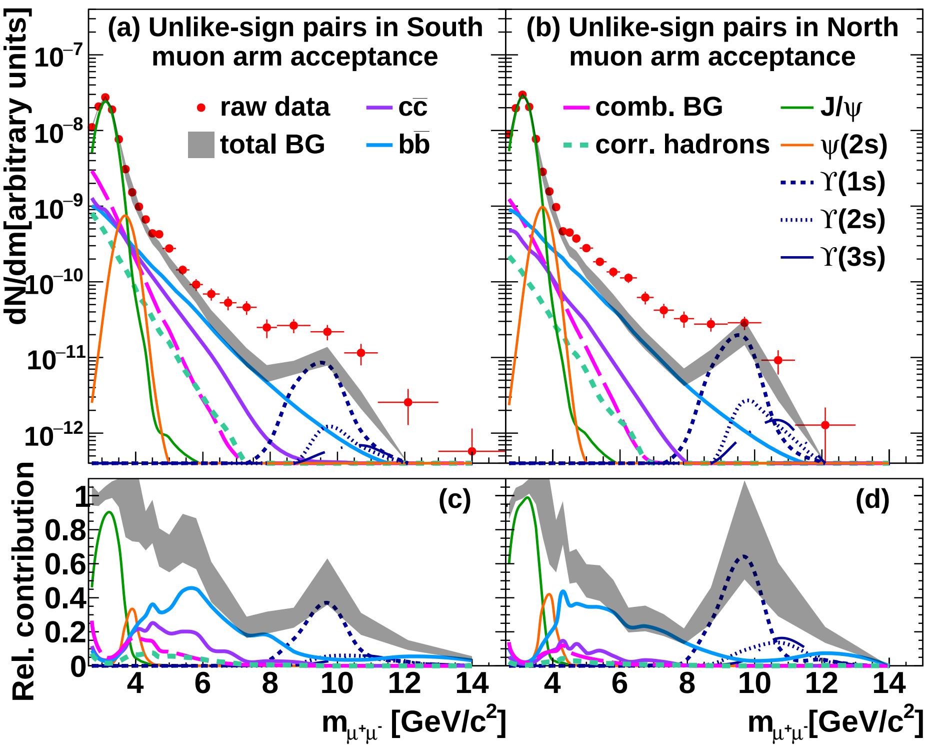

Figure 48: Data and background components for Drell-Yan extraction as a function of mass.

6.3 Acceptance and efficiency

The acceptance and efficiency corrections are determined by PYTHIA simulations, comparing generated pairs with $1.2 < |y_{\mu\mu}| < 2.2$ and reconstructed pairs. The acceptance and efficiency corrections as a function of mass or p_T are shown in Fig. 50. As expected, the acceptance and efficiency is quite flat as a function of p_T because in the high mass region, single tracks have high enough momentum exceeding the threshold of the absorbers and also the dimuon trigger efficiency has saturated.

6.4 Systematic uncertainties

All the systematic uncertainties in p+p analysis apply to p+Au analysis. A summary of all systematic uncertainties can be found in Fig. 51 and 52.

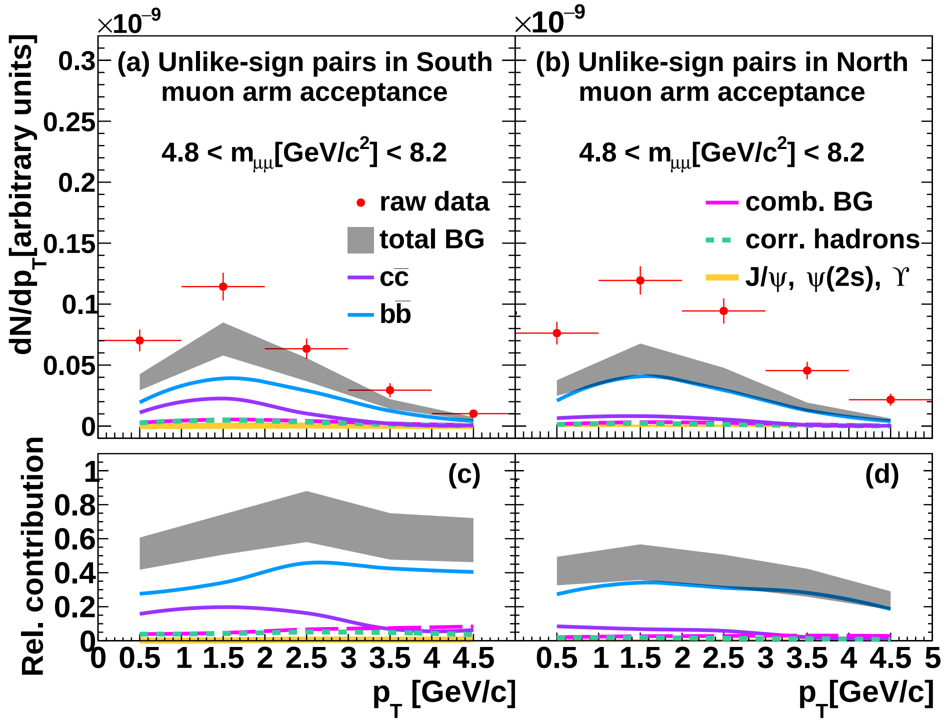

Figure 49: Data and background components for Drell-Yan extraction as a function of pair p_T.

6.4.1 Input hadron spectra (p+p)

Although the hadronic background is negligible in the Drell-Yan mass region, the input hadron spectra can affect the Drell-Yan pairs because the the hadronic background is non-negligible when fitting to the like-sign pairs to obtain the $b\bar{b}$ normalization, which is a large background source for Drell-Yan pairs.

6.4.2 Input hadron spectra (p+Au)

As in the like-sign analysis, the uncertainty in the p+Au spectra includes the uncertainty in the measured R_{pA} and the uncertainty in the extrapolation of R_{pA} to the unmeasured region.

They mainly contribute by modifying the $b\bar{b}$ contribution since $b\bar{b}$ is the most dominant source of background.

6.4.3 $c\bar{c}$ shape (p+p)

Obtained by comparing POWHEG and PYTHIA bottom models.

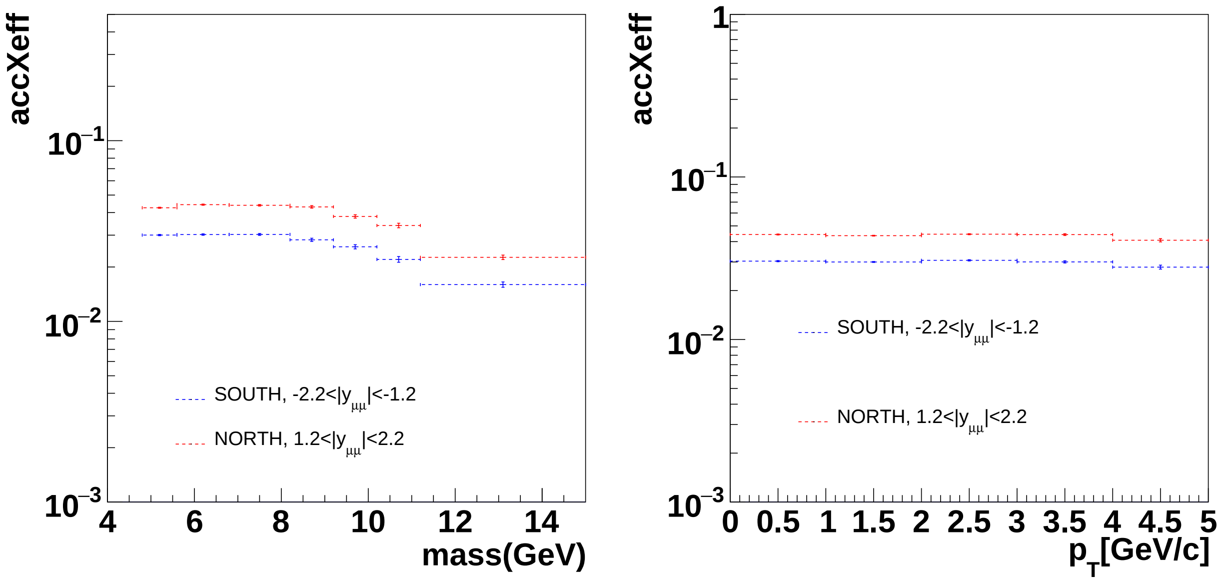

Figure 50: Acceptance and efficiency corrections as a function of mass or p_T.

6.4.4 $c\bar{c}$ shape (p+Au)

The input spectra for $c\bar{c}$ was modified as shown in Fig. 38, which give rise to the systematic bands for $c\bar{c}$ shape as shown in Fig. 39. These are then propagated to the Drell-Yan yields via Eq. 3. Since $c\bar{c}$ is enhanced for the Au-going side, the systematic uncertainties are much larger for the Au-going side compared to the p-going side.

6.4.5 $b\bar{b}$ shape (p+p)

Obtained by comparing POWHEG and PYTHIA bottom models.

6.4.6 $b\bar{b}$ shape (p+Au)

The input spectra for $b\bar{b}$ was modified as shown in Fig. 40, 43, which give rise to the systematic bands for $b\bar{b}$ shape as shown in Fig. 47. These are then propagated to the Drell-Yan yields via Eq. 3. Since $c\bar{c}$ is enhanced for the Au-going side, the systematic uncertainties are much larger for the Au-going side compared to the p-going side.

6.4.7 Statistical uncertainties in fit

The normalization of combinatorial and $b\bar{b}$ backgrounds has an uncertainty related to the statistical uncertainty in the fitting routine using p+Au like-sign data. Likewise, the normalization of correlated hadrons and $c\bar{c}$ contains uncertainties related to the statistical uncertainty in the p+p data.

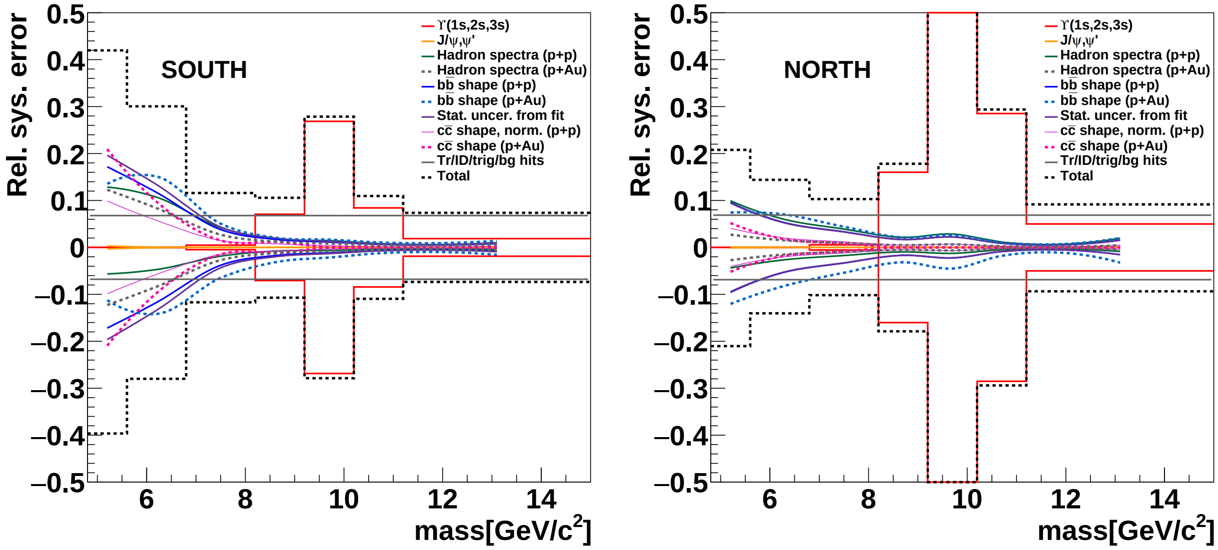

Figure 51: Summary of all systematic uncertainties as a function of pair mass.

6.4.8 ψ',Υ

We have avoided the J/ψ and ψ' by excluding the mass region < 4.8 GeV/c^2 and the Υ the mass region $8.2 - 11.2$ GeV/c^2. The systematic uncertainties for $J/\psi(\psi')$ and Υ are determined by varying the normalization of summing the statistical and systematic uncertainty of the p+p measurement, and then in addition summing the statistical and systematic uncertainty of the $R_{p/d+Au}$ measurements. The resulting uncertainties are negligible due to the mass selection.

6.4.9 Reconstruction efficiency

We assign MuTr(4%), MuID (2%), trigger (1.5%) as systematic uncertainties as above.

6.4.10 Background hits

We assign 5% as systematic uncertainty as above.

6.5 Results

The differential Drell-Yan cross-sections in p+Au collisions at 200 GeV is shown in Fig. 55 as a function of mass and Fig. 56 as a function of p_T for pairs with mass= $4.8 - 8.2$ GeV/c^2. The results are compared to the p+p case and the R_{p+Au} is determined. The p+p data has been rebinned to increase the statistical significance. As such, the bin shift correction has to be redetermined. To estimate the bin shift, we use PYTHIA, which has been verified to reasonably reproduce the Drell-Yan p_T spectra. Fig. 53 shows the dN/dp_T spectra of Drell-Yan pairs from PYTHIA; the bin shift correction is determined by taking the ratio of the total number of counts in one bin(red)

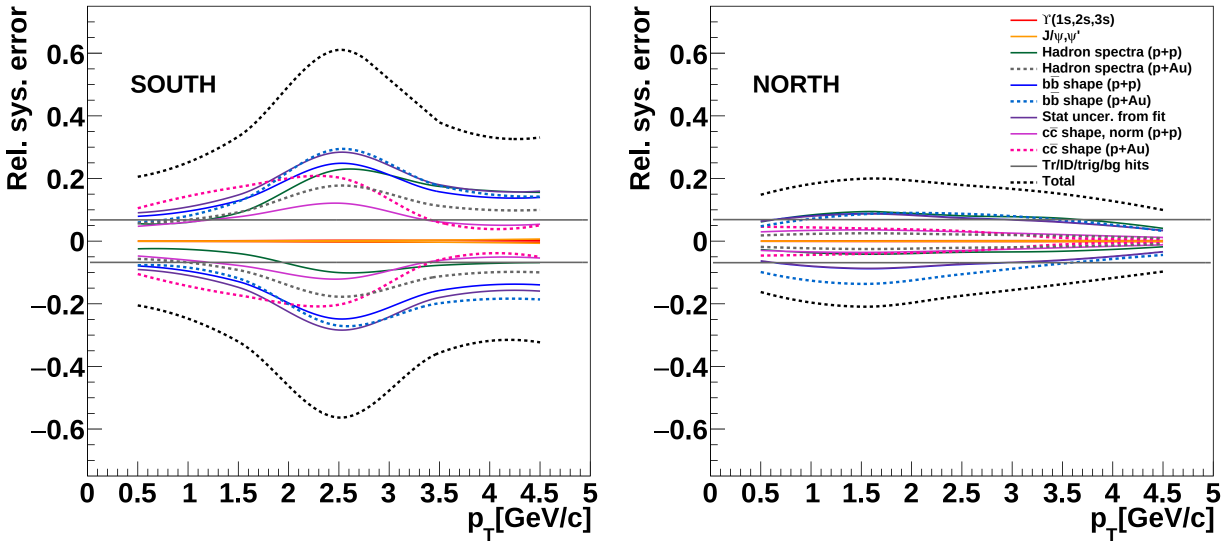

Figure 52: Summary of all systematic uncertainties as a function of pair mass.

divided by the value of dN/dp_T at the center of the bin estimated by the fine binning case(black). The resultant bin shift corrections are shown in the right panel and the uncertainties are statistical of around 3%, which is negligible compared to the other sources of systematic uncertanties.

EPPS16 in conjunction with PYTHIA was used to calculate the expected modification from nPDFs. The uncertainty from EPPS16 is calculated by adding all 20 error sets in quadrature, as shown in Fig. 54.

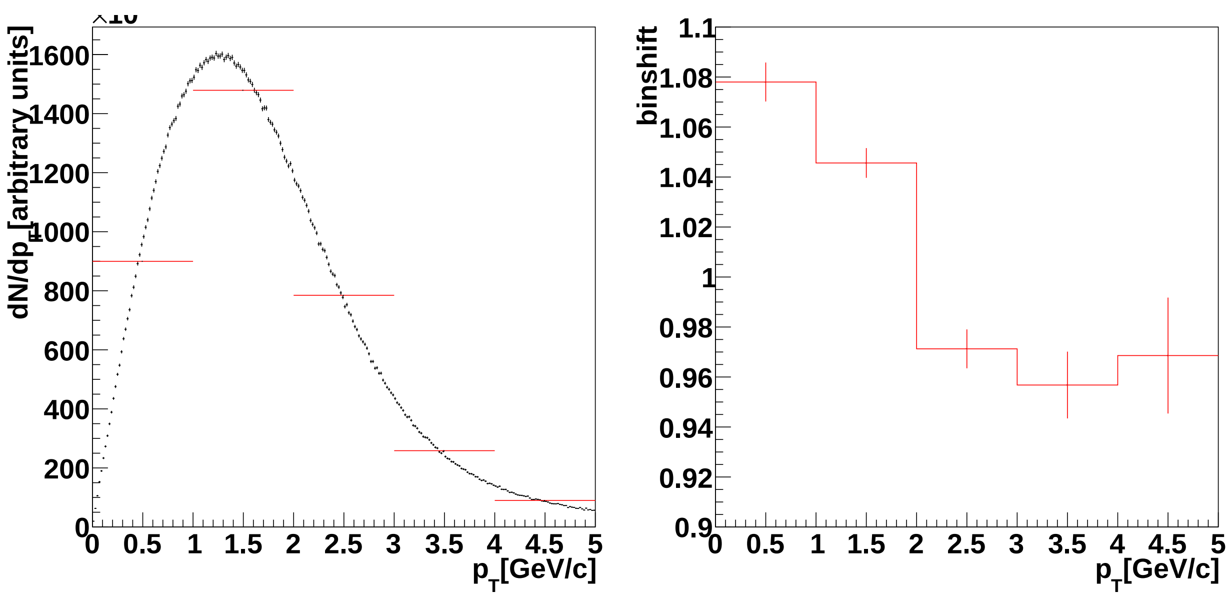

Figure 53: Left panel: dN/dp_T from PYTHIA, with fine binning and binning from data. Right panel: Bin shift corrections as a function of p_T.

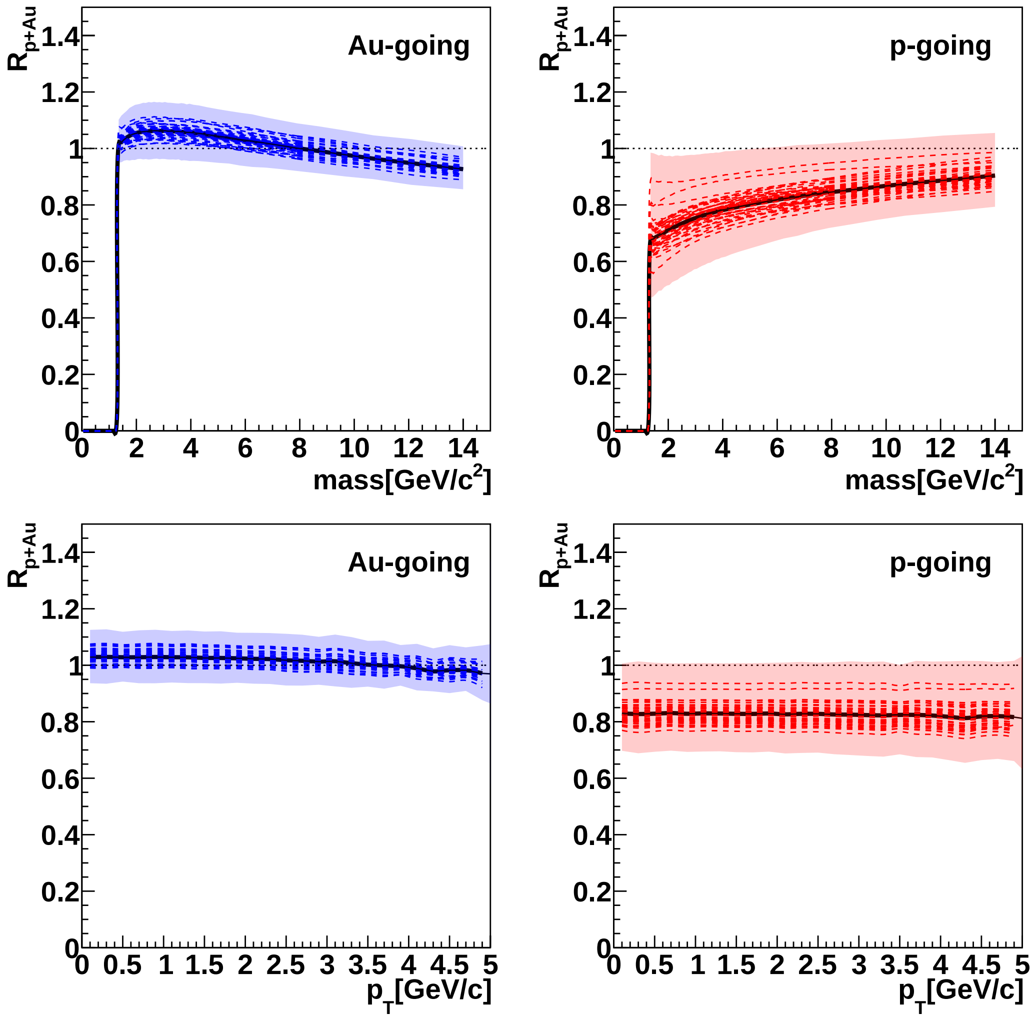

Figure 54: EPPS16 error sets.

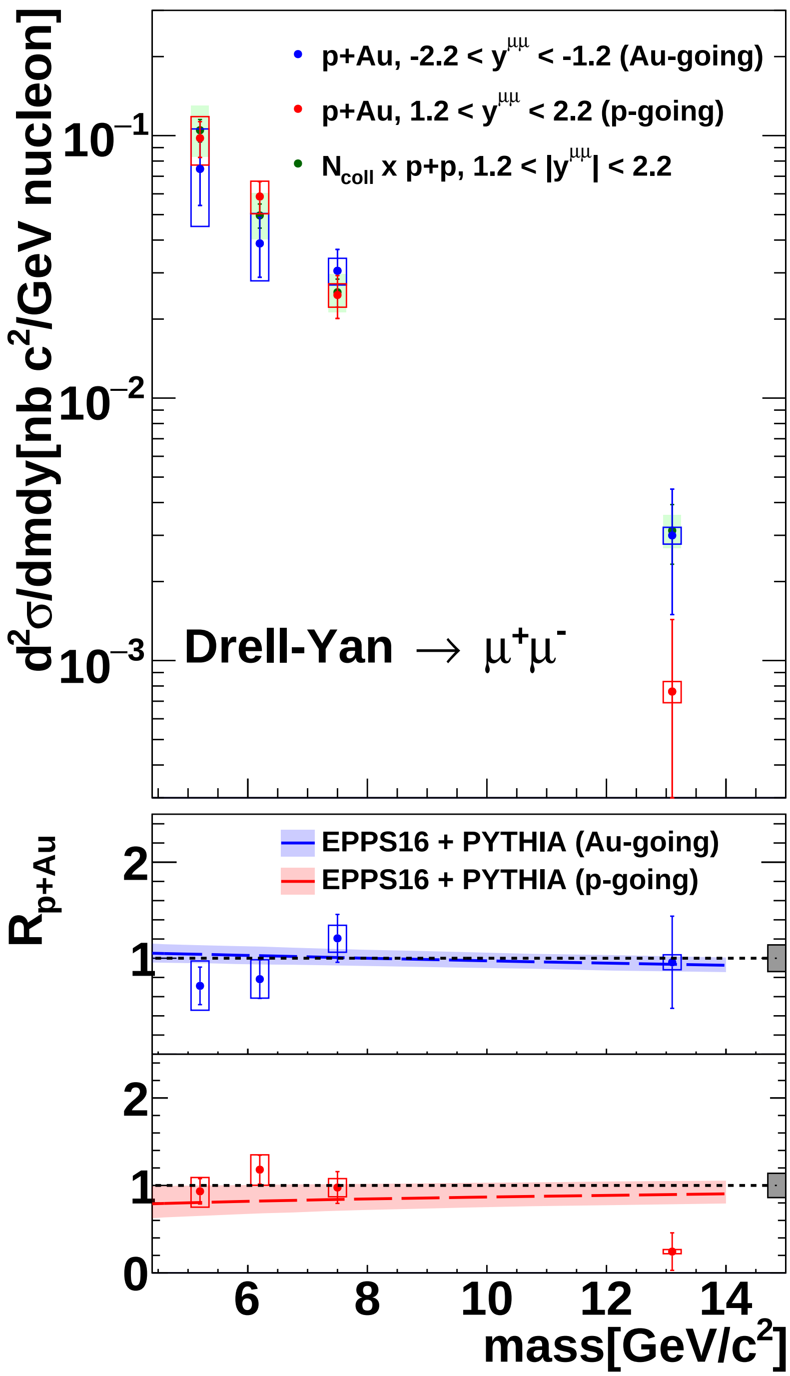

Figure 55: Drell-Yan cross-sections as a function of mass.

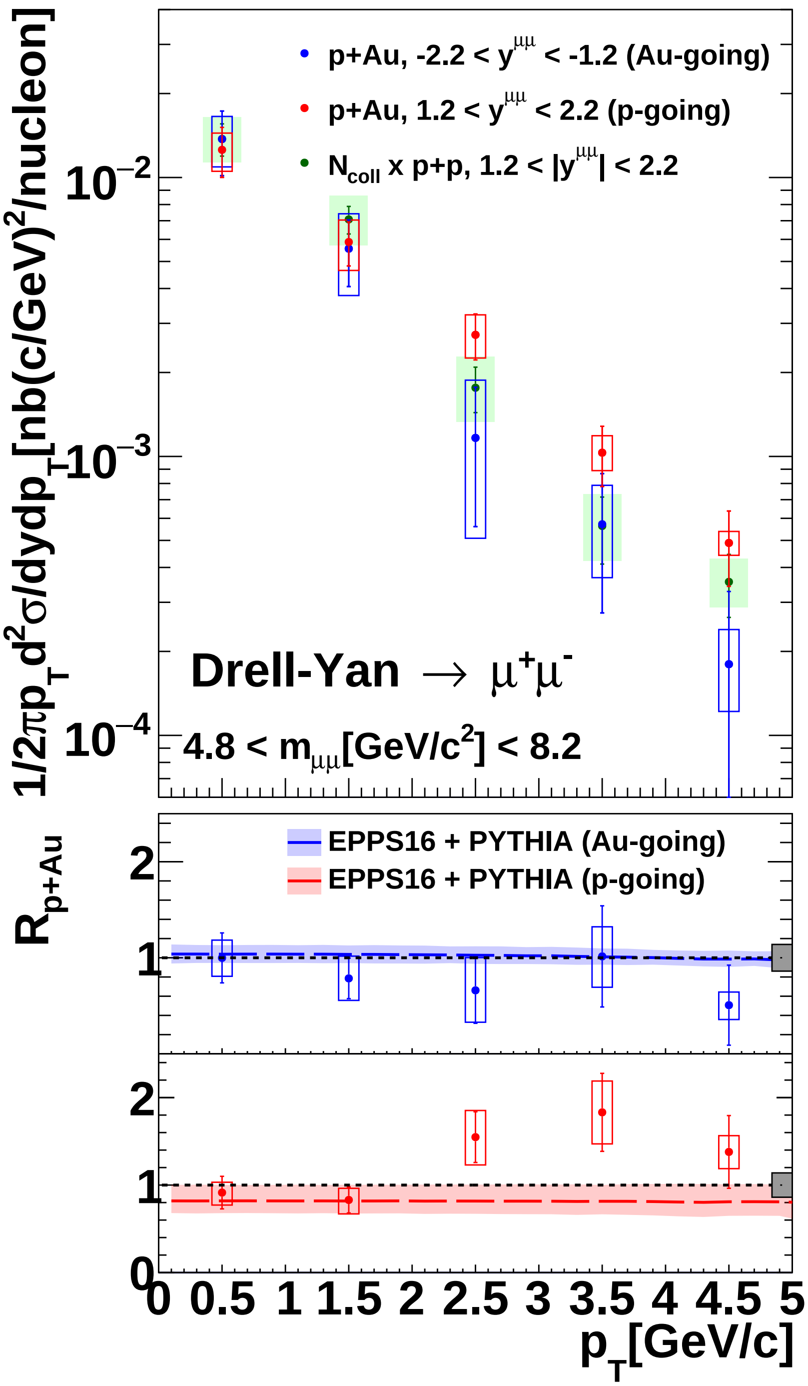

Figure 56: Drell-Yan cross-sections as a function of p_T for pairs with mass$= 4.8 - 8.2$ GeV$/c^2$.

6.6 Crosschecks

6.6.1 Varying the mass window

As a cross-check, two additional mass selection for the p_T measurement was chosen $5.2-8.2$ GeV/c^2, $5.6-8.2$ GeV/c^2. This is motivated by the fact that the background contributions from $c\bar{c}$ and correlated hadrons drop as a function of mass. To confirm this, we compare the backgrounds as a function of p_T for the three mass selections in Fig. 57. The background to inclusive data is also shown in Tab. 4 which clearly illustrates that both $c\bar{c}$ and correlated hadrons relative contribution drops by a factor of two from 4.8GeV/c^2 to 5.6GeV/c^2.

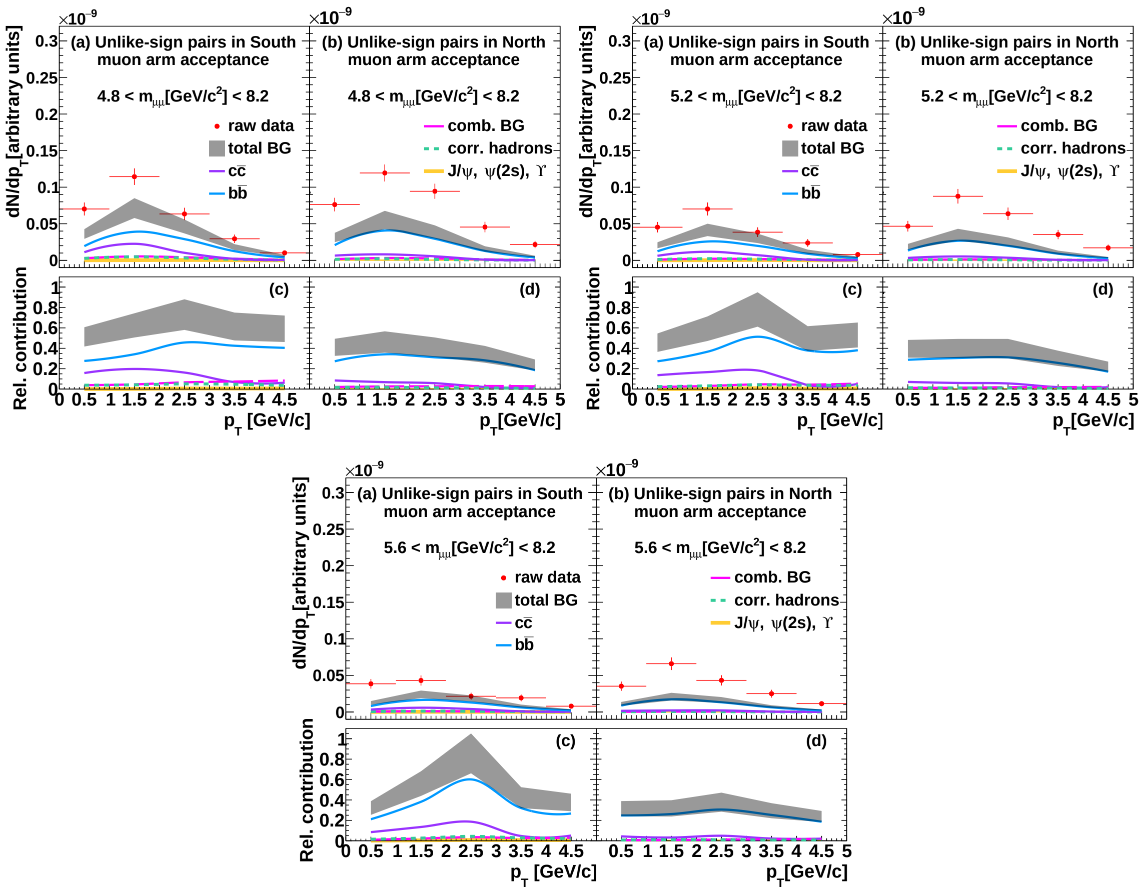

Figure 57: Drell-Yan background components as a function of p_T for three different mass selections.

The same analysis procedure is repeated for all three mass selections and the differential cross-sections as a function of p_T are shown in Fig. 58.

We see the same trend in all mass selections: for the Au-going side the R_{p+Au} scatter around unity, whereas for the p-going side, if we take into account all statistcal and systematic uncertainties, the data points are consistent with unity, but the data points for $p_T > 2$ tend to lie above unity. As the same trend is seen in all mass selections, it is very unlikely that this tendency is due to mis-modelling of backgrounds, as the background components, especially $c\bar{c}$ and correlated hadrons

Table 4: Contributions of background components for three mass selections.

mass interval [GeV/c^2]	corr.hadrons/data	$c\bar{c}$/data	$b\bar{b}$/data
Au-going			
4.8-8.2	0.043 ± 0.003	0.16 ± 0.01	0.36 ± 0.02
5.2-8.2	0.033 ± 0.003	0.14 ± 0.01	0.37 ± 0.03
5.6-8.2	0.026 ± 0.003	0.11 ± 0.01	0.35 ± 0.03
p-going			
4.8-8.2	0.015 ± 0.001	0.060 ± 0.003	0.30 ± 0.02
5.2-8.2	0.011 ± 0.001	0.052 ± 0.003	0.29 ± 0.02
5.6-8.2	0.009 ± 0.001	0.036 ± 0.003	0.26 ± 0.02

drop by almost a factor of two from the different mass selections.

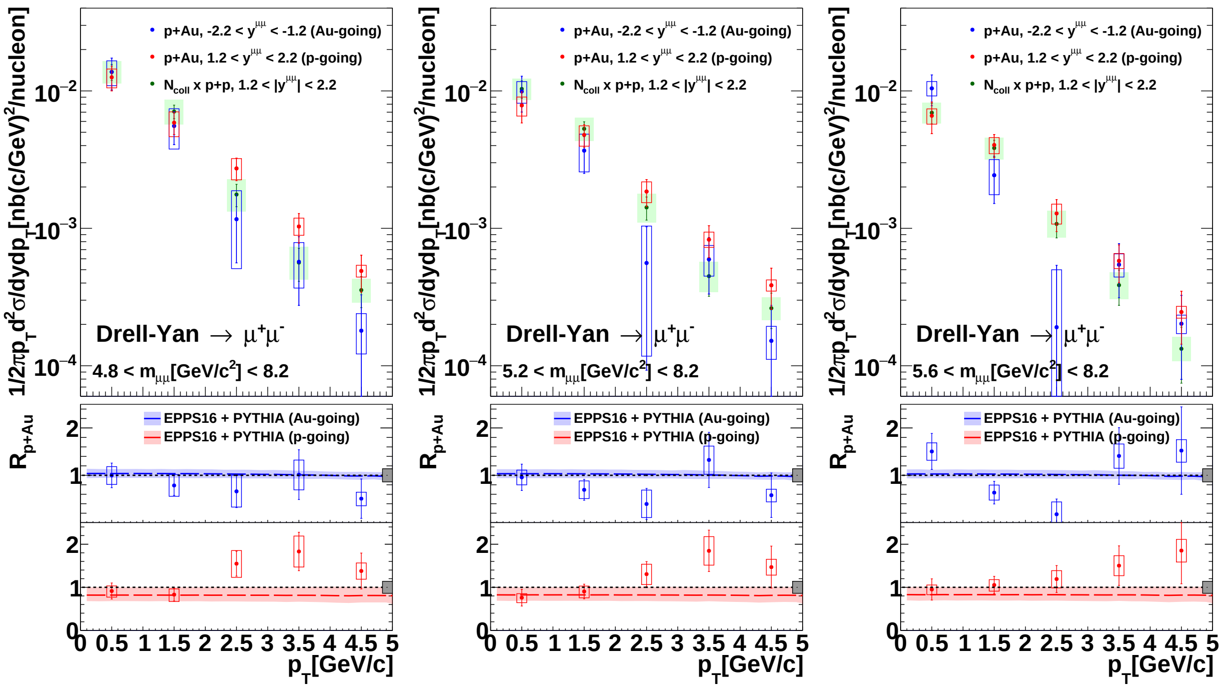

Figure 58: Drell-Yan differential cross-sections as a function of p_T for three different mass selections.

6.6.2 Crosscheck: Like-sign subtraction

For both Drell-Yan $p+p$ and $p+$Au analysis as described above, we have used the (default) subtraction method, in which the Drell-Yan counts are determined using the following formula:

$$N_{DY} = N^{+-}_{inclusive} - N^{+-}_{corr.hadrons} - N^{+-}_{comb.bg} - N^{+-}_{quarkonia} - N^{+-}_{c\bar{c}} - N^{+-}_{b\bar{b}} \tag{4}$$

An alternative method is to apply like-sign subtraction, according to the following:

$$N_{DY} = N^{+-}_{inclusive} - N^{\pm\pm}_{inclusive} - N^{+-}_{quarkonia} - N^{+-}_{c\bar{c}} - (N^{+-}_{b\bar{b}} - N^{\pm\pm}_{b\bar{b}}) \tag{5}$$

Since the like-sign data should in principle be described by its cocktail of components, i.e.

$$N^{\pm\pm}_{inclusive} = N^{\pm\pm}_{corr.hadrons} + N^{\pm\pm}_{comb.bg} + N^{\pm\pm}_{b\bar{b}} \tag{6}$$

It is easy to see that this method therefore assumes the following relations.

$$N^{+-}_{corr.hadrons} = N^{\pm\pm}_{corr.hadrons} \tag{7}$$

$$N^{+-}_{comb.bg} = N^{\pm\pm}_{comb.bg} \tag{8}$$

As we have seen in the $p+p$ analysis and also in the following, these relations do not hold in the low mass region, but they hold well at mass $> 3\text{GeV}/c^2$ (AN1306: Fig.37, AN1306: Fig.52). Hence, we can safely use the like-sign subtraction method for Drell-Yan extraction for the mass selection $(4.8 - 8.2)\text{GeV}/c^2$.

The disadvantage of this method is that it introduces more statistical fluctuations to the background estimation. This is compensated with the advantages of evading the usage of the fastMC in the subtraction, as well as lowering the contribution of $b\bar{b}$ from simulations; since the like-sign $b\bar{b}$ component directly comes from data, and that the modifications of unlike and like-sign $b\bar{b}$ are basically identical in this mass region.

6.7 Cross-sections as a function of mass and p_T (Like-sign subtraction)

Although we do not expect any complications in the Drell-Yan analysis as a function of mass, we start this cross-check by looking at the mass variable to set the stage.

The unlike- and like-sign inclusive data and all cocktail components are shown in Fig. 59.

We make the following observations: (i) The unlike- and like-sign combinatorial background and correlated hadrons overlap; (ii) The sum of all like-sign cocktail well describes the data. We therefore expect no difference to within uncertainties between the Drell-Yan signal between the default subtraction and like-sign subtraction method, and this is shown in Fig. 60.

We then apply the like-sign subtraction method to extract Drell-Yan cross-sections as a function of p_T. The unlike- and like-sign inclusive data and all cocktail components are shown in Fig. 61.

The uncorrected Drell-Yan signal using the default and like-sign subtraction methods are compared in Fig. 62.

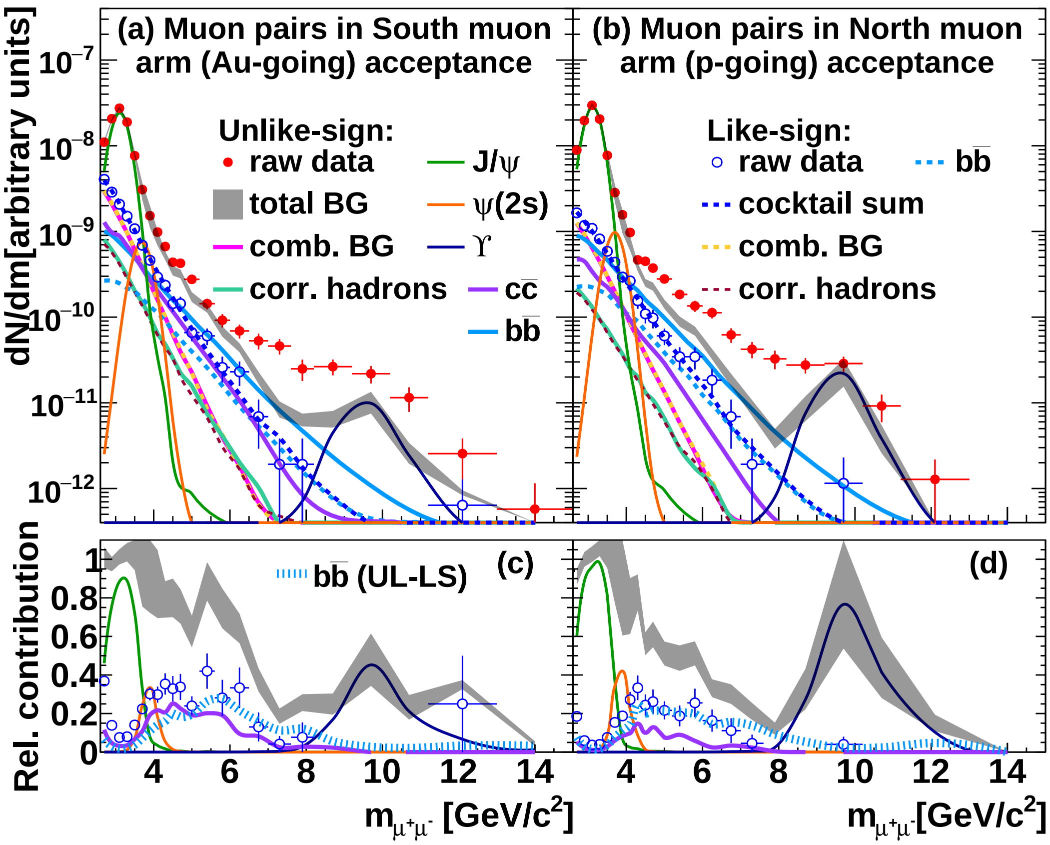

Figure 59: Drell-Yan backgrounds as a function of mass.

We see that even without considering systematic uncertainties, the two methods are consistent to within the statistical uncertainties. Finally, we show the corrected cross-sections as a function of mass and p_T using the like-sign subtraction method in Fig 63. The exact same conclusions are drawn as compared to using the default subtraction method. Since the like-sign subtraction method does not involve the FastMC, we conclude that that mis-modelling of correlated hadronic backgrounds cannot be an issue in this analysis.

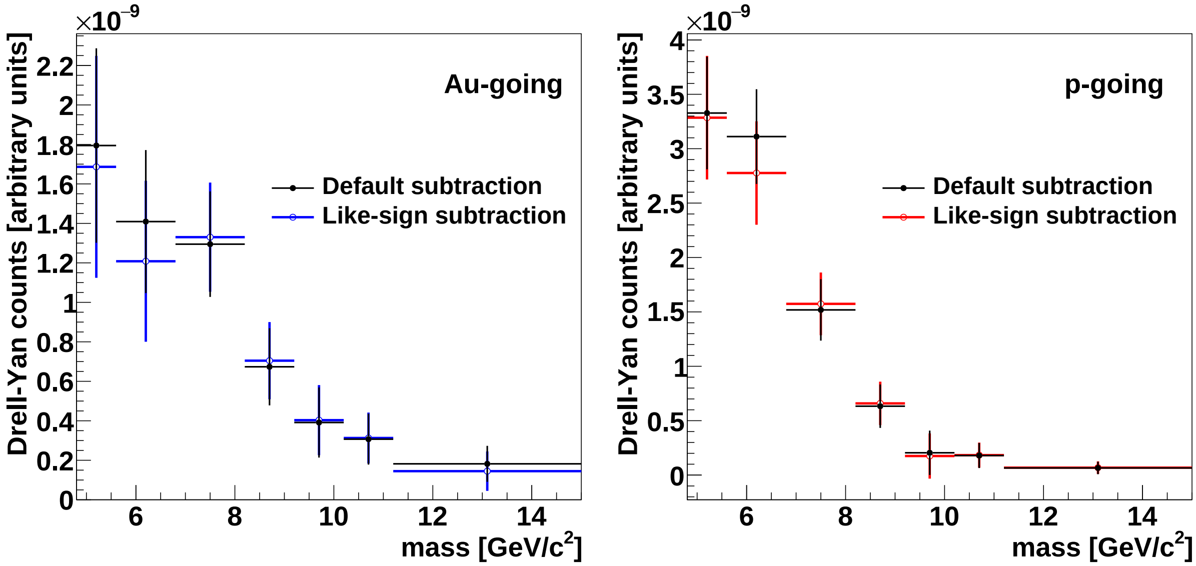

Figure 60: Drell-Yan signal as a function of mass.

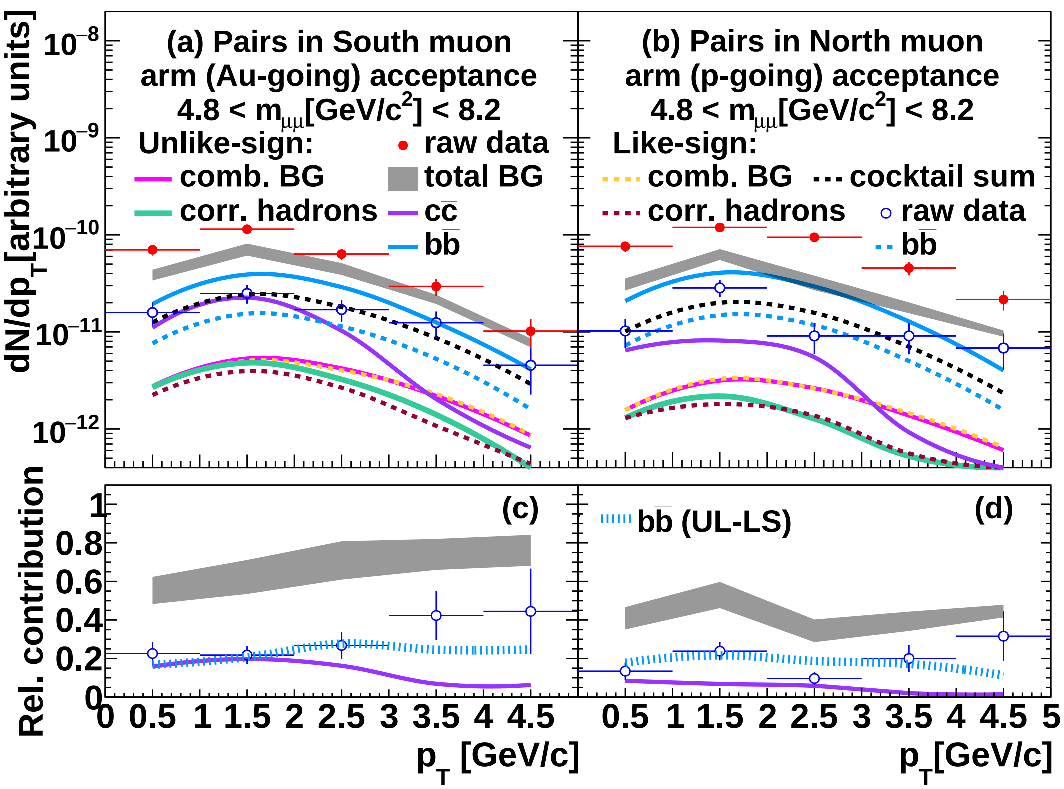

Figure 61: Drell-Yan backgrounds as a function of p_T.

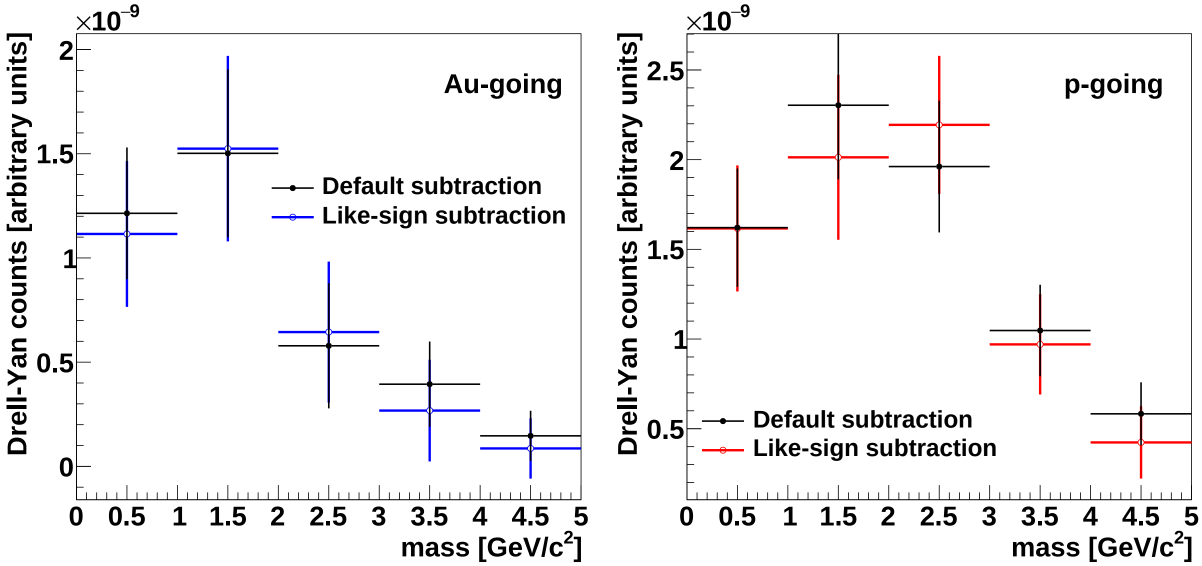

Figure 62: Drell-Yan signal as a function of p_T.

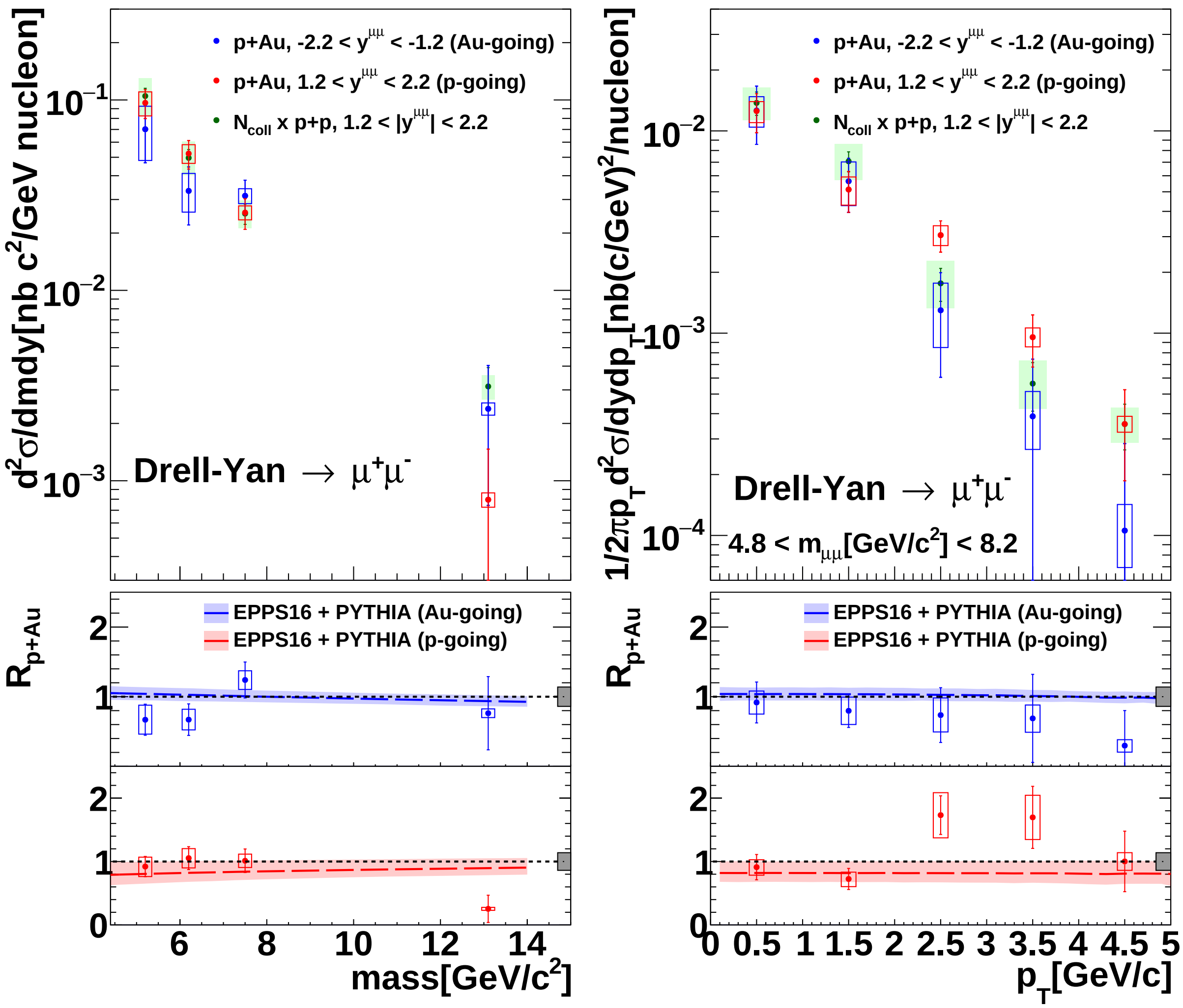

Figure 63: Drell-Yan cross-sections as a function of mass and p_T using the like-sign subtraction.

6.7.1 Crosscheck: Effect of background hits on hadrons

Although we did not see a significant effect of background hits on J/ψ or $b\bar{b}$ simulations that give rise to prompt muons, we have yet to check the effect of such hits on hadrons. We use a flat input p_T distribution of k plus and k minus, and embed into minimum bias p+Au collisions. The ratio of reconstructed muons as a function of p_T between embedded and non-embedded simulations are shown in Fig. 64 for the different charges.

No charge or p_T dependency on efficiency loss is observed to within the assigned 5% systematic uncertainties.

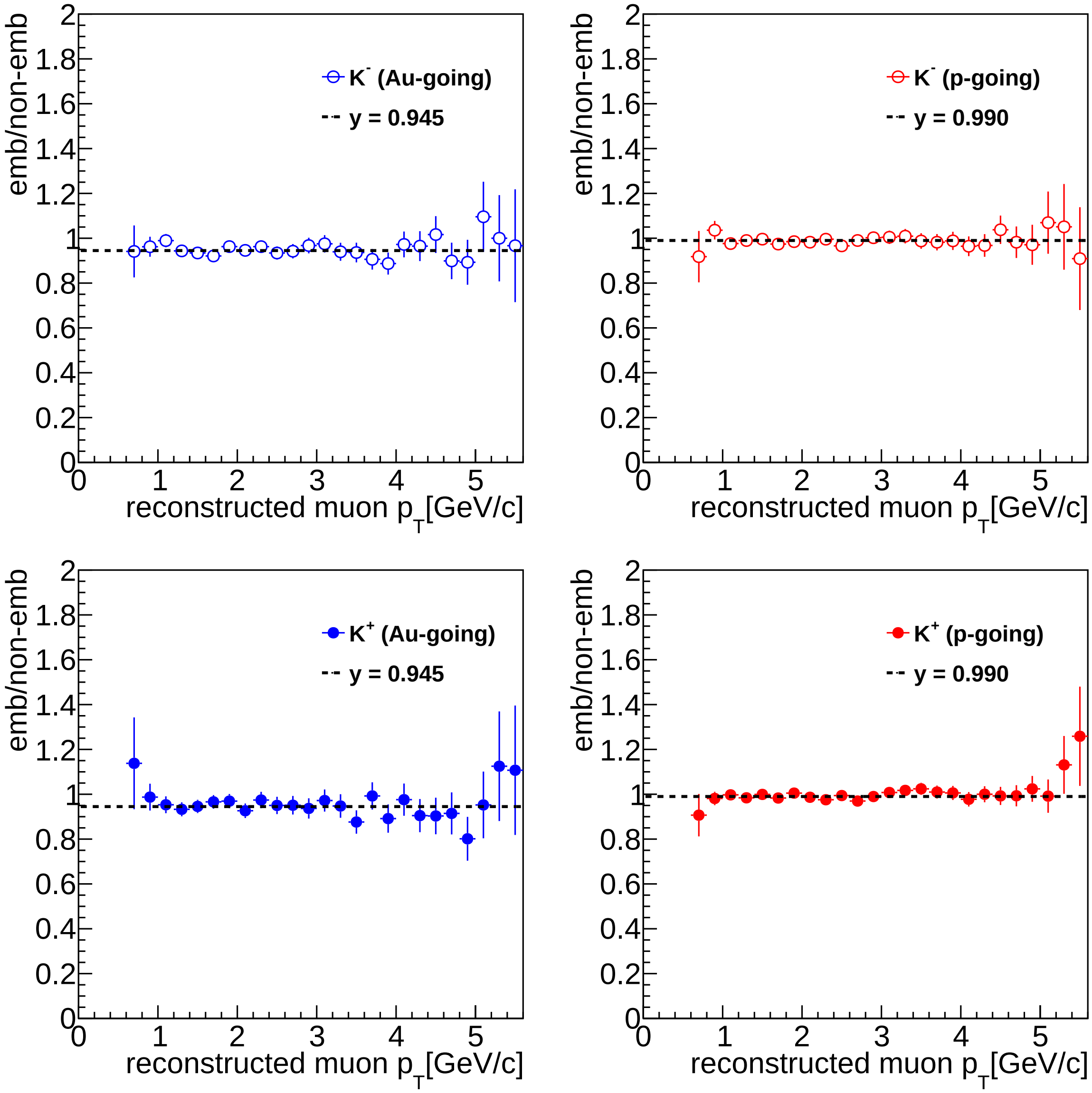

Figure 64: Input kaons with a flat p_T spectra from 1 to 5 GeV/c. Figure shows ratio of embedded to non-embedded simulations as a function of reconstructed muon p_T for different charges and arms. A straight line is plotted to guide the eye.

6.7.2 Crosscheck: Momentum asymmetry

A concern for the high mass region are hadronic backgrounds that may not be reproduced by the fastMC. These hadronic backgrounds usually has large momentum asymmetry, where *asym* is defined:

$$asym = \frac{|p_1 - p_2|}{|p_1 + p_2|} \tag{9}$$

We first check the asymmetry of real data, for the mass region $4.8 - 8.2$ GeV/c^2 used for the Drell-Yan analysis, for unlike- and like-sign pairs. This is shown in Fig. 65.

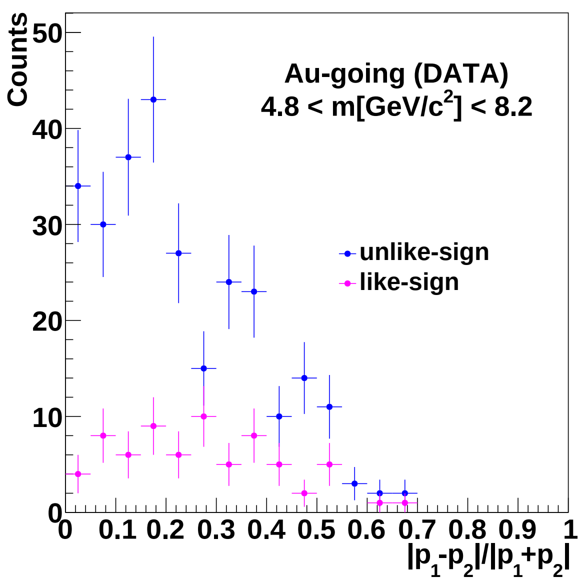

Figure 65: Momentum asymmetry of unlike- and like-sign pairs for the Au-going and p-going sides.

All analysis cuts (except for $asym < 0.55$, of course) are applied. No significant momentum asymmetry is observed. This can be due to a combination of MuTr/MuID proximity cuts, the $p < 20\text{GeV}/c$ cut, $vtxchi2 < 5$ cut and (D)DG0 cuts, all of which have some power to reject hadronic tracks from secondary particles or decays within the MuTr volume resulting in false high p_T particles.

To further confirm that the bump at high p_T for the p-going side is not from rogue hadronic tracks, we separate the unlike-sign data into high asymmetry ($asym > 0.5$) and low asymmetry ($asym < 0.5$) cases. This is shown in Fig. 66.

One can then plot the ratio of high asymmetry ($asym > 0.5$) pairs to low asymmetry ($asym < 0.5$) pairs as a function of p_T. This ratio is compared to the same quantity using Drell-Yan simulations in Fig. 67.

We see there is no indication of rogue hadronic background in the data, and the ratio seen in the data (despite containing small amounts of unsubtracted hadronic background) is consistent with the ratio in Drell-Yan simulations.

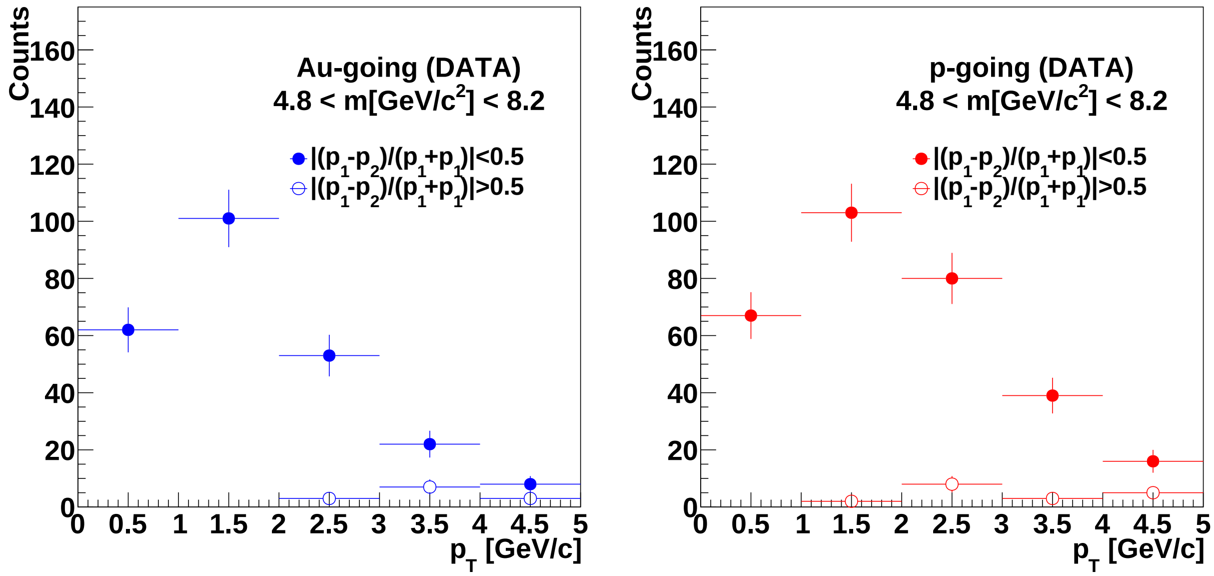

Figure 66: Unlike-sign data, divided into pairs with ($asym > 0.5$) and ($asym < 0.5$)

.

As a final test, we plot the asymmetry distribution of like-sign subtracted data for p_T in data and Drell-Yan simulations. The Drell-Yan simulations are normalized to the integral of the data. The results are shown in Fig. 68.

We do not see evidence of contamination of rogue hadronic tracks.

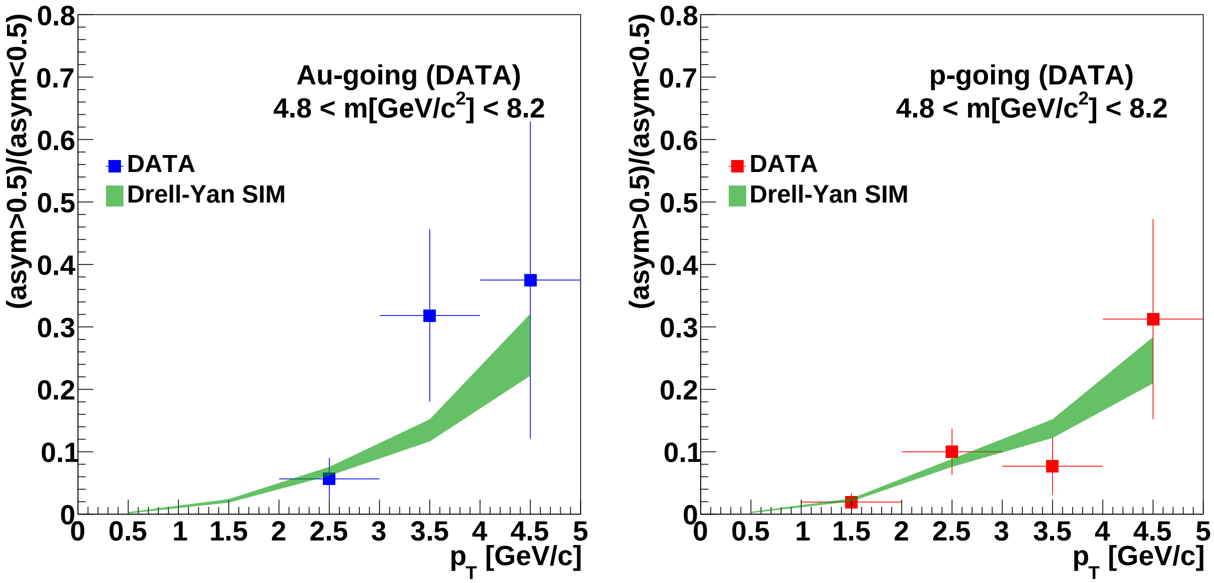

Figure 67: Unlike-sign data, divided into pairs with $(asym > 0.5)$ and $(asym < 0.5)$

.

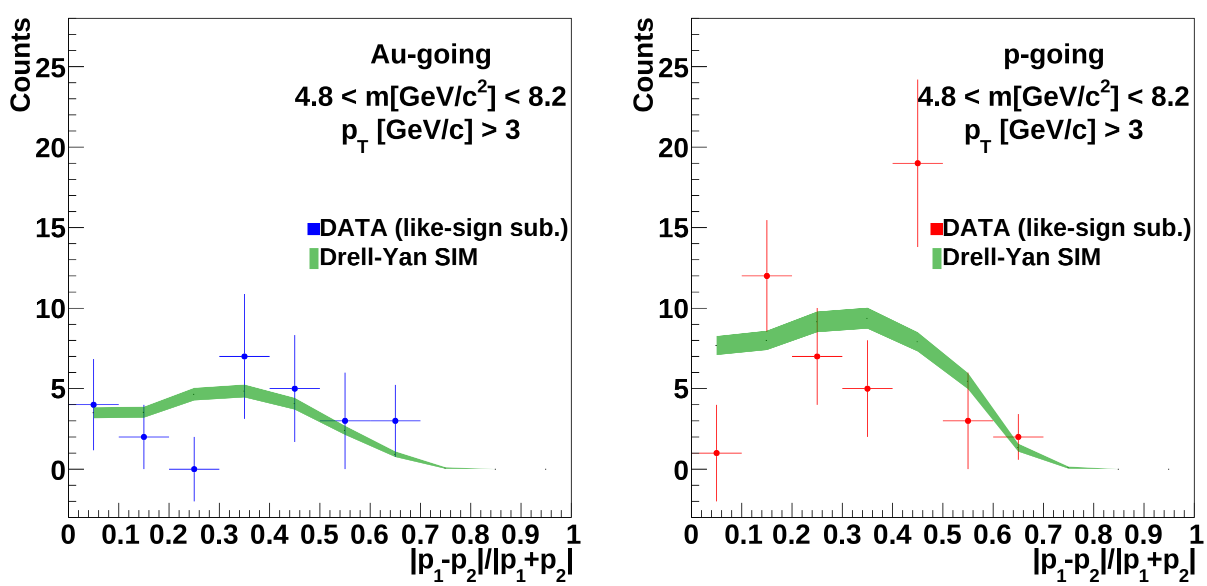

Figure 68: Momentum asymmetry of like-sign subtracted unlike-sign data, compared to Drell-Yan simulations, for mass= $4.8 - 8.2$ GeV/c^2; $p_T > 3$ GeV/c

.

7 References

References

[1] PHENIX analysis note 1306, Measurement of charm, bottom and Drell-Yan cross-sections in p+p collisions in Run15 via dimuons at 200 GeV.

[2] PHENIX analysis note 1354, Inclusive J/psi at muon arms in small collision systems.

[3] PHENIX analysis note 1341, Charged hadrons with FVTX in Run15pp200 and RpA.

[4] PPG153, Cold nuclear matter effects on heavy-quark production at forward and backward rapidities in d+Au collisions at $\sqrt{s_{NN}} = 200$ GeV, arXiv:1310.1005.